

Passive and Stable Impedance Reduction of Hybrid and Flexible Link Serial Robots Using Position, Force, and Acceleration Feedback

A.H.G. Overbeek
Master Thesis Biomedical Engineering, Systems and Control

Document number: BE-786

Faculty of Engineering Technology
Department of Biomechanical Engineering

Graduation Committee:
prof. dr. ir. H. van der Kooij
dr. ir. A.Q.L. Keemink
dr. ir. D. Dresscher
ir. H.C. Voort

June 10, 2021

Abstract

Apparent impedance reduction allows heavy and damped robots to feel lightweight to human users. Doing so passively yields unconditional human-robot stability and thus safety. This fulfills a baseline requirement of rehabilitation robotics: the ability to train unobstructed by robot dynamics, only experiencing therapy dynamics. This work studies and compares two derogatory effects on the safe impedance reduction of serial robots: the discrete-time controller and link flexibility. A simple impedance controller is considered that linearly adds motor position, interaction force, end effector acceleration and their derivatives. Novel passivity conditions reveal that the hybrid system allows very little acceleration and no force feedback, resulting in barely any passive inertia reduction. Underdamped link flexibility is separately studied and is reaffirmed to be fundamentally limited to passively masking actuator inertia. Maximum passive impedance reductions for each case are compared, where both allow complete damping reduction. However, passivity must be forfeit for many applications that require inertia reduction. This theory is applied in a case study to the Gable Core rehabilitation platform. Modern optimal design of a stabilizing, rather than passivating, controller minimizes noise while reducing impedance. The two derogatory system models are compared to the ideal and the mixed system, consisting of both hybrid and flexible dynamics. This reveals that the hybrid model is less restrictive than the flexible model for stable impedance reduction, but more restrictive for passive impedance reduction.

Contents

Abstract	i
Nomenclature	v
I General Introduction	I
1 Introduction	2
1.1 Rehabilitation	2
1.2 Safety	3
1.3 Performance	3
1.4 Problem	3
1.5 Contribution and Outline	4
II Background	5
2 Literature Review	6
2.1 Chronological Overview	6
2.1.1 Analytical Passivity	6
2.1.2 Enforcing Passivity	7
2.2 Classification of Literature	8
2.3 Analysis and Contribution	9
3 Passive Impedance Control Design and Methods	12
3.1 System Description	12
3.2 Safety: Passivity	13
3.3 Performance: Impedance Shaping	14
3.4 Passive/Stable Impedance Reduction	15
3.5 Noise Sensitivity	15
3.6 Optimal Design	16
3.7 Design Case Study: Gable Core	17
3.7.1 System Identification	17
3.7.2 Noise Identification	19
III Analysis and Design	20
4 Rigid Robot With Continuous-Time Controller	21
4.1 System Description	21
4.2 Safety: Passivity	22
4.3 Performance: Impedance Shaping	22
4.4 Passive Impedance Reduction	23
4.5 Noise Sensitivity	23
4.6 Design: Gable Core	24
4.7 Discussion and Conclusion	25

5	Rigid Robot With Discrete-Time Controller	26
5.1	System Description	26
5.2	Safety: Passivity	28
5.2.1	Passivity Conditions Through Passive Environment Closed Loop Stability	28
5.2.2	Separate Discrete-Time Position Feedback	30
5.2.3	Separate Discrete-Time Acceleration Feedback	30
5.2.4	Separate Discrete-Time Force Feedback	30
5.3	Performance: Impedance Shaping	31
5.4	Passive/Stable Impedance Reduction	31
5.4.1	Passive Reduction: Combined Position and Acceleration Feedback	31
5.4.2	Stable Reduction: Force Feedback	33
5.5	Noise Sensitivity	33
5.6	Design: Gable Core	33
5.6.1	Analytical Design	33
5.6.2	Numerical Design	34
5.7	Discussion and Conclusion	36
6	Flexible Link Robot With Continuous-Time Controller	38
6.1	System Description	38
6.2	Safety: Passivity	40
6.2.1	Physical Equivalence	40
6.2.2	Heuristics	41
6.2.3	Positive Real Condition	42
6.3	Performance: Impedance Shaping	43
6.4	Passive/Stable Impedance Reduction	43
6.4.1	Passive Reduction	43
6.4.2	Stable Reduction	44
6.5	Noise Sensitivity	44
6.6	Design: Gable Core	45
6.7	Discussion and Conclusion	48
IV	Conclusions	49
7	Comparison and Discussion	50
7.1	Passivity Analysis	50
7.2	Stability Analysis	52
8	Conclusions	55
V	Appendix	56
A	Appendix to Chapter 3	57
A.1	Definition: LTI Frequency Passivity	57
A.2	Definition: Nyquist Criterion	57
A.3	Real and Imaginary Parts of a Complex Ratio	58
A.4	Manual Physical Equivalent Synthesis	58
B	Appendix to Chapter 4	59
B.1	Rigid Robot Continuous-Time Controller PRC Without Derivatives	59
B.2	Rigid Robot Continuous-Time Controller PRC Including Derivatives	60
B.3	Rigid Robot Continuous-Time Controller PE	61
B.4	Inertia Cancellation of the Rigid Robot Continuous-Time Controller by G_{fd}	62

C	Appendix to Chapter 5	63
C.1	Definition: Starred Transform	63
C.2	Rigid Robot With Discrete-Time Controller Transfer	63
C.3	Rigid Robot Discrete-Time Position Feedback Passivity (Alternative to [1])	64
C.4	Rigid Robot Discrete-Time Force Feedback Passivity	65
C.4.1	Limited Resonance	66
C.4.2	Pure Environmental Stiffness	66
C.5	Lemma: Positive Realness Condition of $A(s)$	67
C.6	Minimal Passive Impedance for Combined Discrete-Time Position and Acceleration Feedback	67
C.7	Discrete-Time Part of Loop Gains	68
C.8	Lemma: Sampling of RHP Passive and RHP Offset Systems	69
C.9	Combined Hybrid and Mixed Loop Marginal Stability for Spring Environments	69
C.10	Complex Region Product Sampling	70
C.11	Physical Interpretation of Uncoupled Pure Inertia Robot Acceleration Feedback	71
C.12	Positive Discrete-Time Acceleration Feedback Passivity	72
C.13	Negative Discrete-Time Acceleration Feedback Passivity	72
C.13.1	Lemma: Conservative Approximation	76
D	Appendix to Chapter 6	77
D.1	Root Separation	77
D.2	Flexible Link Robot Numerator Root Separation	77
D.3	Quadratic-Quadratic Polynomial	78
D.4	Flexible Link Robot Continuous-Time Controller PE Without Derivatives	78
D.5	Flexible Link Robot Continuous-Time Controller PE with Derivatives	80
D.6	Flexible Link Continuous-Time Controller (Noise) Transfer	82
D.7	Second Order Transfer Phase Requirement	82
D.8	Flexible Link Robot HF PRC	83
D.9	Flexible Link Robot with Continuous-Time Controller PRC	83
D.10	Flexible Link Robot Literature Comparison	84
D.10.1	DLR	84
D.10.2	SEA	85
D.11	Derivation of Flexible Link Robot and SEA Equivalence	86
E	Appendix to Chapter 8	88
E.1	Flexible Link Discrete-Time Controller (Mixed) Stability Tradeoff	88
	Bibliography	93

Nomenclature

List of Symbols

X, x	Position in the Laplace and time domain Subscript: relating to position
V, v	Velocity in the Laplace and time domain Subscript: relating to velocity
A, a	Acceleration in the Laplace and time domain Subscript: relating to acceleration
F, f	Interaction force in the Laplace and time domain Subscript: relating to interaction force
t	Time
s	Laplace variable
ω	Frequency
p	Subscript: relating to haptic performance Subscript: relating to proportional feedback gain
Z	Mechanical impedance
r	Subscript: related to unactuated robot
d	Viscous damping Subscript: related to desired apparent impedance Subscript: related to damping Subscript: related to derivative feedback gain
m	Inertia Subscript: relating to inertia Subscript: relating to motor
k	Stiffness Subscript: relating to stiffness
n	Subscript: relating to either sensor (x, a, f)
l	Subscript: relating to either PD (p, d)
e	Subscript: relating to end effector
Ω	Passivity condition
Λ	Stability condition
Ψ	Shaping condition
η	Reduction ratio
G	General feedback controller and its gains
W	Noise transfer
Ξ, ξ	White noise signal in the Laplace and time domain
σ	Variance of sensor white noise Real part of the Laplace variable
M	Noise shaping filter
α	Noise and gain margin tradeoff factor

T	Sample time
z	Discrete-time Laplace variable
N	Subscript: relating to Nyquist frequency
h	ZOH transfer
	Subscript: relating to environment or human
\bar{h}	Backward difference transfer
$[\cdot]^*$	Starred transform of the argument
L	Loop gain
\tilde{D}	Discrete-time part of a loop gain
H	Continuous-time part of a loop gain
$\text{Re}\{\cdot\}$	Real part of the argument
$\text{Im}\{\cdot\}$	Imaginary part of the argument
$\overline{\text{Re}}\{\cdot\}$	Purely real part of the argument (where $\text{Im}\{\cdot\} = 0$)
μ	Tradeoff between discrete-time position(0) versus acceleration feedback(1)

List of Abbreviations

PBIC	Passivity Based Interaction Control
IC	Impedance Control
AC	Admittance Control
LTI	Linear Time Invariant
PD	Proportional-Derivative
LF	Low-Frequency
HF	High-Frequency
PHRI	Physical Human-Robot Interaction
RHP	Right Half-Plane
ZOH	Zero-Order Hold
PRC	Positive Real Condition
PE	Physical Equivalent
IPM	Ideal Physical Model
SEA	Series Elastic Element
DLR	German Aerospace Center
ADC	Analog-to-Digital Converter
LP	Low-Pass

Part I

General Introduction

Chapter 1

Introduction

In a very general sense, physical human-robot interaction (PHRI) can provide superhuman strength, speed, accuracy and repeatability. At the same time, there is room for human learning, versatility and dexterity, combining the best of both worlds. Highly researched PHRI topics include medical applications, such as surgical and rehabilitation robotics on teleoperation and exoskeletal equipment. Another branch is that of robots that share their workspace with humans, called collaborative robots or cobots for short. This technology has few commercial applications as of yet and only in recent years have ISO standards for cobots been introduced, requiring power and force limiting (ISO/TS 15066:2016). However, numerous other fields are developing interest in the application of these haptic devices, such as entertainment, design, education, manufacturing/assembly, medical training, prosthetics, space and marine robotics to name a few [2].

1.1 Rehabilitation

Rehabilitation is one of the branches benefitting most from PHRI, where robotics allows much more efficient training. During traditional rehabilitation several therapists may be required to physically support a rehabilitant. The strength provided by robotics can greatly alleviate physical effort by personnel. As a result, a single therapist can oversee more than one patient at a time, increasing the quantity of rehabilitation. In addition, the greater consistency provided by robotics may increase safety and rehabilitation rates for repetitive exercises.

A novel rehabilitation robot is the Gable Core: a gait and balance training platform developed by Gable Systems B.V. (Hengelo, OV, the Netherlands), shown in fig. 1.1. The system is designed to fully support a user's bodyweight at the hips, which lowers the entry threshold of training to a minimum. As an example, wheelchair-bound rehabilitants can be lifted directly out of their wheelchairs. The self-driving base follows intended user movement, such that rehabilitants are free to move around the training facility. This allows training with a large variety of exercises and equipment, such as treadmill training, sit-to-stand training, balance training and custom obstacle courses. A physical therapist has control over the amount of support, resistance or perturbations the robot administers. In that manner the robot can variably assist or oppose exercises such that it may guide any stage of the rehabilitation process.

The structural strength required to support humans means that full body rehabilitation robots are inherently heavy.



Figure 1.1: Gable Core gait and balance training platform: bodyweight is compensated at the hip. The mobile base and internal actuation facilitate impedance reduction, such that the robot follows the freely moving user unobstructed. Supportive or resistive forces can be applied for training purposes.

Table 1.1: Overview of the chapters and sections in this work.

	Analysis					Design	Conclusions
	System description	Passivity analysis	Impedance shaping	Passive/stable reduction	Noise sensitivity	Optimal design	
General system	3.1	3.2	3.3	3.4	3.5	3.6	
Ideal	4.1	4.2	4.3	4.4	4.5	4.6	4.7
Hybrid	5.1	5.2	5.3	5.4	5.5	5.6	5.7
Flexible link	6.1	6.2	6.3	6.4	6.5	6.6	6.7
Comparison			7.1			7.2	8

However, a rehabilitant using this platform must be hardly aware of the system, to allow natural training. Herein lies one of the challenges of interaction control: reducing the haptic presence of the robot itself. This property is called robot transparency, which requires that the user only experiences dynamics functional to rehabilitation, as determined by the physical therapist. A functional robot must render a range of haptic experiences to the user, from free motion to opposing or promoting exercises. An interaction controller that creates both transparency and these haptics must do so safely, creating a tradeoff between safety and performance. Because the Gable Core is heavy by default, it requires such an interaction controller, and is therefore used as a case study in this work.

1.2 Safety

At the base of all PHRI is the safety of the human during interaction with a robot. Safety can be guaranteed by human-robot stability in all three cases of physical contact: uncoupled, contact transition and coupled [3]. The stability property guarantees that after a human stops exerting effort, both systems will eventually come to a halt. Attaining stability criteria for each of these three cases can be hard. Stability of the uncoupled human and robot systems separately is not sufficient for the other two cases, because the coupling of two separately stable systems is not necessarily stable. Moreover, where robots can be modelled well, humans cannot, because of uncertainty, nonlinearity and time variance. Additionally, contact transition is hard to analyze because such systems are nonlinear by definition. For complex robots and uncertain humans, the three stability criteria can thus be hard to attain.

The property of robot passivity, although more restrictive than robot stability, provides a single condition for stability in all contact cases. Because the coupling, transition and decoupling of passive systems is always stable, the passivity properties of robot and human separately lead to unconditional stability. Because most environments, including inert humans, can be considered passive, robot passivity is the only requirement for stability.

The intuitive time-domain interpretation is that a user can only receive as much energy from the robot as the user has transferred into the robot in the past. Because humans have conscious control over macroscale movements (excluding reflexes) the human is then responsible for his own safety, instead of the robot. Robot passivity thus forms a base for stable and safe PHRI. Active additions, to oppose or assist exercises, then add functionality depending on the application.

In this work, the passivity condition is considered to be the leading target for safety. However, passivity is sometimes too restrictive. In that case, coupled stability must be considered instead, requiring that human dynamics are considered.

1.3 Performance

The goal of interaction control is to render a wide set of different haptic experiences, often far different from the inherent robot dynamics. The apparent impedance determines how a robot *feels* from the user's point of view by dynamically relating interaction variables: velocity and force. The shaping of this dynamic relationship, rather than explicitly controlling a single variable, is the key difference between interaction control and classical mechatronics.

In many cases the target impedance is the rendering of an explicit virtual environment or, in the case of teleoperation, another physical environment. When the target rendering is free space, the apparent impedance should be minimized. During collision with a virtual wall, the impedance should be maximized. Robot functionality is determined by the range of apparent impedances that can be rendered and the accuracy with which this can be done.

1.4 Problem

The two discussed aspects, safety and performance, are necessary for a baseline functional PHRI robot. Safety can thus be guaranteed by robot passivity, and performance by impedance shaping. These aspects can be combined into the notion of passive impedance shaping. The goal of a passive impedance controller is to passively render a range of apparent impedances.

Many factors affect the range of passive apparent impedances that can be rendered. Ch. 2 contains a literature review on relevant research into passivity based interaction control and its challenges. There, five underrepresented themes in modern literature are chosen to be studied: analytical methods, impedance reduction, link flexibility, hybrid systems and additional sensing. The latter topics are described in short here.

- One particular challenge in passive interaction control is the reduction of the minimal apparent impedance, given that many robots are inherently heavy. In other words: a robot that is inherently hard to move, typically due to reflected motor inertia, should not feel as such to the user. The lowest impedance that can be passively rendered is thus a hard requirement for a functional robot, because an unmovable robot is not practical.
- The derogatory effects of the discrete-time controller and link compliance on the minimal passive impedance are especially underrepresented in modern literature. However, they have long been known to fundamentally limit the amount of passive impedance reduction that can be done, as shown in particular by the seminal work of Colgate and Schenkel in [1] and Colgate in [3].
- Feedback of interaction force and acceleration is rarely applied in impedance control, and the feedback of their derivatives is even rarer. Investigating the effect of these feedback options may lead to new strategies.

1.5 Contribution and Outline

To investigate these issues this work studies passive impedance reduction using PD feedback of position, interaction force and acceleration on systems with two detrimental effects: the discrete-time controller and the flexible link. The generalized impedance controller is considered: linearly feeding back PD position, acceleration and force, resulting in six feedback paths, without preconceptions of internal controller structure.

The resulting body of this work is split into four chapters, each concerned with one robot description:

- (Ch. 3, General system) Introduce the general serial robot, impedance control, design targets and methods for analysis and design.
- (Ch. 4, Rigid robot continuous-time controller) Analyze the ideal rigid haptic robot and set its advantages as reference for the following suboptimal chapters. Also referred to as the ideal model.
- (Ch. 5, Rigid robot discrete-time controller) Analyze the rigid hybrid system with the discrete-time controller including the sampler, zero-order hold and finite difference differentiation. Also referred to as the hybrid model.
- (Ch. 6, Flexible link robot continuous-time controller) Analyze the flexible link robot, introducing non-collocation of actuation and end effector sensing. Also referred to as the flexible model.

Each chapter follows the same structure. First, traditional analysis attempts to derive the largest safe impedance reduction. If this is not possible passively, numerical stability is considered instead. Second, modern optimal controller design is done for the Gable Core case study robot, to aid interpretation of the results. For each of these four chapters the structure is:

- (Sec. 1, System description) Introduce the system technically.
- (Sec. 2, Passivity analysis) Derive passivity conditions if possible, otherwise derive stability conditions.
- (Sec. 3, Impedance shaping) Derive requirements to shape the target impedance.
- (Sec. 4, Passive/stable reduction) Obtain the minimal safe impedance by combining the passivity or stability conditions with shaping requirements.
- (Sec. 5, Noise sensitivity) Derive sensitivities to noise.
- (Sec. 6, Optimal design) Design a controller for passive/stable reduction that minimizes noise sensitivity (or a trade-off with robustness) for the case study robot.
- (Sec. 7, Conclusion) Discuss results and draw conclusions.

Because of this structure chapters can be read independently, but all refer to ch. 3 for methods and goals. After separate analyses, the hybrid and flexible link results are compared to each other, to the ideal system and to the combined system in ch. 7. Finally, global conclusions are drawn in ch. 8, while more detailed conclusions can be found in each respective chapter. An overview of this work and structure is shown in table 1.1.

Part II

Background

Chapter 2

Literature Review

This chapter will give an overview of major results in passivity-based impedance control (PBIC), since its conception until contemporary literature. Research is first discussed by theme and in chronological order. Second, a classification identifies uncommon themes. Third, the focus of this work, already mentioned in sec. 1.5, is derived from the lacking literature.

All literature are publications or PhD theses that *explicitly* take passivity into account. This is in contrast to literature on interaction control literature preceding PBIC by e.g. Hogan [4], [5], [6] and Kazerooni et al. [7], [8], which deal with coupled stability traditionally. Literature here only introduces novel analyses or strategies, not the application of previous ones. Furthermore, analyses must be applied to at least an example system, presenting new results.

Teleoperation literature is not included here, even though haptics can be seen as a subset of teleoperation. The problems in one-sided haptic interfaces are often on a smaller time scale, and are thus not dominated by transmission delays in teleoperation. Additionally, series elastic actuator (SEA) literature is left out, because end effector position measuring is not realistic in serial robots in general.

2.1 Chronological Overview

Literature here will be split into two major themes: analytical passivity and passivity enforcement. The former indicates the a priori analysis of conditions that theoretically guarantee passivity during robot runtime. The latter indicates the continuous regulating of interaction energy during runtime, essentially enforcing passivity. The two major approaches and their subjects are discussed in chronological and topical order.

2.1.1 Analytical Passivity

Colgate and Hogan [3] were the first to extensively use passivity in the design and evaluation of interaction control robots. Colgate concluded that, while coupled stability has been extensively researched, the passivity property offers an advantage in the form of a much simpler criterion. Namely one that is independent of the environment dynamics. Among his main contributions was a framework to analyze passivity by the positive real condition (PRC). He also proposed the passive physical equivalent (PE) as an intuitive way to analyze haptics and passivity, which is heavily based on the classic work of Hogan [4].

A sequence of papers by Colgate et al. follow in [9], [10], [11], [1], which contain one of the most important results in PBIC literature. A hybrid robot, having both continuous and discrete-time dynamics, rendering a virtual wall is shown to have an elegant passivity condition. The derivation is done through a frequency domain approach of the modified small gain theorem for coupled stability, not through his proposed PRC. This work is significant because including the sampler in a hybrid passivity analysis is difficult, and is often purposefully ignored by assuming brick-wall filtering. These papers refer to mixed systems including the sampler as sampled data systems, here they are referred to as hybrid systems.

The same result was later obtained by Kim and Ryu [12] through a time-domain derivation. Haddadi and Hashtrudi-Zaad [13] derive a very similar passivity condition for the Tustin difference instead of the backward difference, giving less restrictive passivity conditions. The neglectance of sampling by brick-wall filtering is studied as well, and underlined to be dangerous. In addition, velocity sampling is found to be much less restricting, allowing any virtual damping and stiffness. This is confirmed by Liu et al. [14], [15], who also argue that the original passivity conditions by Colgate are restrictive, even though they are universally accepted.

Colgate et al. [16] introduced the concept of virtual coupling. Here, an element between virtual environment and controller clips the stiffness in real time to one that, according to analysis, can passively be rendered. Adams [17] extended and generalized this idea into impedance control (IC) and admittance control (AC), but mainly considered stability rather than passivity. Brown [18] investigated numerical implementations of different passive haptic renderings.

Stramigioli [19] named the idea of specifically designing controllers with Hogan’s PE in mind physical control. This implies that the control has a physical interpretation, which simplifies intuition and passivity analysis. However, the body of the paper is about the damping injection framework: a way estimate velocity in an energetically consistent manner. The method introduces a virtual spring between controller and output, such that the causality of the virtual model is inverted into admittance form, which has a smooth velocity.

Colgate [3] briefly discussed AC passivity before others, upon which Newman [20] expanded and coined the AC name. Both publications, along with Dohring [21], investigate the passivity properties of AC, especially during mass reduction. The latter discusses three practicalities that negatively influence the passivity of mass reduction. Kim et al. [22] restates the non-physical interpretation of AC and proposes bidirectionality of the controller to remedy effects such as wall-sticking. Keemink [23] derives and combines guidelines for the design of passive AC mass reduction.

Albu-Schaefer et al. in [24], [25], [26] introduced a method to shape the end effector impedance of a flexible link robot, while maintaining passivity. Additionally, motor inertia is reduced to lower total apparent inertia. Ott et al. [27] proposed a switching IC/AC scheme for the same method as a solution to the trade-off between IC/AC strengths. Ye et al. [28] applied the singular AC form of the same control scheme.

Abbott and Okamura [29] expanded on discrete-time controller literature by studying quantization and nonlinear friction on renderable passive impedances. This approach is in the time domain, which sets it apart from most approaches. Colonnese and Okamura [30] considered the IC stiff wall problem, with a known bound human impedance.

2.1.2 Enforcing Passivity

In the early 2000s a different approach to PBIC was proposed, rooted in reaction rather than precaution. Hannaford and Ryu [31] proposed the time domain passivity approach (TDPA), of which the goal is to measure energy exchange in real time and react accordingly. Upon measuring activity, purposeful damping in the virtual environment dissipates the extra energy. The original proposition was to scale the damping factor with the activity, such that the energy is to be dissipated in a single computation cycle. Several iterations by Ryu et al. [32], [33], [34], [35], Ye et al. [36], Mannewarm and Tothawornyuenyong [37] and others have expanded upon this idea. Balachandran et al. [38] applied TDPA to closed-loop IC, where most other methods assume open-loop IC or do not need to specify an interaction controller.

Most of these works base energy measuring on Stramigioli et al. [39], who showed that measuring energy at a ZOH interaction port with position sensing measures the true energy. Several authors have suggested modifying the virtual environment states when activity is observed. Stramigioli et al. [40], [41] and Franken and Stramigioli [42] only allow virtual states that maintain passivity, and describe methods to find states close to the active ones. This form of passivity enforcement acts before activity occurs, rather than after.

Kim et al. [12], [43], [44], [45] proposed an energy bounding algorithm, which indirectly monitors the net energy generated at the ZOH, limiting the output force to maintain passivity. However, they note that this approach can be more conservative than other methods. They applied the scheme to AC as well in [46].

Lee and Huang [47] propose bounding of the position signal, called passive-set-position-modulation. This work relates to the position modulation of a spring in a damping injection framework, and thus indirectly limits output force. The adjusting output-limiter of Lee and Doo [48], [49] is related to this approach, which limits output force based on the worst-case energy generation of the ZOH and delays. Even though the estimate is relaxed by a dissipation estimation, it may be conservative. The method is applicable to AC if direct force control is possible. Kim et al. [50], [51] and Baek et al. [52], [53] propose a force bounding approach, which appears very similar but no comparisons are made in either publication. Both methods suffer from dissipation memory effects, requiring a way of resetting the energy difference.

Jafari et al. [54] use the input-to-state stable approach for IC to stabilize a virtual wall, due to the same effects as the previously mentioned authors, but analyzes the ZOH as a pure hysteresis. Multiple other authors choose to guarantee stability rather than passivity, such as Morbi and Ahmadi [55] guaranteeing bounded tracking error in AC, which bounds activity to a known value.

Ryu and Yoon [56] proposed a memory based passivation approach, which records the energy inserting trajectory during interaction with a unilateral virtual wall. This trajectory is traced during energy retrieval, minimizing the effects of ZOH and resolution activity. Several TDPA have been applied to AC, especially in later years, including De Stefano et al. [57], Nabeel et al. [58], Totorkulov and Ryu [59], on which Keemink [23] comments that AC has fundamental passivity violations, which TDPA only hides rather than solves.

All passivity enforcing approaches up to Ryu et al. [60] have been in the time domain, who proposed and implemented frequency domain enforcement. A real time discrete Fourier transform estimates the interaction power spectrum and enables a damper if high frequency activating oscillations occur. However, the fundamental tradeoff between frequency resolution and recording time limits reaction time. A reaction time of a hundred milliseconds may be acceptable in some cases, but does not guarantee strict passivity.

2.2 Classification of Literature

The classification of literature is done by the themes listed below, which surface from frequent observations in the literature. The first theme, approach, has already been discussed historically as the distinction between sub-themes analytical passivity and enforcing passivity. Because publications may contain multiple (sub-) themes, none are mutually exclusive.

Some themes correspond so often that they are considered coupled. For example, practically all literature on enforcing passivity takes place in the time domain. Therefore, the themes of Approach and Domain have coupled sub-themes, seen in the title of the next paragraph. The exceptions are considered in the following paragraphs.

The first three themes are prerequisites for every publication: each publication must contain an approach, causality and goal. The auxiliary themes are optional extensions, such as including more complicated dynamics.

Approach (Analytical Passivity, Enforcing Passivity) & Domain (Frequency, Time) This distinction of approach was already discussed in sec. 2.1: the a priori analysis versus enforcement during runtime. The distinction of domains is straightforward: most analytical research is done in the frequency domain, while most enforcement research is done in the time-domain. This is due to most analyses being much more powerful in the frequency domain for LTI systems, as is the case for much control engineering. In contrast, runtime frequency domain enforcement is fundamentally limited as shown in [35]. Literature that analyses passivity in the time-domain is limited to [39], [12] [29]. The work of [1] uses both domains to prove its message.

Causality (IC, AC) & Rendering (High Impedance, Low Impedance) Even though the distinction between control causalities can be unclear, it can still serve as a useful distinction. The application of a fixed causality strategy can be impractical for certain robots, given their sensory options. This theme almost always aligns with the target rendering of the virtual environment. In general, IC is better at rendering low impedances while AC is better at rendering high impedances. Therefore, the goal of much research is to try and render the opposing, challenging, impedance. Literature on IC thus mainly focuses on rendering stiff walls, while literature on AC focuses on rendering low inertias.

Goal (Passivity, Bounded Activity) Some authors allow temporary activity as a way of relaxing the passivity condition, still guaranteeing stability. Bounding the generated energy will stabilize many systems as long as there is enough inherent or enforced damping. The distinction with coupled stability is made because allowing bounded activity is still a different approach than fully allowing activity. Only the enforcement methods studied here allow bounded activity, while analysis studies require strict passivity by design. In some cases, bounding the activity is simply using a different energy reference, and an approach can both attempt passivity enforcement and activity bounding.

Auxiliary (Digitization, Flexibility, MDOF, Discontinuities, Force) The auxiliary theme contains some often-present dynamics that complicate control. The effects of digitization are among such well-known factors, as is flexibility introducing non-collocation between actuation and sensing. It is important to know if analyses or strategies have been generalized for MDOF, which is a requirement for many practical applications. Discontinuities can contain physical effects such as backlash, realistic friction and saturation. In general these effects make a system nonlinear, complicating analysis. In that case, analysis in the time domain is often more powerful than the frequency domain.

Because motor position sensing is in practice always necessary for current control, the feedback of position in a larger control loop is almost always used. In addition to position sensing, interaction force is sometimes added. This has three main applications in PBIC: the explicit control of interaction force by SEA type paradigms, reference generation in AC, and the measuring of interaction energy. As a result, force sensing is always used in AC, but much less so in IC.

2.3 Analysis and Contribution

Table 2.1 orders literature by theme correlation, showing quantitatively which themes are explored with respect to other themes. The top row percentage indicates total theme coverage. Discontinuities for example are studied the least, likely due to difficulty in analyzing nonlinear systems. Each column and row considers one sub-theme and the amount of literature it shares with other sub-themes by absolute number and percentage. Darker squares indicate literature gaps and, although some theme combinations are not very practical, it does give some insight into what literature is unexplored. For example, passivity and bounded activity have a 0% overlap, meaning that no publication considers these two at the same time. Consequently, it may be fruitful to research the comparison between the two.

Table 2.2 orders literature chronologically. If an author has multiple publications on the same subject with related content, only the earliest work is shown. One use of this table comes from recognizing trends over time. Alternatively, it can be used to find literature considering a certain theme of interest.

Several themes are shown by tables 2.2 and 2.1 to be underrepresented in modern literature. Five of these are discussed here in the following three paragraphs. These themes are then to be studied in this work, as described in 1.5. The themes are: analytical analysis, digitization, impedance reduction, flexibility, force and acceleration feedback.

Analytical Approach One chronological trend from table 2.2 is the shift from the analytical approach to the enforcement approach. It is reasonable to first analyze a problem, and only if analysis does not yield satisfactory results attempt to solve the problem by enforcement. These methods are promising, but are somewhat brute force approaches as they ignore the fundamental reasons why activity occurs in the first place. Therefore, they are hard to generalize, something that is paramount in interaction with uncertain environments. To achieve truly robust interaction control, fundamental passivity analysis is still critical.

		Causality, Rendering		Goal		Approach, Domain		Auxiliary																		
		Impedance, High Z	Admittance, Low Z	Passivity	Bounded activity	Analysis, Frequency	Enforcement, Time	Digitization	Flexibility	MDOF	Discontinuities	Force														
Total		59	100%	45	76%	15	25%	43	73%	10	17%	29	49%	29	49%	26	44%	6	10%	11	19%	2	3%	17	29%	
Causality, Rendering	Impedance, High Z	45	100%																							
	Admittance, Low Z	5	11%	15	100%																					
Goal	Passivity	36	80%	11	73%	10	100%																			
	Bounded activity	8	18%	3	20%	0	0%	10	100%																	
Approach, Domain	Analysis, Frequency	23	51%	9	60%	24	56%	4	40%	29	100%															
	Enforcement, Time	24	53%	7	47%	22	51%	7	70%	4	14%	29	100%													
Auxiliary	Digitization	25	56%	3	20%	20	47%	5	50%	16	55%	12	41%	26	100%											
	Flexibility	5	11%	2	13%	6	14%	0	0%	5	17%	1	3%	1	4%	6	100%									
	MDOF	9	20%	3	20%	8	19%	2	20%	4	14%	6	21%	5	19%	3	50%	11	100%							
	Discontinuities	2	4%	0	0%	1	2%	0	0%	2	7%	0	0%	2	8%	0	0%	0	0%	2	100%					
	Force	8	18%	13	87%	13	30%	3	30%	11	38%	7	24%	3	0%	4	67%	4	36%	0	0%	17	100%			

Figure 2.1: Correlation matrix of literature on PBIC of table 2.2, only including novel approaches and excluding SEA and teleoperation literature. Left columns (white lettering) shows number of publications per correlating theme, right column (black lettering) shows percentage of that column's theme. For example: only one publication considers enforcement and flexibility at the same time, 3% of publications on enforcement, whereas 49% of all publications is on enforcement.

Digitization Another trend seen in 2.2 is a decrease in research into digitization. The argument is sometimes made that, with computing power increasing at a still rapid pace, research studying the effects of digitization (most predominantly time discretization) is becoming less relevant. However, passivity is a system-wide property and if true passive control is to be attained, fundamental understanding is essential. Especially when robots must be passive in all contact cases, the effects of digitization (which occur at high frequencies) can be relevant when interacting with much stiffer environments than humans. Therefore, aiming for passivity in hybrid systems is still attractive because full robustness is only obtained with a passivity guarantee.

Where the analyses of purely discrete-time systems are similar in complexity to that of continuous systems, the type of hybrid systems studied here are significantly harder to analyze. Analysis is harder mainly because of the sampler, introducing aliasing, which can cause hybrid systems to become time varying. That is, they are not time invariant to delaying the input signal. In contrast, the ZOH and finite difference differentiation are relatively straightforward to analyze. Although the total amount of research into digitization is sizeable, very little of the modern literature fully include the effect of the sampler [61], [14], [15]. Often, approximations of the sampler are made or brick-wall filtering is assumed. However, Colgate and Schenkel [10] have shown that the sampler can be fully included and can result in elegant passivity conditions. It is therefore viable to investigate whether this theory, including the sampler, can be applied to more systems.

Flexibility, Impedance Reduction and Force/Acceleration Sensing Only three publications on IC consider link flexibility: the analysis of Colgate [3] and the design of Ott et al. [25] and Albu-Schaeffer et al. [24]. And, although not visible in the tables due to coupled sub-themes, these are the only publications on IC to consider impedance reduction.

The former publication finds that passive inertia reduction of the undamped flexible link robot with force feedback is fundamentally limited to masking motor inertia. While the argument is convincing, a valid question is whether the addition of more sensors or damping might allow larger reduction.

The latter work reduces motor inertia in an inner torque loop, while leaving link inertia unchanged. It mainly focuses on cartesian passive impedance shaping, and assumes robots are sufficiently light by design to not require more inertia reduction. However, because IC robots cannot always be designed to be lightweight, as is the case for the Gable Core, impedance reduction remains an overlooked problem.

Apart from the rare application of force feedback in IC, acceleration feedback has to the author's knowledge not been applied in PBIC literature. However, acceleration feedback can be worth investigating within the context of inertia reduction, because of its natural relation to inertia.

Another reason for the apparent lack of modern flexible link literature can be explained by a shift towards the SEA paradigm, where mechanical compliance is intentionally included rather than seen as derogatory. Although these approaches are popular, especially for human robot interaction, SEA strategies can in general not be applied to flexible serial robots. This is because serial robots end effectors are suspended in free space, which makes their coordinates very hard to measure accurately.

Theme, Coupled theme		Causality, Rendering			Goal	Approach, Domain			Auxillary				
Sub-theme, Coupled sub-theme		Impedance, High Z	Admittance, Low Z	Passivity	Bounded activity	Analysis, Frequency	Enforcement, Time	Digitalization	Flexibility	MDOF	Discontinuities	Force	
First author	Year												
<u>Colgate phd</u>	1988	x	x	x		x			x			x	
<u>Newman</u>	1992		x	x		x						x	
<u>Colgate</u>	1992	x		x		x							
<u>Colgate</u>	1993	x		x		x		x					
<u>Colgate</u>	1994	x		x		x		x					
<u>Colgate</u>	1995	x		x		x	x	x					
<u>Stramigioli</u>	1996	x		x		x		x					
<u>Brown phd</u>	1997	x	x	x		x		x				x	
<u>Gillespie</u>	1999	x		x		x		x					
<u>Adams phd</u>	1999	x	x		x	x						x	
<u>Hannaford</u>	2000	x	x	x			x						
<u>Stramigioli</u>	2002	x		x			x						
<u>Ryu</u>	2003	x		x			x		x				
<u>Ryu</u>	2003	x		x			x						
<u>Dohring</u>	2003		x	x		x						x	
<u>Albu Schafer</u>	2004	x		x		x			x	x		x	
<u>Kim</u>	2004	x			x	x	x	x					
<u>Gil</u>	2004	x			x	x		x					
<u>Abbott</u>	2005	x		x		x		x			x		
<u>Ryu</u>	2005	x		x			x						
<u>Stramigioli</u>	2005	x		x			x						
<u>Maneewarn</u>	2006	x		x			x	x					
<u>Diolaiti</u>	2006	x				x		x			x		
<u>Ott</u>	2006	x		x		x			x	x			
<u>Lee</u>	2007	x	x	x			x	x		x		x	
<u>Kim</u>	2008	x			x		x	x		x			
<u>Kang</u>	2008		x							x		x	
<u>Ryu</u>	2008	x			x		x						
<u>Franken</u>	2009	x		x			x						
<u>Kim</u>	2010	x			x		x	x					
<u>Lee</u>	2010		x	x			x	x					
<u>Haddadi</u>	2010	x		x		x		x					
<u>Franken phd</u>	2011	x		x			x	x					
<u>Kim</u>	2011	x		x			x						
<u>Ye</u>	2011	x		x			x						
<u>Colonesse</u>	2012	x			x	x							
<u>Totorkulov</u>	2012	x		x			x					x	
<u>Ryu</u>	2013	x		x			x	x		x			
<u>Kim</u>	2014	x		x			x			x			
<u>Hulin</u>	2014	x		x		x		x					
<u>Liu</u>	2010	x		x		x		x					
<u>Morbi</u>	2015		x		x		x					x	
<u>Nabeel</u>	2015		x		x		x					x	
<u>Stefano</u>	2015		x	x		x	x					x	
<u>Liu</u>	2015	x		x		x		x					
<u>Kronander</u>	2016	x		x		x				x			
<u>Ye</u>	2016		x	x		x			x	x		x	
<u>Kim</u>	2016		x	x		x						x	
<u>Jafari</u>	2017	x			x		x	x		x			
<u>Baek</u>	2017	x		x			x	x					
<u>Keemink phd</u>	2017		x	x		x	x					x	
<u>Balachandran</u>	2017	x		x			x					x	
<u>Schindeler</u>	2018	x		x		x		x					
<u>Baek</u>	2019	x		x			x	x		x			

Figure 2.2: Novel literature on PBIC, only including major new approaches, ordered chronologically and by containing themes and sub-themes.

Chapter 3

Passive Impedance Control Design and Methods

This chapter serves as a technical introduction to methods and design for control of a general robot. First, the general impedance controlled serial robot considered in this work is presented. Afterwards, functional safety and impedance reduction targets are described in a technical sense, as well as the methods used for their analysis. An optimal controller design procedure is given to minimize noise sensitivity during impedance reduction. The dynamics and noise sensitivities of the Gable Core are identified, and are to be used as a case study for controller design in the following chapters.

3.1 System Description

The generalized impedance controlled serial robot is shown in fig. 3.1. The robot consists of total inertia m_r , due to rotor and link inertias, and damping d_r due to motor and bearing friction. It is assumed that there is no stiffness connecting the motor to the ground and negligible ground damping on the end effector, which is a practical consideration for many serial robots. Three models of this robot are studied in the rest of this work: the ideal rigid continuous-time robot, the rigid continuous-time robot with discrete-time controller, and the flexible link continuous-time robot, in respectively ch. 4, ch. 5 and ch. 6.

Motor position $x_m(t)$ is measured by a motor encoder, commonly available due to its necessity for current control. Accurately measuring end effector position is not possible in many serial robots, because the end effector is suspended in free space and compliant in six dimensions. Acceleration $a_e(t) = \ddot{x}_e(t)$ can be measured by an IMU, and interaction force $f(t)$ by a load cell, both located near the end effector. The distal load cell inertia is neglected, or can be seen as a small inertia adding to the environment. The three quantities are linearly added in the general controller G , which asserts an effort $f_m(t)$ on the rotor:

$$f_m(t) = [G_x \quad G_f \quad G_a] \begin{bmatrix} x_m(t) \\ f(t) \\ a_e(t) \end{bmatrix}. \quad (3.1)$$

It is assumed that feedback of each variable and their first derivatives are available. Integration and double differentiation are assumed impractical due to drift and noise amplification respectively. For each signal the PD controller is therefore:

$$G_n = G_{n_p} + G_{n_d} \frac{d}{dt}. \quad (3.2)$$

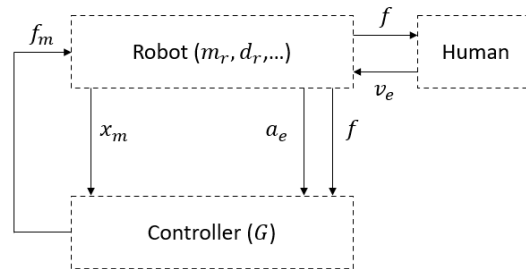


Figure 3.1: Conceptual diagram of the general haptic robot, no assumptions are made about the nature of the controller, nor about the physical system itself. Position is measured at the motor. Acceleration and interaction force are measured at the end effector.

There are thus six gains G_{nl} , where subscript n denotes the measured variable $n = \{x, f, a\}$ and subscript $l = \{p, d\}$ the proportional or derivative gain. For example, G_{ad} is the derivative feedback gain of the acceleration measurement, feeding back the jerk.

A human that interacts with the system at the end effector *feels* apparent impedance $Z(s)$, rendered by the combination of inherent dynamics and controller. The goal of the controller is to shape $Z(s)$ passively to desired impedances $Z_d(s)$. Attaining $Z_d(s)$ is the performance requirement, while maintaining passivity is the safety requirement. Consequently, the properties of performance and safety can be considered separately.

3.2 Safety: Passivity

The safety target of a robot is considered to be the passivity property. In that case, coupling and decoupling with any other passive system, such as a human at rest, results in unconditional stability. The fundamental requirement for passivity of a one-dimensional power port is that energy leaving the system is bound by the energy that has entered it:

$$E(t) = \int_{-\infty}^t f(\tau)v_e(\tau)d\tau \geq 0, \quad (3.3)$$

where $f(t)$ and $v_e(t)$ are the power-conjugated variables at the interaction port. The fundamental condition of (3.3) can sometimes be used to obtain passivity conditions directly. However, when a time-domain analysis is required a storage function approach is often more powerful. In this work, three other methods of passivity analyses are used: the PRC, the PE, and arbitrary passive environment closed loop stability.

- If the system is linear time-invariant (LTI), the frequency domain yields a convenient equivalent condition: the positive real condition (PRC) of apparent impedance $Z(s)$, defined in app. A.1. This method results in the exact passivity conditions, but for higher order systems these can get involved.
- A more conceptual energy-based analysis is that of the physical equivalent (PE): an interpretation of the system impedance $Z(s)$ from the perspective of the interaction port. This interpretation only consists of the simple physical elements: masses, dampers and springs and is derived by network synthesis. A PE can give powerful insight into the energetic behavior and haptic interpretation of a robot, but does not always exist [3]. Integrating position for example, as done in PID controllers, does not have a physical interpretation.
- Another alternative to analyze passivity uses the following reasoning: *robot passivity implies that closing the loop with any passive environment should result in a stable closed loop system*. This can be reversed as well: *the stability conditions of a robot coupled to any passive, but otherwise arbitrary environment, are equivalent to passivity conditions* [1]. Passivity conditions can then be analyzed by conventional stability analysis, such as by the Nyquist criterion defined in app. A.2.

Passivity conditions can in general be nonlinear conditions in controller and system parameters. The passivity conditions for a system will be denoted Ω . For a robot to be passive then requires that the control parameters are in the passive set:

$$G_{nl} \in \Omega.$$

The stability conditions Λ of a system are a subset of these passivity conditions, such that to be stable requires:

$$G_{nl} \in \Lambda \subseteq \Omega.$$

In addition to controller and robot parameters, the stability conditions also depend on environment parameters. The stability conditions for all passive environments are then also the passivity conditions. Thus, when a system is passive it is also always stable, which is exactly the strength of a passive robot.

Stability conditions can in general be analyzed well numerically or in simulations, when analytical conditions cannot be derived. Testing whether a system is stable is conveniently tested by exciting the system and observing the response. Passivity conditions however require much stronger testing, possibly for all input signals and all environments and are therefore not considered suitable for numerical analysis. It is this property that highlights the importance of analytical passivity conditions.

3.3 Performance: Impedance Shaping

The performance goal of interaction control is to modify the dynamic interaction between robot and user. Altering the apparent robot impedance $Z(s)$ felt by the user at the interaction port to a desired impedance $Z_d(s)$ is:

$$Z_{LF}(s) \rightarrow Z_d(s) = m_d s + d_d + k_d s^{-1}, \quad \forall \omega \in [0, \omega_p]. \quad (3.4)$$

Where \rightarrow represents a design target and $Z_{LF}(s)$ is the low-frequency (LF) apparent impedance. The desired impedance is chosen to be a simple mass-spring-damper equivalent.

Although passivity follows from perfectly matching to a mass-spring-damper over all frequencies, $Z_d(s)$ need not be attained for all frequencies. The LF impedance must only match the desired impedance up to a performance frequency of e.g. $\omega_p = 30$ Hz, because of the limited actuation and kinesthetic proprioception bandwidth of humans.

Typically, the impedance target consists of a low baseline inertia for simulating free motion, and a range of compliance and damping relevant to the application. This requires lowering the inherent robot inertia m_r and damping d_r by some factor e.g. $\eta_m = 10$ and $\eta_d = 10$ respectively, depending on robot design and application. The summary of such targets can be expressed as follows:

$$\begin{aligned} m_d &= \frac{m_r}{\eta_m} \\ d_d &\in \left[\frac{d_r}{\eta_d}, d_{\max} \right] \\ k_d &\in [0, k_{\max}]. \end{aligned} \quad (3.5)$$

In the case that pure impedance reduction is considered, it is acceptable for either apparent parameter (m_d, d_d) to be reduced more than η_m or η_d . This dynamic range in which impedances can be passively rendered has been coined impedance-width (Z-width) [3]. It is assumed that there is always inertia behavior required at the performance frequency, such that

$$\frac{d_d}{m_d} < \omega_p.$$

This assumptions is made to simplify analysis. These targets are visualized for the general robot in fig. 3.2. The controller gains that achieve the LF target impedance $Z_d(s)$ will be denoted Ψ . For the LF impedance to be matched, the controller parameters must thus be:

$$G_{nl} \in \Psi. \quad (3.6)$$

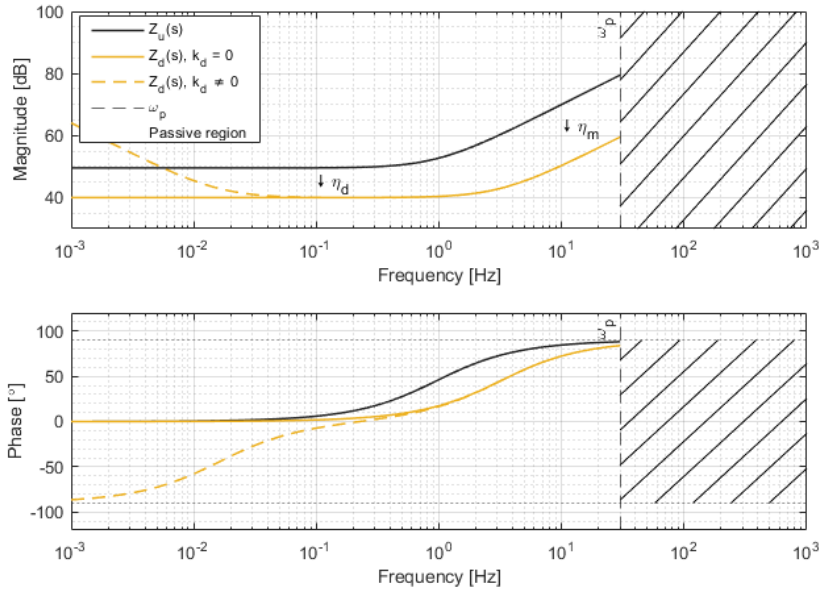


Figure 3.2: General target of shaping apparent robot impedance from unactuated $Z_r(s)$ to target $Z_d(s)$: lower the minimal apparent inertia by η_m , lower the minimal apparent damping by η_d , and vary the apparent damping and stiffness over a range up to the performance frequency ω_p . The hatched regions indicate areas to which the impedance must be bound; passive by the PRC but otherwise arbitrary.

3.4 Passive/Stable Impedance Reduction

The previous sections describe the passivity conditions as Ω , stability conditions as Λ , and the impedance shaping conditions as Ψ . Combining these conditions then results in whether a robot impedance can be safely reduced enough, either passively or stable, and therefore whether it will be a functional robot. If the intersection of robot passivity and impedance shaping conditions are not empty:

$$\Omega \cap \Psi \neq \emptyset, \quad (3.7)$$

then the target impedance of (3.5) can be reached passively. Fig. 3.2 visualizes this design target, requiring a good LF fit and passive behavior over all frequencies. The minimal LF passive impedance that can be achieved is denoted as ${}^{\Omega} \hat{Z}(s)$.

If the target impedance cannot be reached passively, it is assumed that impedance matching Ψ is reached regardless. In that case, passivity conditions Ω are violated and stability conditions Λ will be considered instead. If the combination of robot stability and impedance shaping conditions are not empty:

$$\Lambda \cap \Psi \neq \emptyset, \quad (3.8)$$

then sufficient stable reduction can be done. The minimal LF passive impedance that can be achieved is denoted as ${}^{\Lambda} \hat{Z}(s)$.

The goal is thus to find the minimal passive or stable LF impedance, expressed as a function of the reduction ratios:

$${}^{\Omega/\Lambda} \hat{Z}(s) = \frac{m_r}{\eta_m} s + \frac{d_r}{\eta_d}.$$

In the stable reduction case, the stability conditions Λ depend on the environmental dynamics as well, meaning that there are passive environments for which the system will be unstable. In many cases it is acceptable for the destabilizing environment to be a high impedance one, because humans are limited in their impedance. A stiff pure spring for example is acceptable, but only when interacting purely with humans. If a robot risks collision with much stiffer environments, such as physical walls, this may not be a safe requirement, which is why passivity is preferred.

In addition to a destabilizing spring environment, it may not be acceptable for there to exist a minimum destabilizing pure damping environment. A coupled system may then be stable when coupled to a damped human, but not when decoupled, because environmental damping is assumed negligible. For passive robots, all of these stability conditions are guaranteed, again underlining the advantages of the passivity property.

It may be the case that a target impedance can be attained safely in more ways than one. In that case there are degrees of freedom (DOF) left in the choice of controller gains. A good idea is then to choose a controller that minimizes the effects of noise.

3.5 Noise Sensitivity

Above the performance frequency ω_p , a robot should be inert for good impedance fidelity; the accuracy of a haptic rendering. Because humans are highly receptive to low amplitude mechanical vibrations of up to 1 kHz [62], a haptic robot may not be comfortable if it is erratic, even though it is passive.

The assumed system has three sensors $n = \{x, f, a\}$ used for feedback, and thus three noise sources $\xi_n(t)$ with Laplace transforms $\Xi_n(s)$. The manner in which these enter the system is shown in fig. 3.3.

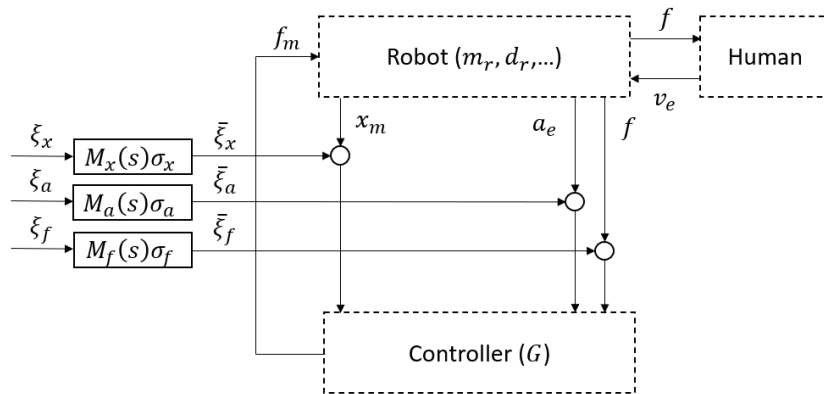


Figure 3.3: Noise sources $\xi_n(t)$ entering the controller $G(t)$ and generalized robot, exerting a force $f(t)$ on a human.

If the system is LTI and $F(s)$ is considered the output of the impedance controlled system, the system equations can be written as:

$$F(s) = Z(s)V(s) + \sum_n W_n(s)\Xi_n(s). \quad (3.9)$$

Where the transfers from noise sources $\Xi_n(s)$ to output $F(s)$ are defined as:

$$W_n(s) = \frac{F(s)}{\Xi_n(s)}.$$

The pure relationship between $V(s)$ and $F(s)$ in (3.9) realizes the apparent impedance $Z(s)$, whereas any additions by $W_n(s)\Xi_n(s)$ distract from that relationship in an uncorrelated manner. Noise sources are assumed to be of Gaussian distribution:

$$\xi_n(t) \sim \mathcal{N}(0, \sigma_n^2),$$

with known variance σ_n^2 and zero mean. These white noise sources enter the system as $\bar{\Xi}_n(s)$ in fig. 3.3. Such noise sources, uncorrelated to other signals, are assumed to not influence passivity because their phases are random. A time domain interpretation is as follows: although passivity may be affected over a short time, for the infinite horizon problem the random phase is expected to dissipate as much energy as it generates.

The power spectral density of white noise signals is known by Parseval's theorem to be equal to its variance [63]:

$$S_{\xi_n}(\omega) = \sigma_n^2.$$

Given the definition of the power spectral density:

$$S_{\xi_n}(\omega) = |\Xi_n(\omega)|^2,$$

it can be inferred that the measured Laplace transform $\Xi_n(s)$ of a white noise signal $\xi_n(t)$ has constant magnitude σ_n and random phase, even though analytically the Laplace transform does not exist for random signals. Each white noise source $\Xi_n(s)$ with unit variance is scaled by a standard deviation σ_n and shaped by filter $M_n(s)$. This obtains an estimate of colored sensor noise $\bar{\Xi}_n(s)$. Then, the magnitude of colored noise is:

$$|\bar{\Xi}_n(s)| = \sigma_n |M_n(s)| |\Xi_n(s)| = \sigma_n |M_n(s)|,$$

given that the amplitude of each white signal $|\Xi_n(s)|$ is unity. All noise transfers can be collected in a row vector:

$$W(s) = [W_x(s) \quad W_f(s) \quad W_a(s)].$$

Noise sensitivity can be minimized by requiring that the cumulative effects of the transfers $W(s)$ should be small. The minimization of its H_2 system norm minimizes the expected value of the output variance, given that the input signals are white [64]. This guarantees that the user haptically experiences the minimal amount of noise. For the purpose of norm minimization, the environment is assumed to be locked, such that no knowledge of the environment is necessary to derive the noise transfers.

3.6 Optimal Design

Previous sections described the passivity conditions as Ω and shaping conditions as Ψ . Combining these conditions then results in a safe robot that has desired and reduced impedance $Z_d(s)$. Furthermore, to optimize user comfort, the noise sensitivities $W(s)$ of a system should be minimized. The optimal control parameters are then such that the H_2 norm of the noise transfer vector is minimal:

$$G_{n_i,o} = \arg \min_{G_{n_i}} \|W(s)\|_2, \quad (3.10)$$

subject to controller parameters that result in a passive Ω and impedance shaped Ψ robot.

Alternatively, when passive impedance reduction can not be done sufficiently, stability conditions Λ are considered. In that case, measures of robustness such as the modulus, gain or phase margin can be included in the optimization. In this work, the gain margin for an environmental spring k_h is considered:

$$G_{n_i,o} = \arg \min_{G_{n_i}} \left(\alpha \|W(s)\|_2 + \frac{1 - \alpha}{\hat{k}_h} \right), \quad \alpha \in [0, 1], \quad (3.11)$$

where α represents a tradeoff between minimization of noise and inverse robustness. In this way, the stiffness of a marginally stable spring \hat{k}_h is maximized in tradeoff with noise sensitivity. The solutions to the general H_2 problem of Doyle et al. [65] cannot be used here, because of the nonlinear constraints and the fixed structure controller. Therefore, it is best to look for numerical solutions, in this work done with the Matlab nonlinear optimization toolbox.

3.7 Design Case Study: Gable Core

To illustrate controller design, a case study is done on a section of the Gable Core described in sec. 1.1. This rehabilitation robot has two types of actuation: fast three dimensional cartesian motion in its internal structure, seen in fig. 3.4, and slower omnidirectional planar base motion. The sagittal axis of the internal actuation (marked \vec{x}) is designed to fully support humans in the gravity field, while being transparent in the horizontal plane. This part of the system can be seen as a linear serial robot.

The stiffness required to support humans results in an inherently high inertia, much higher than suitable for training purposes. Therefore, impedance reduction is required to achieve an apparent inertia of 5 kg and damping of 100 Nsm⁻¹. Note that this damping is relative to the mobile base, and is therefore sufficiently low.

The following sections identify the robot, noise spectra and impedance reduction targets. Given this data, finding optimal controllers through (3.10) or (3.11), subjected to passivity Ω (or stability Λ) and shaping Ψ conditions, then facilitates design for this system.

3.7.1 System Identification

The Gable Core is modelled in two different ways. ch. 4 and ch. 5 assume a rigid robot, modelled by a single mass-damper. Ch. 6 assumes a robot with internal compliance, with a single underdamped flexible mode. The rigid model is of order one and the flexible model of numerator order three and denominator order two, as seen in their respective chapters.

Identification of the Gable Core was done by excitation of its own actuator and position data collected at the same motor encoder, rather than at the interaction port. The transfer from motor velocity $sX_m(s)$ to motor effort $F_m(s)$ of the flexible system of ch. 6 is:

$$Z_{id, flex}(s) = \frac{Z_1(s)Z_2(s) + Z_{12}(s)(Z_1(s) + Z_2(s))}{Z_2(s) + Z_{12}(s)}, \quad (3.12)$$

where

$$\begin{aligned} Z_1(s) &= m_1 s + d_1 \\ Z_{12}(s) &= d + ks^{-1} \\ Z_2(s) &= m_2 s. \end{aligned}$$

Note that this is a different impedance than the apparent impedance. The rigid robot studied in ch. 4 and ch. 5 is then the LF approximation of that system:

$$Z_{id, rigid}(s) = m_r s + d_r, \quad (3.13)$$

where

$$\begin{aligned} m_r &= m_1 + m_2 \\ d_r &= d_1. \end{aligned}$$

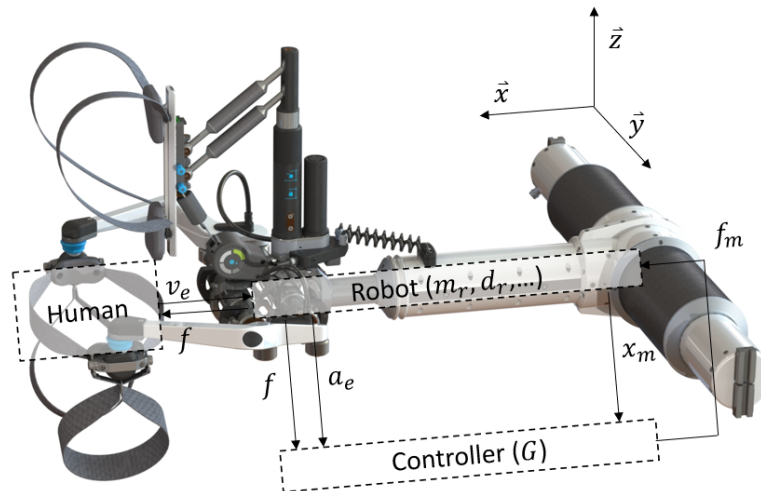


Figure 3.4: Internal structure of the Gable Core, shown in fig. 1.1, with generalized controller overlay of fig. 3.1. The end effector is actuated in the three cartesian directions, of which \vec{x} extends the forward structure forward out of the sleeve.

The system was actuated by a multisine of 50 frequencies, linearly spaced on $[10, 500]$ Hz at a 250 N excitation amplitude. Data was gathered over one minute at a sample frequency of 2 kHz and the frequency response extracted only at the given frequency peaks. A spectral estimate of the transfer is then obtained by dividing the Fourier transforms of the actuation effort $F_m(s)$ by the measured velocity $sX_m(s)$. Fig. 3.5 shows the estimate of the transfer at these 50 points, showing a flexible mode around 100 Hz.

The DC gain is assumed by (3.12) and (3.13) to consist of a pure damper. However, the spectral data suggests that this damper is of magnitude 90 dB, an unmovable impedance for humans, magnitudes larger than the experienced damping when a user actuates the unactuated system. Reasons for this mismatch, such as nonlinearity in stick-slip or hidden dynamics, are discussed in sec. 7.2. To address the DC gain, the damping parameter is estimated by a human induced velocity, measuring the reaction force.

The parametric models of (3.12) and (3.13) can then be fitted to the estimated frequency response points. The identified parameters of the flexible model of ch. 6 are rounded to $m_1 = 25$ kg, $m_2 = 25$ kg, structural stiffness $k = 15 \cdot 10^6$ Nm⁻¹, structural damping $d = 5 \cdot 10^3$ Nsm⁻¹ and base damping $d_1 = 300$ Nsm⁻¹. The rigid robot model (3.13) then has total mass $m_r = m_1 + m_2 = 50$ kg and base damping $d_r = d_1 = 300$ Nsm⁻¹.

Both models are shown in fig. 3.5. Given this data, the reduction targets are set at an inertia reduction ratio of $\eta_m = 10$ and a damping reduction ratio of $\eta_d = 3$ to obtain the apparent inertia of 5 kg and apparent damping of 100 Nsm⁻¹. To illustrate the effects of varying the reduction, three other sets of reductions are added: $(\eta_m = 10, \eta_d = 10)$, $(\eta_m = 10, \eta_d = 20)$, $(\eta_m = 20, \eta_d = 20)$.

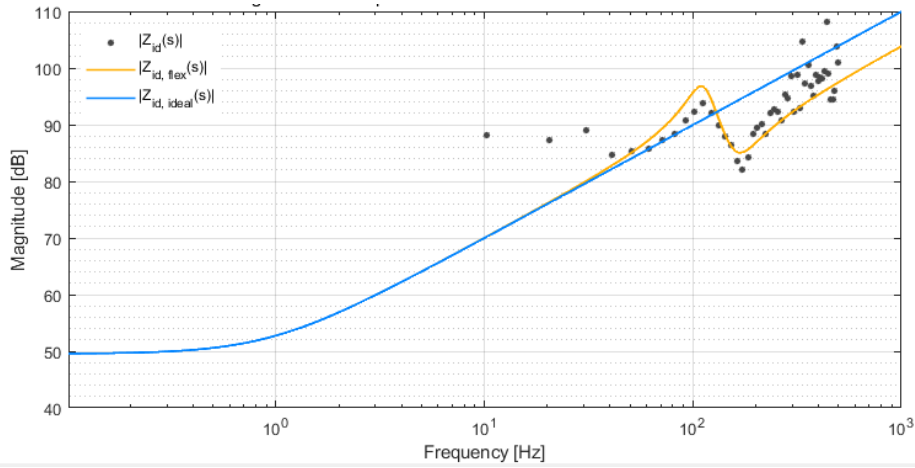


Figure 3.5: Gable Core x-axis impedance from motor velocity to motor force, identified in the HF range by a multisine at the point frequencies and by manual damping identification in the LF. A rigid model $Z_{id, rigid}$ and flexible model $Z_{id, flex}$ are fitted to match the data.

3.7.2 Noise Identification

The three sensors of (3.1) facilitate impedance reduction: motor position encoding, interaction force sensing and acceleration sensing. The robot is designed to measure the latter two as close to the end effector as possible.

The noise spectra of the optical 17 bit encoder $\Xi_x(s)$, MTi3 accelerometer $\Xi_a(s)$ and custom strain gauge with 16 bit ADC $\Xi_f(s)$ have been measured separately for a minute at rest. The standard variation of these signals were determined from the time series, while the their bandwidth is approximated from the Fourier transforms of fig. 3.6. Their bandwidth is modelled by noise shaping filters of first order, for each sensor n :

$$M_n(s) = \frac{1}{s/\omega_n + 1}$$

The encoder has a standard deviation $\sigma_x \approx 1.41 \cdot 10^{-5}$ m after translational transformation with no roll-off visible up to 1 kHz. The force sensor has a standard deviation $\sigma_f \approx 67.4 \cdot 10^{-3}$ N with first order roll-off starting at $\omega_f = 200$ Hz. The accelerometer has a standard deviation $\sigma_a \approx 30.6 \cdot 10^{-3}$ ms⁻² with first order roll-off starting at $\omega_a = 100$ Hz.

The lack of roll-off in encoder measurements (up to the measured frequency) is due the naturally high bandwidth of optical position sensing, whereas force and acceleration sensing have notable low-pass characteristics by design. However, because the used H_2 optimization requires zero gain at $\omega = \infty$, a low-pass filter must be included and is set at $\omega_x = 1$ kHz.

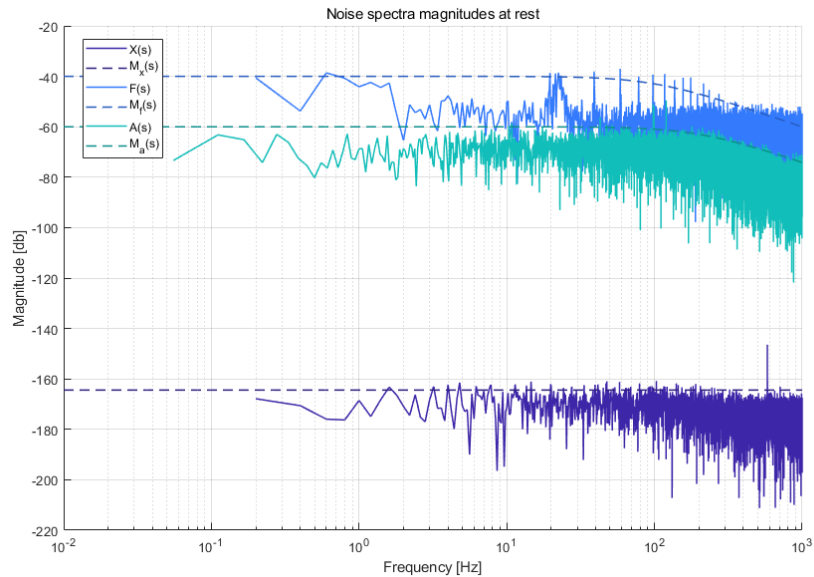


Figure 3.6: Measured noise spectra over one minute at rest for MTi3 accelerometer, custom strain gauge with 16 bit ADC, and optical rotary 16 bit encoder transformed to linear motion. First order shaping filters are assumed for each.

Part III

Analysis and Design

Chapter 4

Rigid Robot With Continuous-Time Controller

The following chapter studies the ideal robot, assumed to be rigid and controlled by a continuous-time controller. Studying the ideal system presents the advantages of the feedback options. The results derived here then serve as reference for the rest of the work. The main findings are:

- Impedance reduction of the ideal system is straightforward, any impedance can be passively attained in a variety of ways.
- Practical application prefers the use of force over position or acceleration feedback.
- Equal inertia and damping reduction is recommended, such that exclusively force feedback is sufficient.
- Some force derivative feedback is recommended for noise reduction and a well posed design problem.

4.1 System Description

The bond graph of the rigid robot equivalent of fig. 3.1 is shown in fig. 4.1. It consists of a single mass m_r and damper d_r , which combine into an inherent robot impedance:

$$Z_r(s) = m_r s + d_r.$$

Because the system and controller are LTI, the Laplace transforms of (3.1) and (3.2) can be taken to describe the controller.

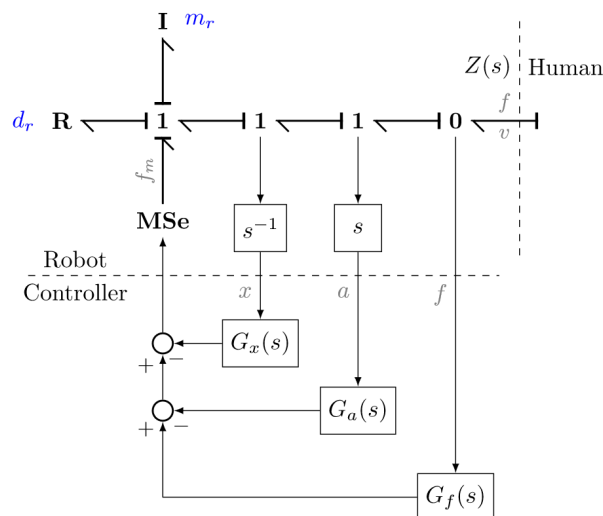


Figure 4.1: Bond graph of an ideal serial robot consisting of a mass-damper, the controller linearly feeds back collocated position, acceleration and interaction force.

Due to the single rigid inertia m_r , all measurements are collocated: measuring position $X(s)$, acceleration $s^2X(s)$, and interaction force $F(s)$. The apparent impedance of the controlled system is:

$$Z(s) = \frac{G_{a_d}s^2 + (m_r + G_{a_p})s + (d_r + G_{x_d}) + G_{x_p}s^{-1}}{G_{f_d}s + 1 + G_{f_p}}. \quad (4.1)$$

The effects of feedback can be intuitively derived from this transfer and its PE, given in fig. 4.2. Position PD feedback introduces a spring-damper equivalence. Proportional acceleration feedback can increase or decrease the apparent inertia. Proportional force feedback conveniently scales all dynamics. The effects of either is clearly visible in fig. 4.2 (b). Derivative force and acceleration feedback add elements, and are shown by the PE of fig. 4.2 (a) to complicate the physical interpretation. Additionally, both significantly modify all present elements.

4.2 Safety: Passivity

Conditions for robot passivity can be obtained directly from the PE derived in app. B.3, shown of fig. 4.2. Intuitively, if all physically equivalent elements are passive, then surely the system is passive at the interaction port. This requires that all elements have positive coefficients, leading to the following passivity conditions:

$$\begin{aligned} G_{x_p} &\geq 0 \\ G_{x_d} &\geq -d_r \\ G_{f_p} &\geq -1 \\ \frac{(d_r + G_{x_d})(1 + G_{f_p})}{G_{x_p}} &\geq G_{f_d} \geq 0 \\ G_{a_p} &\geq -m_r \\ \frac{(m_r + G_{a_p})G_{f_d}}{1 + G_{f_p}} &\geq G_{a_d} \geq 0. \end{aligned} \quad (\Omega_{\text{ideal}})$$

The same requirements can be derived from the PRC of transfer (4.1), as shown in app. B.2. This means that the passivity conditions from the PE are the exact conditions, and are not conservative. The reason for the first three and fifth conditions is evident from their physical interpretations in fig. 4.2 (b), requiring positive coefficient elements.

Novel is the condition that force and acceleration derivative feedback (G_{f_d} , G_{a_d}) is allowed. The limit of force derivative feedback is inversely proportional to the rendered stiffness. Thus, without a rendered stiffness during impedance reduction, force derivative feedback may be infinitely large. Acceleration derivative feedback is allowed only when there is force derivative feedback.

4.3 Performance: Impedance Shaping

Equation (4.1) allows convenient shaping of the apparent impedance to the target impedance of (3.4) using a selection of available feedback. Position PD feedback and proportional force feedback, for example, is a straightforward method to match the apparent impedance to (3.4). An alternative is positional PD feedback in combination with proportional acceleration feedback.

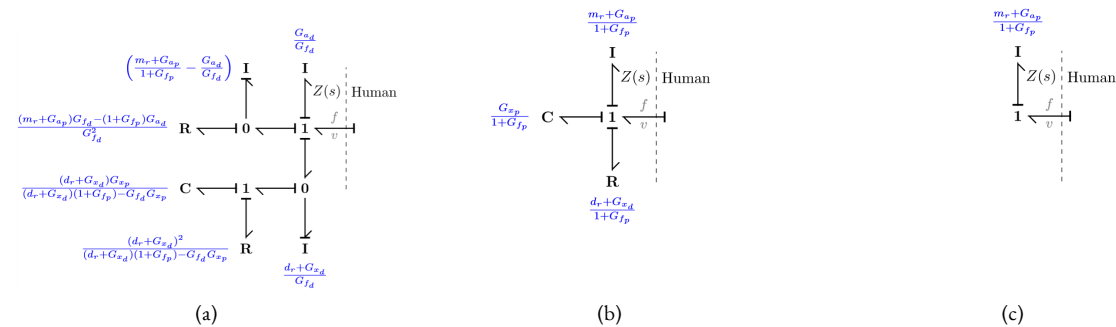


Figure 4.2: PE of the rigid continuous-time controller system with position, force, and acceleration PD feedback (a). This reduces to the middle PE for $G_{f_d} = G_{a_d} = 0$ in (b) and the undamped system of [3] with additionally $G_{a_d} = G_{x_d} = G_{x_p} = d_1 = 0$ in (c).

Therefore, LF impedance shaping to (3.4) is done by setting controller parameters to the following:

$$\begin{aligned}\frac{m_r + G_{a_p}}{1 + G_{f_p}} &= m_d, \\ \frac{d_r + G_{x_d}}{1 + G_{f_p}} &= d_d, \\ \frac{G_{x_p}}{1 + G_{f_p}} &= k_d.\end{aligned}\tag{\Psi_{ideal}}$$

Each condition represents one PE element as seen in fig. 4.2 (b) to match (3.4). Without force feedback, impedance reduction requires damping and inertia compensation.

Derivative feedback (G_{f_d}, G_{a_d}) can influence the HF range, as seen in (4.1) by their adding HF roots. If either gains is too large, the LF impedance is affected and the mass-spring-damper-like behavior up to ω_p is distorted. Requiring the HF pole and zero not to influence below the performance frequency can be done by requiring both to be:

$$\frac{1 + G_{f_p}}{G_{f_d}} \leq \gamma\omega_p, \quad \frac{m_r + G_{a_p}}{G_{a_d}} \leq \gamma\omega_p.\tag{\Psi_p}$$

This requires each roots to be some factor larger than the performance frequency, the maximum is set at $\gamma = 5$. This guarantees that the behavior is mass-like up to ω_p , resulting in a maximum phase error of about 10° . Limiting the size of (G_{f_d}, G_{a_d}) is done for reasons discussed in sec. 4.7.

4.4 Passive Impedance Reduction

The passivity conditions of Ω_{ideal} do no inhibit the reduction of the target impedance by any Ψ_{ideal} . Therefore, any passive impedance shaping can be attained. The minimal passive impedance can be completely reduced, preferably by large G_{f_p} , resulting in zero minimal passive impedance:

$$\Omega \hat{Z}_{ideal}(s) = 0.\tag{4.2}$$

As a result, the Z-width of the ideal haptic robot is positive infinite for apparent masses, springs and dampers.

Of the given feedback options, force feedback has an advantage in its scaling of all dynamics, and is therefore a good choice when the goal is impedance reduction. The natural intuition is that the magnitude of the user's effort is magnified, rendering the user stronger by a factor $(1 + G_f)$ from the robot's perspective. This is similar to how electronic power steering in the automotive industry drastically reduces the effort to steer a vehicle. Note that this reduction includes the downscaling of non-linear dynamics, because the time-domain relationship is:

$$F(t) = \frac{(m_r + G_a)\ddot{x}(t) + d_r(\dot{x}, x)\dot{x}(t) + g(x) + G_x x(t)}{G_f + 1}.$$

This is an advantage in the case of gravity or non-linear effects, such as motor cogging and stick-slip.

In general there are three DOF left in the problem after matching the impedance: one in Ψ_{ideal} , and either size of G_{f_d}, G_{a_d} , although constrained by Ψ_p . If so, the DOF in controller gains can be used to minimize noise sensitivity.

4.5 Noise Sensitivity

From fig. 4.1, the ideal system can be derived to have noise transfers from white noise sources $\Xi_n(s)$ to output force $F(s)$:

$$W_{n,ideal}(s) = \frac{G_n(s)M_n(s)\sigma_n}{1 + G_f(s)},$$

for each sensor $n = \{x, F, a\}$. Because each $W_n(s)$ has the same denominator, minimization favors force over position or acceleration feedback. Additionally, G_{f_d} is useful because it adds roll-off to all noise spectra. In fact, when $W_x(s)$ or $W_a(s)$ use derivatives (G_{x_d}, G_{a_d}) without G_{f_d} , their gains at $\omega = \infty$ are non-zero. In that case the H_2 norm is infinite, and optimization is theoretically nonsensical. Therefore, the ideal system requires the added roll-off of the force derivative feedback G_{f_d} for a well-posed optimization problem.

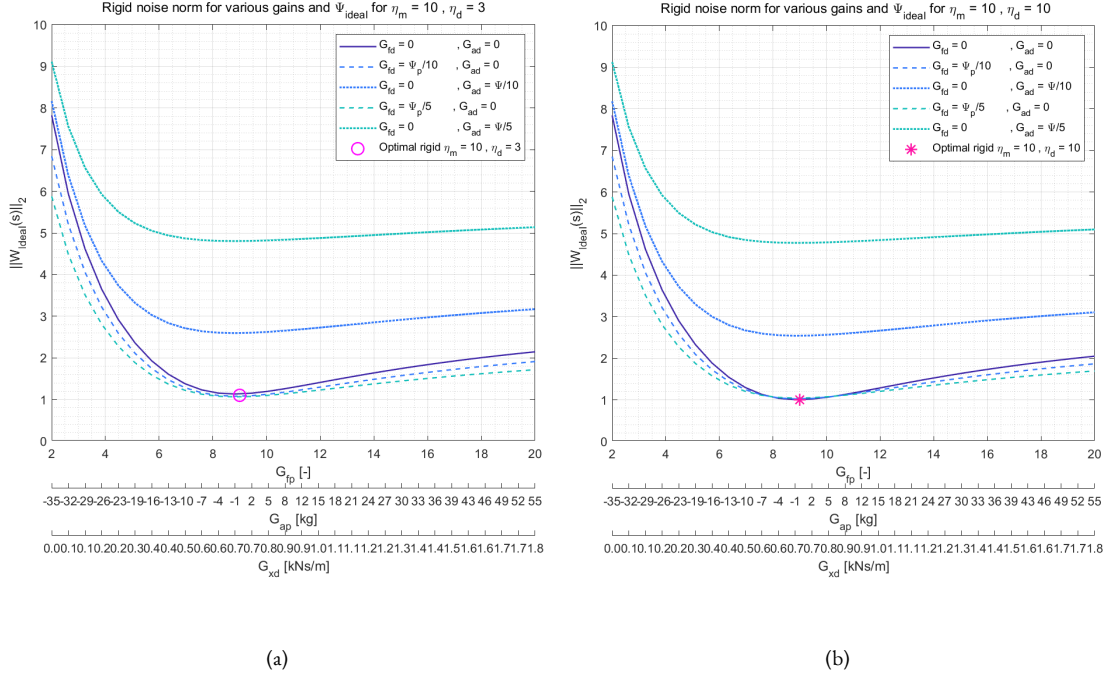


Figure 4.3: Noise norms for different gain sets according to Ψ_{ideal} , choosing G_{fp}, G_{fd}, G_{ad} as DOF. All solutions are passive. (a) reduces damping more than inertia, while (b) equally reduces inertia and damping. The gains for the marked optimal points are shown in tab. 4.1. The x-axes parameters are related linearly through Ψ_{ideal} .

4.6 Design: Gable Core

Sec. (4.4) showed that the ideal system can passively achieve any impedance reduction. The reduction targets set for the Gable Core in sec. 3.6 can thus also be achieved passively.

The passive optimization of (3.10) is used for this system, purely focused on minimizing noise. Minimization of the noise norm subjected to trivial passivity conditions Ω_{ideal} and shaping rules Ψ_{ideal} and Ψ_p is:

$$\min \|W_{\text{ideal}}(s)\|_2. \quad (4.3)$$

Because there are three DOF left, three controller parameters can be chosen freely, such as G_{fp}, G_{fd}, G_{ad} . The first is chosen as the free parameter from Ψ_{ideal} , which determines how large G_{xd}, G_{ap} will be. Derivative gains G_{fd}, G_{ad} are limited to a fifth of their limit in Ψ_p , to maintain low LF impedance matching error. Because any optimization follows both these shaping rules, their LF impedance matching errors are equally low.

Fig. 4.3 shows the noise norms as a function of the three DOF, when two sets of (η_m, η_d) are achieved. The derivative gains are chosen as a fraction of their maximum allowable value bound by Ψ_p . In either figure it is always optimal to increase G_{fd} and forego G_{ad} .

Fig. 4.3 (b) shows that equal reduction ($\eta_m = \eta_d$) of inertia and damping has slightly better noise variance than unequal reduction, even though inertia is reduced more than necessary. The reason for this is that if equal reduction is desired, only G_{fp} is necessary and optimal. Then, $W_{\text{ideal}, f}$ is the only noise transfer. When matching unequally, feedback of another signal in G_{ap} or G_{xd} must be added. In that case, damping compensation with G_{xd} is better than G_{ap} to reduce noise sensitivity.

Table 4.1: Selection of optimal parameters for the minimization of $\|W_{\text{ideal}}\|_2$ for the case study robot, assuming the ideal robot model. The first two are shown in fig. 4.3 (a) and b.

η_m	η_d	Constraints	$\ W_{\text{ideal}}\ _2$ [N]	G_{xp} [$\frac{N}{m}$]	G_{xd} [$\frac{Ns}{m}$]	G_{fp} [-]	G_{fd} [s]	G_{ap} [kg]	G_{ad} [kgs]
10	3	$\Omega_{\text{ideal}}, \Psi_{\text{ideal}}, \Psi_p$	1.0646	0	700	9	0.01061	0	0
10	10	$\Omega_{\text{ideal}}, \Psi_{\text{ideal}}, \Psi_p$	1.0421	0	0	9	0.01061	0	0
10	20	$\Omega_{\text{ideal}}, \Psi_{\text{ideal}}, \Psi_p$	1.0432	0	-150	9	0.01061	0	0
20	20	$\Omega_{\text{ideal}}, \Psi_{\text{ideal}}, \Psi_p$	1.0792	0	0	19	0.021221	0	0

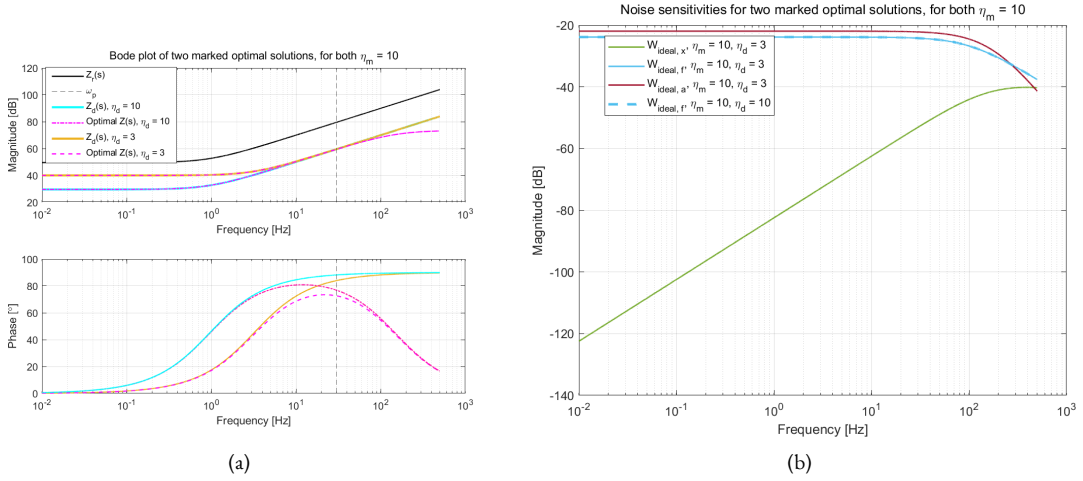


Figure 4.4: Frequency responses (a) and noise transfers (b) of the optimal solutions to the case study design problem of fig. 4.3 in comparison with unactuated $Z_r(s)$ and target $Z_d(s)$ impedance. Only the magnitude of the noise transfers are shown because the phase is not relevant for random noise.

4.7 Discussion and Conclusion

This chapter studied the passive impedance reduction of the ideal haptic system: a rigid robot with continuous-time controller. The main findings in short are described at the beginning of this chapter.

Passive Reduction The passivity conditions have been derived by the PE and the PRC, of which most feedback options have intuitive conditions. Impedance reduction can be done through inertia compensation by acceleration feedback, damping compensation by position feedback. Force feedback can lower both inertia and damping simultaneously and additionally reduces parasitic nonlinear dynamics. Because the passivity conditions do not interfere with reduction, the minimal passive impedance was found to be zero in (4.2). The robot dynamics can thus be completely reduced ($\eta_d = \infty, \eta_m = \infty$).

The derivative feedback of force and acceleration feedback were shown to complicating the physical interpretation. Force derivative feedback is allowed and has been shown to be useful in reducing noise sensitivity. Acceleration derivative feedback is allowed if force derivative feedback is present, although here it does not provide any apparent advantages.

Passive Optimal Design The Gable Core case study was shown to have optimal passive solutions that minimize noise contribution. These are always at $G_{f_p} = \eta_m - 1$, preferring no acceleration feedback but possibly velocity feedback to achieve the required damping reduction η_d . Unequal reduction ($\eta_m \neq \eta_d$) results in more noise variance than equal reduction ($\eta_m = \eta_d$), because the preferred method is always solely force feedback. Maximum allowable derivative feedback then lowers noise.

Limited Derivative Feedback The force and acceleration derivative feedback gains (G_{f_d}, G_{a_d}) here are only used in a very limited sense, constrained in size by Ψ_p . That way, they barely influence the LF range intentionally and can only be used in smaller amounts for noise reduction.

This limiting is done for three reasons. First, practical application forbids these gains to be large, because in practice they have a finite bandwidth not included in this analysis affecting passivity. Second, the systems of the next chapters (ch. 5 and ch. 6) do not allow these gains large due to their additional dynamics. To allow a fair comparison between systems this requires similar size gains. Third, because the minimal passive impedance was shown to be completely reducible already by G_{f_p} , the large use of G_{f_d} is not very relevant. This is because the use of a proportional signal is always more practical than its derivative.

However, theoretically there can be merit in larger derivative gains: app. B.4 shows that it is possible to completely cancel the apparent inertia.

Chapter 5

Rigid Robot With Discrete-Time Controller

This chapter introduces the discrete-time controller to the otherwise ideal rigid robot, resulting in a hybrid system. This complicates analysis for several reasons and forces the analysis to consider the discrete-time position, force and acceleration feedback loops somewhat separately. The key findings are:

- Discrete-time position feedback can passively completely compensate damping, although this is a known result from [1].
- Discrete-time acceleration feedback can passively compensate half the inertia, but requires large damping or sample time.
- Discrete-time force feedback is not passively allowed, although simple sufficient stability conditions can be derived.
- Position and acceleration feedback can be applied at the same time, although the restrictive acceleration conditions limit practical use.
- Many modern designed systems, including the case study, must consider stable reduction rather than passive reduction due to naturally restrictive passivity conditions.
- Design of the case study follows the same recommendations as ch. 4 in general, preferring solely force feedback and its derivative.

5.1 System Description

Fig. 5.1 shows the bond graph of the rigid haptic robot, now including discrete-time dynamics in the sampler, ZOH and finite difference differentiation using sample time T . In the entirety of this work the z operator is used interchangeably with its identity $z = e^{sT}$ to shorten notation, although application is always in the s domain. In addition, the tilde operator denotes the z -transformed version of a transfer.

The Laplace transform of the continuous-time motor effort of (3.1), using the discrete-time controller, is:

$$F_m(s) = \frac{\bar{h}(z)}{s} \begin{bmatrix} \tilde{G}_x(z) & \tilde{G}_f(z) & \tilde{G}_a(z) \end{bmatrix} \begin{bmatrix} X(s) \\ F(s) \\ s^2 X(s) \end{bmatrix}^* \quad (5.1)$$

Here the zero-order hold $h(s)$ is split into the backward difference $\bar{h}(z)$ and continuous-time integrator $\frac{1}{s}$:

$$h(s) = \frac{\bar{h}(z)}{s}, \quad \bar{h}(z) = \frac{1 - z^{-1}}{T}.$$

The continuous-time controller of (3.2) is replaced by its discrete-time counterpart $\tilde{G}_n(z)$ where the finite difference $\bar{h}(z)$ replaces the continuous-time differentiator s :

$$\tilde{G}_n(z) = G_{n_p} + \bar{h}(z)G_{n_d}.$$

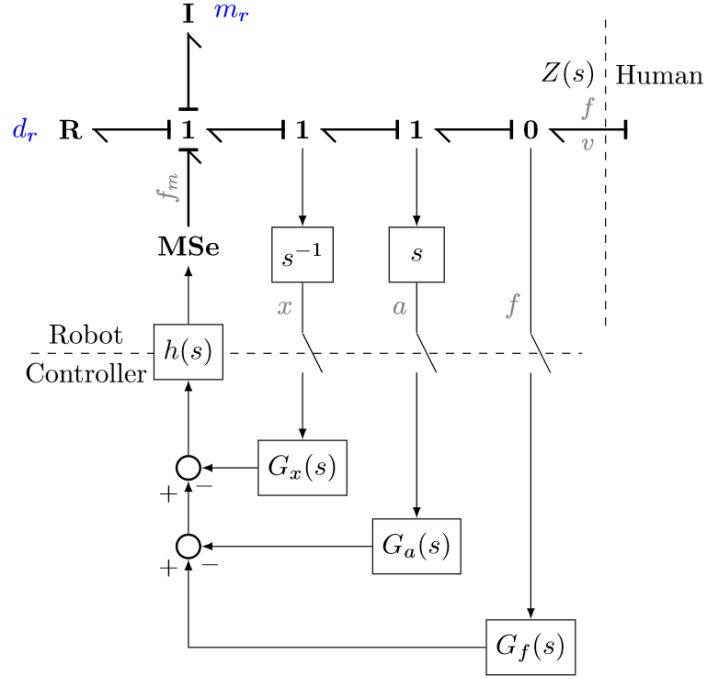


Figure 5.1: Bond graph of the rigid robot with discrete-time controller including sampler, ZOH and finite differences derivatives, resulting in hybrid time varying dynamics at the interaction port.

The operation $[\cdot]^*$ in (5.1) represents the starred transform of its argument, defined in app. C.1, as a result of sampling the measured continuous-time signals. It is the Laplace transform of the sampled time signal, for example for $x(t)$:

$$[X(s)]^* = \mathcal{L}\{x^*(t)\}(s).$$

Or alternatively, the z-transform $\tilde{X}(z)$ with the identity $z = e^{sT}$ substituted, which reinstates the dependence on sample time:

$$\mathcal{Z}\{x(t)\}(z) \Big|_{z=e^{sT}} = \tilde{X}(e^{sT}).$$

The hybrid system is shown in fig. 5.1. It is shown in sec. C.2, following Ragazzini [66], that the continuous-time velocity $V(s)$ of this system subjected to a continuous-time input force $F(s)$ is given by:

$$V(s) = Y_r(s)F(s) - Y_r(s) \frac{\tilde{D}(z) [N(s)Y_r(s)F(s)]^*}{1 + \tilde{D}(z) [N(s)Y_r(s)]^*}, \quad (5.2)$$

where $\tilde{D}(z)$ contains the inherently discrete-time dynamics of the feedback loop:

$$\tilde{D}(z) = \frac{h(z)}{s} \begin{bmatrix} \tilde{G}_x(z) & \tilde{G}_f(z) & \tilde{G}_a(z) \end{bmatrix},$$

and $N(s)$ is used to add the three loops:

$$N(s) = \begin{bmatrix} s^{-1} \\ Z_h(s) \\ s \end{bmatrix}.$$

The system equation of (5.2) is the closest this system can get to an apparent transfer function. The right-hand argument of equation (5.2) contains $F(s)$ within the starred transform and, because the starred transform is not distributive in general, $F(s)$ cannot be separated. Therefore, there exists no closed-form impedance transfer function $Z(s)$ from $F(s)$ to $V(s)$.¹ The reason for this is that the system is time-varying due to the sampler: delaying the input signal does not yield the same delayed output signal. The output is dependent on the input both at and in between sample intervals, and thus requires the exact input signal to compute the output [67][68].

¹Note that technically (5.2) does not lead to an apparent impedance, because $N(s)$ contains $Z_h(s)$. The point here is only to illustrate that an apparent impedance cannot be derived.

The nonexistence of an apparent transfer function is in contrast to the class of hybrid systems studied in much literature and textbook. There, both the input and output are sampled, in which case the apparent transfer is again LTI and described fully by the z -transform. In such cases, sampling itself does not influence passivity, as shown in app. C.8. However, for the type of hybrid system studied here, the sampler is not placed on the input or output, but on internal paths only. It is possible that phase provided by the ZOH and transformative properties of the sampler can influence passivity at the interaction port of such a hybrid system.

5.2 Safety: Passivity

Due to the absence of a closed-form impedance transfer function from (5.2), passivity cannot be analyzed by the PRC. Moreover, a PE would not consist of a finite number of elements or representable by the simple elements and therefore cannot be derived. This is in contrast to the case in fig. 4.2. To illustrate, a physical interpretation of the acceleration feedback closed loop with $Z_h(s) = 0$ and $Z_r(s) = m_r s$ is derived in app. C.11. A different method to analyze passivity is therefore needed.

As mentioned in sec. 3.2, the strength of a passive robot is that closing the loop with any passive environment results in a stable closed loop. This argument works the other way around as well: if the closed loop is shown to be stable for *any* passive environment, then the robot itself must be passive. In other words, the stability conditions of the closed loop with any passive environment are the robot passivity conditions. These conditions are attainable because the denominator of the closed loop hybrid system of (5.2) can be derived; the denominator only contains system properties in the starred transform.

5.2.1 Passivity Conditions Through Passive Environment Closed Loop Stability

Determining closed loop stability, given a passive environment, requires inclusion of environment impedance $Z_h(s)$ into the closed loop, of which the only known property is that it is passive. In this case, such an environment may represent a human at rest applying no voluntary movement. Robot passivity analysis is now a matter of stability for the closed loop with passive arbitrary $Z_h(s)$. As a relevant example, the transfer $V(s)/F_h(s)$ from conscious human effort to velocity could be considered, and should be stable for any $Z_h(s)$ for the robot to be passive.

For the transfer $V(s)/F_v(s)$ of virtual force to velocity the system of fig. 5.1 can be rewritten to the block diagram of fig. 5.2. This conveniently shows three feedback loops for each sensor n with loop gains:²

$$L_n(s) = \tilde{D}_n(z)[H_n(s)]^*. \quad (5.3)$$

The hybrid loop gains $L_n(s)$ have been split into two parts: The discrete-time part $\tilde{D}_n(z)$ contains the discrete-time PD controller and the finite difference of the ZOH:

$$\tilde{D}_n(z) = \bar{h}(z)(G_{n_p} + G_{n_d}\bar{h}(z)).$$

The continuous-time parts $H_n(s)$ contains the passive environmental dynamics $Z_h(s)$, robot dynamics $Z_r(s)$ and the continuous-time integrator $1/s$ from the ZOH model:

$$H_x(s) = \frac{1}{s^2} \frac{1}{Z_h(s) + Z_r(s)}, \quad (5.4)$$

$$H_f(s) = \frac{1}{s} \frac{Z_h(s)}{Z_h(s) + Z_r(s)}, \quad (5.5)$$

$$H_a(s) = \frac{1}{Z_h(s) + Z_r(s)}. \quad (5.6)$$

The coupled stability properties of the three isolated loops are considered first, afterwards their combinative properties are discussed.

The Nyquist criterion, defined in A.2, can be used to determine closed loop stability given the loop gains $L_n(s)$. This requires the number of its unstable poles and the number of clockwise encirclements of the critical point -1 . Loop gain $L_n(s)$ itself is stable because its only poles come from $[H_n(s)]^*$, which has denominator $Z_h(s) + Z_r(s)$. This denominator is stable because an addition of two passive transfers cannot have unstable poles or zeros. The sampled version $[H_n(s)]^*$ then is stable as well, because sampling preserves stability according to app. C.1 or app. C.8. Therefore, the only cause of closed loop instability can be due to clockwise encirclements of -1 by $L_n(s)$. There are two methods used here to investigate passivity with the Nyquist criterion. Afterwards, they are applied to the three separate hybrid loops.

²The same loop gains can be derived for $V(s)/F_h(s)$, but the corresponding block diagram of fig. 5.2 does not have clearly separated loops.

All Passive Loci

Because the passive, but otherwise arbitrary, environmental impedance $Z_h(s)$ can lie anywhere in the RHP, it is more convenient to consider it as an element of the RHP region \mathbf{Z}_0 of complex numbers as done in [1]:

$$Z_h(s) \in \mathbf{Z}_0 \subseteq \mathbb{C} \quad \forall s.$$

Where \mathbf{Z}_0 spans the RHP and is therefore not a function of frequency. Representing $Z_h(s)$ in this manner lead to loop gain loci that themselves are frequency dependent regions:

$$L_n(s) \in \mathbf{L}_n(s) \subseteq \mathbb{C} \quad \forall s.$$

Dependent on the robot parameters and frequency, $\mathbf{L}_n(s)$ might or might not encircle -1 . An example is visualized in fig. 5.3.

Assuming that the loop gain loci are closed regions³ over the entire Nyquist contour and $L_n(s)$ contains no unstable poles, a sufficient condition for the Nyquist stability criterion is that the loop gain loci never contain -1 anywhere on the Nyquist contour. A sufficient passivity requirement is then:

$$-1 \notin \mathbf{L}_n(i\omega + \sigma) \quad \forall \omega \quad \forall \sigma \geq 0. \quad (5.7)$$

Alternatively, if some $\mathbf{L}_n(s)$ touches -1 there exists a $Z_h(s)$ that encircles the critical point at that complex frequency s . Therefore, there is a destabilizing passive environment and the robot itself is not passive. This is the same small-gain theorem reasoning used in [1], although not so explicitly defined.

This theory can be applied to each of the three loops separately to obtain passivity conditions for each, as is done in the following subsections.

Worst-type Loci

When the powerful theory of (5.7) cannot be used, a specific form of $Z_h(s)$ is used here that is based on [3]. A robot may have a single worst type of environment: one that, regardless of its parameters, is always the most restrictive ("first") cause of activity. The stability conditions with that environment lead to the passivity conditions themselves. For any LTI interaction controller a purely imaginary (i.e. non dissipative) environment is the worst type environment. This is either a pure spring or pure inertia, because these add the most phase. The conjecture used here is that this logic can be extended to the class of hybrid systems, where $Z(s)$ does not have a closed-form. It was shown in [3] that the worst environment of discrete-time position feedback was a pure spring. This work assumes that the worst environment can be found in an environmental mass-spring-damper.

³Only for closed surfaces is (5.7) necessary and sufficient for closed loop stability. Non-closed surfaces contain holes in which the crucial point -1 may lie, requiring a different analysis.

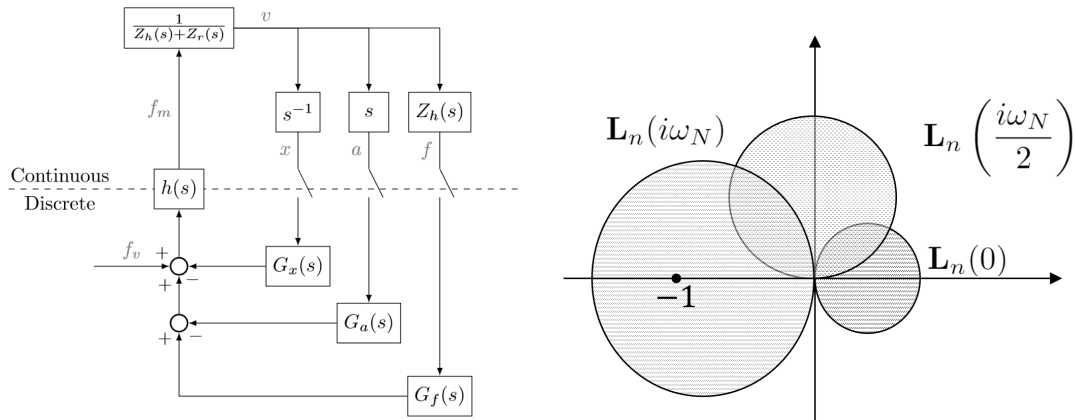


Figure 5.2: Block diagram of fig. 5.1 with virtual input F_v , with explicit splitting of the three parallel loops for position, force and acceleration feedback. These loops result in the loop gains of (5.5) Figure 5.3: Three loci of a single loop gain $\mathbf{L}_n(s)$ at three different frequencies on the Nyquist contour. The left-most locus violates the Nyquist criterion; there exists an environment which destabilizes the closed loop and the robot is not passive.

5.2.2 Separate Discrete-Time Position Feedback

In their seminal work Colgate and Schenkel [1] found for pure discrete-time position feedback the sufficient and necessary closed loop stability conditions with arbitrary passive environment, and therefore passivity condition, to be:

$$d_r > G_{x_p} \frac{T}{2} + |G_{x_d}|, \quad G_{x_p} \geq 0. \quad (\Omega_{\text{hybrid},x,[1]})$$

This yields the famous and simple condition between inherent robot damping d_r , sample time T and the virtual spring G_{x_p} and damper G_{x_d} parameters. It shows that damping compensation is still allowed, although now hampered by the presence of a virtual spring. If no spring is being rendered, damping compensation may be large as physical damping, such that any inherent damping can be compensated.

The proof of sufficiency is repeated in a more geometric manner in app. C.3, which avoids the cumbersome manipulations of [1] and the transformations of [11].

5.2.3 Separate Discrete-Time Acceleration Feedback

Positive acceleration feedback is shown in app. C.13 to have the following sufficient passivity condition:

$$|G_{a_d}| < G_{a_p} \frac{T}{2}, \quad G_{a_p} \geq 0. \quad (5.8)$$

Where theoretically there is no upper limit; the apparent mass can be passively increased indefinitely. However, negative acceleration feedback is more relevant to impedance reduction, as it can compensate inertia. According to app. C.13, when the feedback parameters are bound to:

$$G_{a_p} \leq 0, \quad G_{a_d} \leq |G_{a_p}| \frac{T}{6}, \quad (5.9)$$

the following is a good approximation of the sufficient passivity condition:

$$G_{a_p} + G_{a_d} \frac{2}{T} \geq -\frac{m_r}{2} \left(1 - e^{-\frac{d_r T}{2m_r}}\right). \quad (\Omega_{\text{hybrid},a})$$

The amount of inertia compensation (negative G_{a_p}) is thus limited by the inertia, damping and sample time. Additionally, small positive G_{a_d} can allow larger negative G_{a_p} and thus more apparent inertia reduction.

A notable property here is that smaller sample times restrict the magnitude of negative gains and consequently restrict impedance reduction. This is in contrast to the reasonable assumption that converging to continuous-time ($T = 0$) should result in the passivity condition ($G_{a_p} > -m_r$) of the continuous-time time system in Ω_{ideal} . This contradiction is discussed further in 5.7.

These restrictive conditions mean that in practice it is unlikely that enough inertia can be passively compensated. Stability conditions, rather than passivity conditions are not likely to have an analytical form either, as described in app. C.13, and are best evaluated numerically.

5.2.4 Separate Discrete-Time Force Feedback

Force feedback is shown in app. C.4 to not be passively allowed. The passivity condition for discrete-time force feedback is therefore:

$$G_{f_p} = G_{f_d} = 0. \quad (\Omega_{\text{hybrid},f})$$

And thus no impedance reduction is passively possible. Therefore, it is worth investigating the stability conditions of force feedback. According to app. C.4.1, if the environment is of parallel form:

$$Z_h(s) = m_h s + d_h + k_h s^{-1},$$

and has sufficient damping as follows:

$$d_h(d_h + d_r) \geq k_h(2m_h + m_r), \quad (5.10)$$

then a sufficient stability condition is:

$$|G_{f_d}| < G_{f_p} \frac{T}{2}, \quad G_{f_p} \geq 0. \quad (\Lambda_{\text{hybrid},f,\text{damped}})$$

For sufficiently damped environments then, any positive feedback gains (G_{f_p}, G_{f_d}) result in a stable system. In that case stable and arbitrary impedance reduction is possible.

The condition of (5.10) can be applied to almost all combinations of parallel environment (mass-damper, spring-damper etc.). One exception is if the environment consists of a pure spring:

$$Z_h(s) = k_h s^{-1}.$$

According to app. C.4.2, the problem can then be shown to be analogous to that of discrete-time position feedback. Then the solution is analogous too, and a sufficient stability condition for force feedback given a pure environmental spring is:

$$\frac{d_r}{k_h} > G_{fp} \frac{T}{2} + |G_{fa}|, \quad G_{fp} \geq 0. \quad (\Lambda_{\text{hybrid}, f, k_h})$$

Increasing damping and/or sample time will increase stiffness of the destabilizing spring. This condition also inherently states that no passive force feedback is allowed: passivity requires stability for any spring, but $k_h = \infty$ demands that no feedback is allowed, as in $\Omega_{\text{hybrid}, f}$.

5.3 Performance: Impedance Shaping

Because all effects of time discretization become significant near the Nyquist frequency, which in any reasonable case should be far above the haptic performance frequency $\omega_N \gg \omega_p$, their effect on the apparent impedance can be neglected. The LF impedance can thus be assumed to that of the ideal model of ch. 4. Therefore, the same controller parameterization Ψ_{ideal} can be used to shape the LF impedance. To not influence the LF behavior, Ψ_p must be used as well.

In short, the shaping conditions do not change with respect to the ideal model, only the passivity properties.

5.4 Passive/Stable Impedance Reduction

The previous sections have shown the passivity conditions of the separate feedback loops: $\Omega_{\text{hybrid}, x, [i]}$, $\Omega_{\text{hybrid}, a}$ and $\Omega_{\text{hybrid}, f}$. Of these, the latter is zero, but simple stability conditions were found instead in $\Lambda_{\text{hybrid}, f, \text{damped}}$ and $\Lambda_{\text{hybrid}, f, k_h}$. The shaping conditions of the ideal system Ψ_{ideal} and Ψ_p can still be used.

These passivity and stability conditions can now be combined with the shaping conditions. This gives the options for safe impedance reduction, either passively or stable. The following two sections investigate either option respectively.

5.4.1 Passive Reduction: Combined Position and Acceleration Feedback

Because force feedback is never passive, force feedback cannot be used. However, it is sufficient to consider inertia compensation by acceleration feedback and damping compensation by position feedback. Their separate passivity conditions can be combined using the following argument.

- Consider a user attached to two identical robots, both with impedance $Z_r(s)$, of which one is controlled by position and one by acceleration feedback. In that case, the robots can be seen as two power ports, as visualized in fig. 5.4. If both passivity conditions of $\Omega_{\text{hybrid}, x, [i]}$ and $\Omega_{\text{hybrid}, a}$ are fulfilled for each of the two $Z_r(s)$ separately, then the system is passive at the interaction port as well.
- Instead of using two identical robots, a single real robot can be conceptually split in two, by a factor $\mu \in [0, 1]$. In that way, the total robot impedance is still $\mu Z_r(s) + (1 - \mu) Z_r(s) = Z_r(s)$, and the two robots still *feel* like the single robot. If both of the conceptual robots are then passive, by their separate condition on $\mu Z_r(s)$ and $(1 - \mu) Z_r(s)$, then so is the interaction port.

These combined conditions are restrictive, but apply both controllers at the same time. The minimal passive LF impedance using both loops is shown in app. C.6 to be:

$$\Omega \hat{Z}_{\text{hybrid}}(s) = m_r \left(1 + \mu \frac{3}{4} \left(e^{-\frac{d_r T}{2m_r}} - 1 \right) \right) s + \mu d_r. \quad (5.11)$$

This is a tradeoff between inertia reduction versus damping reduction parametrized by $\mu \in [0, 1]$, which can be chosen arbitrarily. Because force feedback cannot be passively added, this is also the minimal passive impedance for the combined hybrid system.

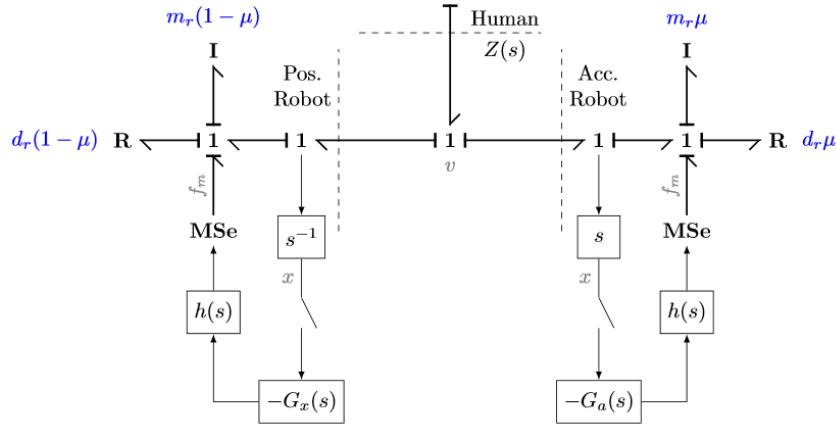


Figure 5.4: Position and acceleration feedback of one robot split in two by μ . The left position feedback assumes a robot scaled by $(1 - \mu)$, and the right acceleration feedback assumes a robot scaled by μ . Splitting the robot is valid because the conceptual two robot impedances act on the same one-junction.

Because μ relates to η_d by its inverse $\eta_d = \mu^{-1}$ in this impedance, the inertia reduction is also a function of damping reduction:

$$\eta_m = \frac{\eta_d}{\eta_d + \frac{3}{4} \left(e^{-\frac{d_r T}{2m_r}} - 1 \right)}.$$

The maximum passive reduction ratios for damping and inertia of this curve are shown in fig. 5.5. This again shows that for fast underdamped systems, such as the Gable Core, only a negligible amount of inertia can be passively reduced.

When all focus is on inertia reduction by acceleration feedback ($\mu = \eta_d = 1$), the minimal passive acceleration feedback impedance is:

$$\Omega \hat{Z}_{\text{hybrid,a}}(s) = \frac{m_r}{4} \left(1 + 2e^{-\frac{d_r T}{2m_r}} \right) s + d_r. \quad (5.12)$$

The lowest passive apparent inertia is $m_r/4$, such that the inertia reduction is $\eta_m = 4$, counterintuitively at large sample times. The damping then remains the same.

When all focus is instead on impedance reduction by position feedback ($\mu = 0$), the minimal passive impedance is:

$$\Omega \hat{Z}_{\text{hybrid,x}}(s) = m_r s. \quad (5.13)$$

This completely compensates damping, while maintaining the natural apparent inertia. This is the same damping compensation that can be achieved in the ideal robot case, although without the inertia reduction.

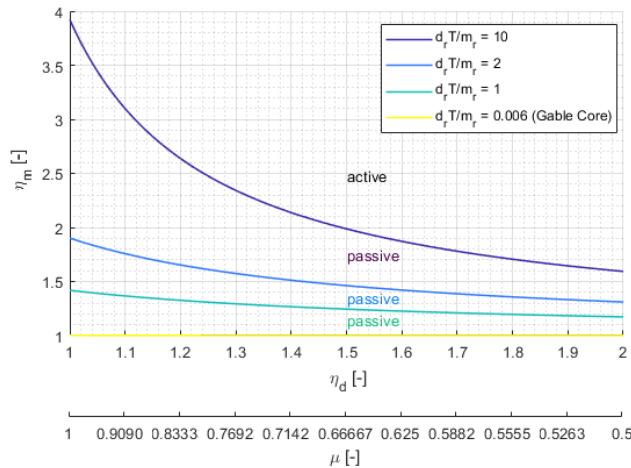


Figure 5.5: Maximum inertia reduction ratio η_m and damping reduction ratio η_d for passive discrete-time feedback: allowing only position and acceleration feedback, such that $G_{x_p} = G_{f_p} = G_{f_d} = 0$ and $G_{a_d} = G_{a_p} T/6$. The tradeoff between position and acceleration compensation is made by μ . Passivity is guaranteed below each of the respective lines.

5.4.2 Stable Reduction: Force Feedback

Because no force feedback is passively allowed in $\Omega_{\text{hybrid},f}$, the minimal passive impedance using force feedback is the original impedance:

$$\Omega \hat{Z}_{\text{hybrid},f}(s) = m_r s + d_r, \quad (5.14)$$

and thus there is no reduction ($\eta_m = \eta_d = 1$). For sufficient environmental damping it was shown that any positive force feedback is stable in $\Lambda_{\text{hybrid},f,\text{damped}}$. In that case, the lowest stable impedance is zero, and the maximum impedance reduction is infinite ($\eta_m = \eta_d = \infty$):

$$\Lambda \hat{Z}_{\text{hybrid},f,\text{damped}}(s) = 0 \quad (5.15)$$

For a pure spring environment, the stability condition was shown to be $\Lambda_{\text{hybrid},f,k_h}$. For maximum impedance reduction by G_{f_p} , no derivative ($G_{f_d} = 0$) is a straightforward choice. The stable minimal impedance using proportional force feedback is:

$$\Lambda \hat{Z}_{\text{hybrid},f,k_h}(s) = \frac{m_r s + d_r}{1 + \frac{2d_r}{T k_h}} \quad (5.16)$$

Here, the reduction ratios are always equal ($\eta_m = \eta_d = 1 + \frac{2d_r}{T k_h}$). This approaches zero impedance in the continuous-time limit or when the environmental spring is infinitely compliant. If inertia reduction is much more important than damping reduction, increasing mechanical damping is beneficial.

5.5 Noise Sensitivity

As mentioned in sec. 5.1, the output force of this hybrid system requires the exact Laplace transform of the input signal itself. Similarly, the noise sensitivity transfers from noise sources to output force require the exact force signal due to human interaction. As a result, noise transfers cannot be determined either. For this reason, sampling cannot be included in the noise analyses and approximations are made instead.

The approximate noise transfers of the hybrid system then include the ZOH and finite difference in $\tilde{G}_n(s)$, but not the sampler:

$$W_{n,\text{hybrid}}(s) = \frac{h(s)\tilde{G}_n(s)M_n(s)\sigma_n}{1 + h(s)\tilde{G}_f(s)},$$

for each sensor n . Here, the ZOH adding roll-off to all spectra is beneficial from a noise sensitivity point of view. This addition causes finite H_2 norm of each $W_{n,\text{hybrid}}(s)$, in contrast to sec. 4.5, creating a well-posed optimization problem.

5.6 Design: Gable Core

Sec. 5.4 showed that with the analysis in this work, there are two ways to safely reduce impedance: passively through position and acceleration feedback of (5.11) or stable by force feedback of (5.16). Apart from these analytical solutions, numerical stability analysis can be done as well. The former is discussed shortly in the next section, followed by numerical stability analysis of the optimal tradeoff.

5.6.1 Analytical Design

Substituting the Gable Core into the minimal passive impedance of (5.11) shows that the target damping reduction of $\eta_d = 3$ can be achieved passively. This can be done by partial velocity feedback ($\mu \approx 1e - 2$). However, at best an inertia reduction of $\eta_m = 1.005$ can be passively achieved, where the target was $\eta_m = 10$. No practical passive inertia reduction can be achieved for this and many other systems. Thus, the target impedance of the case study system can not be reached passively.

Stable force feedback of (5.15) or (5.16) can lower both inertia and damping safely, but only equally at the same time. When the environment is a pure spring, and the required reduction ratios are $\eta_d = \eta_m = 10$, the destabilizing spring is approximately 60 kNm^{-1} , which is more than acceptable. The total inertia reduction is thus larger than necessary, but fulfills both reduction requirements. Because there are no DOF left in this reduction problem ($G_{f_p} = 9$ is the only gain), there is no noise sensitivity minimization to be done.

5.6.2 Numerical Design

For stable reduction the design problem can be defined as in (3.8): a tradeoff between the noise sensitivity and stability margin, assuming a pure environmental spring. This section studies in-depth how to obtain an optimal trade-off between noise sensitivity and robustness.

The optimization, subjected to shaping rules Ψ_{ideal} , Ψ_p and stability condition $\Lambda_{\text{hybrid}, f, k_h}$, is:

$$\min \left(\alpha \|W_{\text{hybrid}}(s)\|_2 + \frac{1 - \alpha}{\hat{k}_h} \right), \quad \alpha \in [0, 1],$$

where \hat{k}_h is the marginally stable spring following from the stability conditions and α is a linear tradeoff between costs.

Three DOF remain in the controller parametrization, here chosen to be G_{f_p} , G_{f_d} , G_{a_d} . The first is chosen as the free parameter from Ψ_{ideal} , which determines how large G_{x_d} , G_{a_p} will be. Derivative gains G_{f_d} , G_{a_d} are limited to a fifth of their limit in Ψ_p . Because any optimization follows these shaping rules, their LF impedance errors are equally low.

The marginally stable spring can be approximated numerically from C.9 and noise sensitivity from sec. 5.5. In that way, the design problem can be numerically investigated.

Numerical Analysis Fig. 5.6 (a) and fig. 5.7 show the effects of varying the DOF on the noise norm and marginally stable spring. Note that this is a different graph than that of the previous chapter in fig. 4.3. The curves trace $G_{f_p} = [5, 40]$ with G_{x_d} , G_{a_p} linearly following Ψ_{ideal} , starting at the right of every curve. The derivatives are varied as fractions of their allowed limit in Ψ_p .

Fig. 5.6 (a) shows that increasing G_{f_d} is beneficial in both lowering noise norm and increasing marginally stable stiffness, where G_{a_d} is detrimental. This holds true for any of the tested reduction sets (η_m, η_d) in fig. 5.7.

In fig. 5.6 (a) and fig. 5.7 there is a clear optimal point for each curve to minimize the amount of noise: the point where $G_{f_p} = \eta_m - 1$. At that parametrization, no acceleration feedback is necessary $G_{a_p} = 0$. However, increasing the gains increases robustness, visualized by following the curves left and up.

Optimal Design To obtain the optimal controller designs of this system, fig. 5.7 shows the four reduction sets (η_m, η_d) with increasing gains. The optimal paths, as a function of tradeoff α , then trace the bottom-leftmost points. These optimal paths are estimated by piecing their bottom-leftmost points together.

The optimal paths for these reduction sets are shown in fig. 5.6 (b). It is seen that requiring twice the inertia reduction more than halves the robustness. Increasing the required damping reduction above the minimal $\eta_d = 3$ shifts the optimal curve to slightly lower noise.

These graphs do not directly say anything about the gains used along the curves, nor what α is, only what the best reachable tradeoff is. Gain information can be derived from fig. 5.7, when following the optimal curve, varying α from small (more emphasis on robustness) to big (more emphasis on noise attenuation).

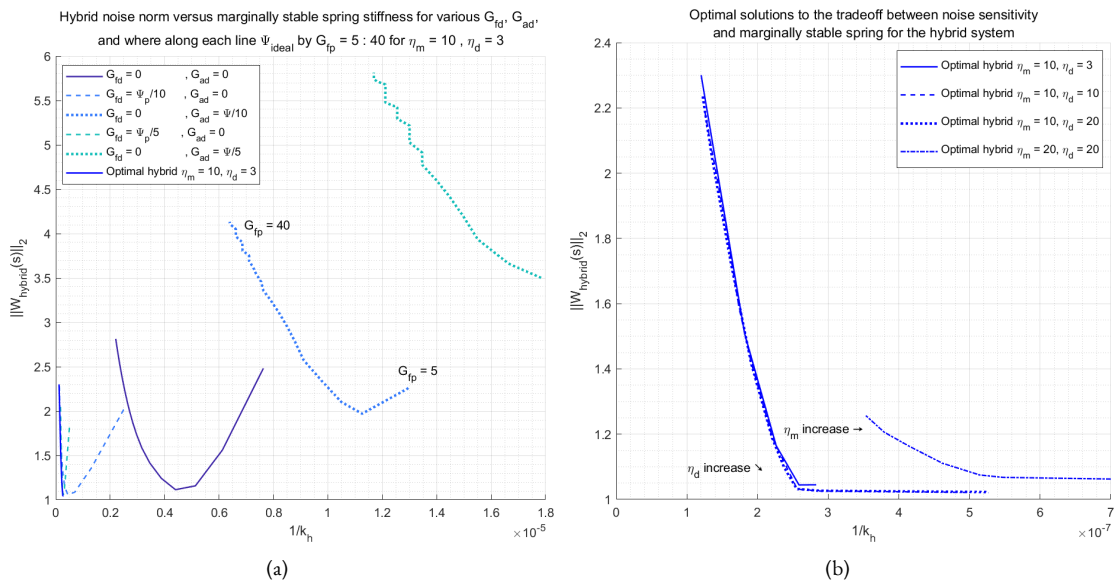


Figure 5.6: Noise norms versus marginally stable stiffness, for varying gains. The stiffness axis is inverted such that the bottom and left is more desirable. (a) shows an example of the effect of increasing G_{a_d} , G_{f_d} . (b) is the combination of optimal curves derived from the graphs of type a., shown in fig. 5.7.

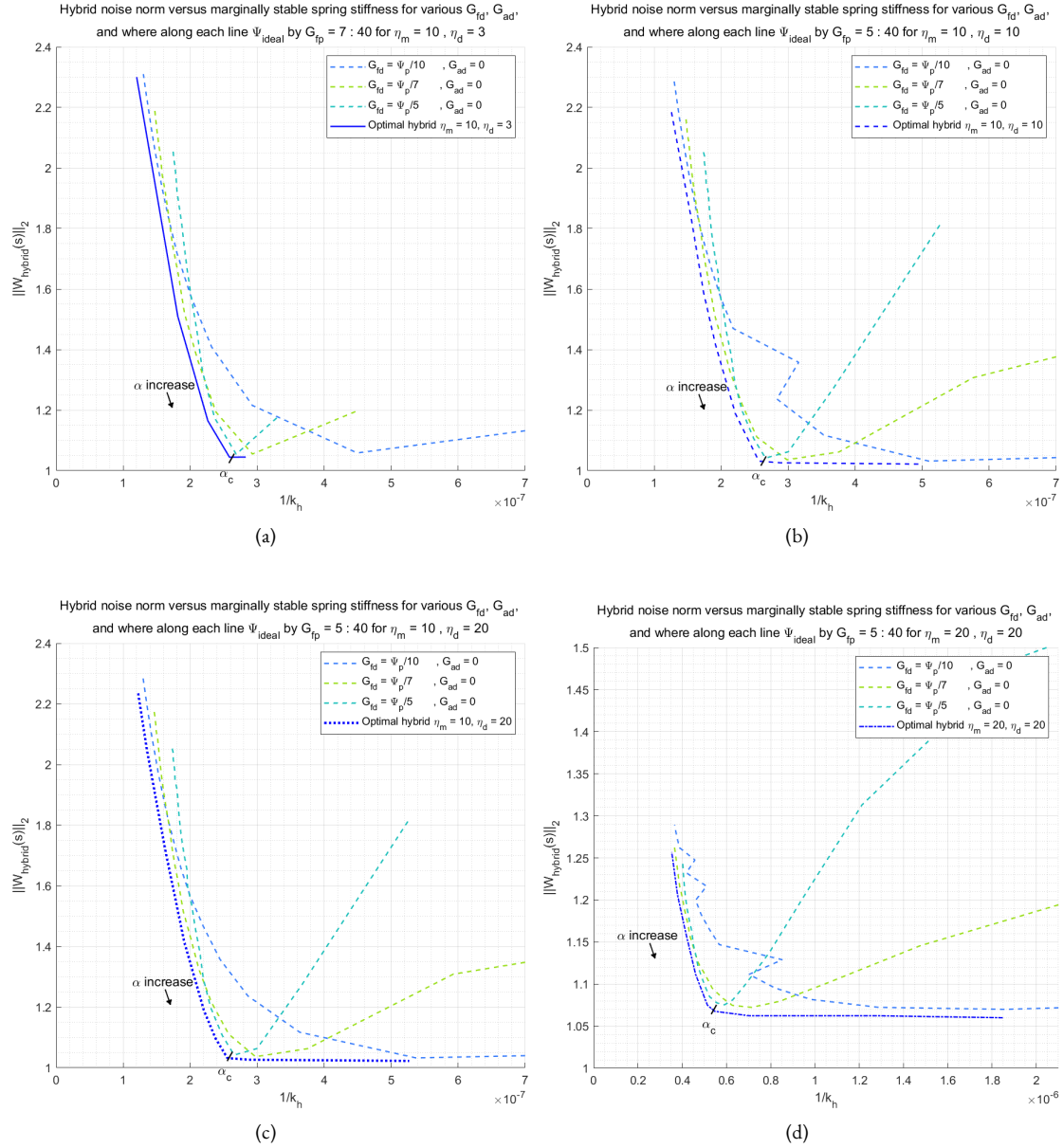


Figure 5.7: Noise norms versus destabilizing stiffness for varying G_{fp}, G_{fd}, G_{ad} and four different η_m, η_d . Optimal paths are obtained by following the bottom-most and left-most curves, and are shown slightly offset for visibility reasons. Note that (d) has different axes.

There is a corner tradeoff α_c at $G_{f_p} = \eta_m - 1$ and related gains of Ψ_{ideal} , where maximum allowable G_{f_d} is optimal. Below α_c , along the left of the optimal curves, the optimal G_{f_p} and the related gains of Ψ_{ideal} increase while G_{f_d} decreases. Above α_c , along the bottom of the optimal curves, the optimal G_{f_p} and the related gains of Ψ_{ideal} are fixed at $G_{f_p} = \eta_m - 1$ while G_{f_d} decreases.

For minimum noise thus, G_{f_p} and the related gains of Ψ_{ideal} must be $G_{f_p} = \eta_m - 1$. Increasing G_{f_d} then increases robustness. For even larger robustness, but increased noise sensitivity, G_{f_p} and the related gains of Ψ_{ideal} can be increased, while G_{f_d} decreases.

Apparent impedances cannot be shown because the HF apparent impedance is not defined, as discussed in sec. 5.1. The LF impedances can be shown, but LF matching is accurate due to Ψ_{ideal} and Ψ_p . Therefore, they are practically equal to the LF impedances of the ideal robot, visible in fig. 4.4 (a), accurate up to the performance frequency ω_p .

5.7 Discussion and Conclusion

This chapter studied the hybrid system: a rigid robot with discrete-time controller. The main findings in short are described at the beginning of this chapter. Passivity conditions for discrete-time feedback of position $\Omega_{\text{hybrid},x,[1]}$, force $\Omega_{\text{hybrid},f}$ and acceleration $\Omega_{\text{hybrid},a}$ with full inclusion of the sampler and ZOH were derived. Minimal safe impedances are presented and applied to the case study system, which must focus on stability rather than passivity to achieve its reduction targets.

Position Feedback Discrete-time position feedback is again shown to be able to passively compensate damping ($\eta_d = \infty$). Its condition was derived in a simpler geometric manner than Colgate and Schenkel [1], Liu [14] or Kim and Ryu [12], but was merely proven to be sufficient. Proving necessity is harder than sufficiency, and might require a time domain analysis, as done by Colgate and Schenkel [1].

Force Feedback It has been shown that force feedback can never be used passively in $\Omega_{\text{hybrid},f}$. In contrast, the stability conditions $\Lambda_{\text{hybrid},f,\text{damped}}$ show that if the environment is damped enough, any force feedback is stable. Moreover, a condition for pure human spring in $\Lambda_{\text{hybrid},f,k_h}$ scales well for fast control loops and damped robots. The stability conditions for discrete-time force feedback were thus shown to be more than acceptable, whereas the passivity conditions are zero. This is a testament to the argument that passive control can be too restrictive.

Acceleration Feedback According to sec. 5.4, without derivative feedback half of the robot inertia can be compensated ($\eta_m = 2$). With derivative feedback, three quarters of the robot inertia can be compensated ($\eta_m = 4$). Apart from the acceleration conditions $\Omega_{\text{hybrid},a}$ being based on the conjecture of 5.2.1, the derivation makes several assumptions based on numerical observation. It is therefore not an exact proof, and requires rigorous validation.

The most interesting feature of acceleration feedback is that, counterintuitively, lower sample times do not promote a higher inertia reduction. In contrast, robot damping does promote inertia reduction, which holds for position and force feedback too. For modern robot design with fast control and low damping, these conditions allow very little inertia reduction. Moreover, in the limit of an infinitely fast controller, the condition does not approach the ideal model condition of Ω_{ideal} . In fact, the infinitely fast discrete-time controller does not allow any passive inertia reduction. This is in contrast to the reasonable assumption that an infinitely fast discrete-time controller is the same as a continuous-time one, which in ch. 4 allowed full inertia reduction.

The technical reason for the mismatch is that there always exists a worst-case pure environmental spring that scales inversely with sample time, as shown in app. C.13. The spring is tuned such that the combined mass-spring-damper system's natural frequency is at the first Nyquist frequency. The same worst type environment was found by Colgate and Schenkel [1] on discrete-time position feedback. For both types of feedback, decreasing the sample time infinitely then increases the worst spring to infinite stiffness.

The only difference in loop gain with position feedback is a factor s^{-2} , as seen in 5.6. This results in the loop gain of position feedback approaching a finite value towards continuous-time. In contrast, the loop gain of acceleration feedback approaches infinity. The lack of this term is also what prevents the use of the same method of Colgate and Schenkel [1]. An intuitive reason for the mismatch is lacking, but three possibilities are provided here.

First, if the worst-type environment is not in the mass-spring-damper, there may be a worse unbound environment that always activates the system. In that case acceleration feedback may actually never be passive. The derivation in this work is then not a passivity condition, but a stability condition.

Second, the discrete-time controller is a fundamentally different system, and the assumption that an infinitely fast discrete-time controller is the same as a continuous-time controller is false in the modelling of this robot.

Third, approaching continuous-time and increasing worst-case environmental spring stiffness to infinity is not a well-posed limit. Such an infinitely stiff environment would not allow any energy exchange, and the concept of passivity is nonsensical.

The passive compensation of inertia is theoretically interesting. However, the restrictive conditions, in combination with limited bandwidth, means that in practice this method is unlikely to be applied.

Combined Feedback A passivity condition for the entire hybrid system Ω_{hybrid} was shown as an interpolation between acceleration $\Omega_{\text{hybrid},a}$ and position $\Omega_{\text{hybrid},x,[1]}$ feedback, because the condition for force feedback $\Omega_{\text{hybrid},f}$ was zero. This resulted in a conservative tradeoff between (η_d, η_m) , of which the latter in practice is close to unity. The only significant reduction is then by position feedback, which may completely compensate $(\eta_d = \infty)$ damping.

Validation With the exception of $\Omega_{\text{hybrid},x,[1]}$, all given passivity and stability conditions are merely shown to be sufficient, not sufficient *and* necessary. This means that they need not be the exact conditions, and may be overly restrictive for practical purposes, requiring validation. The passivity conditions are derived in two ways: similar to Colgate [1] or by assuming a simple worst type of environment. The assumption that such single worst types of environments exist and lead to the passivity conditions is known for LTI systems, but in this work is based on an assumption.

All conditions have seen limited validation in simulation by Matlab's Simulink and 2o-sim. Proving passivity of these types of hybrid systems in simulation technically requires evaluating energy exchange for *every* signal, because each input signal aliases differently. Even when limiting to sinusoids, this requires evaluation of *every* frequency, because the system is not periodic at the interaction port. Passivity can therefore not be verified in simulation, which is exactly why analytical passivity conditions are paramount.

Stable Optimal Design Analytically, it was found that the case study design requires stable design rather than passive. Because any solution to the reduction problem already has destabilizing stiffness far above human stiffness, it is recommended to focus on noise reduction. To minimize noise, equal reduction of inertia and damping is recommended, such that only force feedback is necessary at $G_{f_p} = \eta_m - 1$. The maximum allowable G_{f_d} then increases robustness.

Chapter 6

Flexible Link Robot With Continuous-Time Controller

The following chapter introduces a single underdamped flexible mode to the serial robot, with the otherwise continuous-time controller. This added complexity results in a model for which the passivity conditions are best analyzed numerically, done for the case study system. Still, some useful insight can be heuristically derived. The key results are:

- No matter what feedback options are available, passivity requires that only the motor inertia can be masked.
- The main factor that limits how close passive reduction may get to masking the motor inertia is base damping.
- Reaching this passivity limit exactly is theoretically always possible, although not robust.
- The case study system must forego passivity to reach its inertia reduction target.
- Closed loop stability conditions are much more manipulable with the added sensory options.

6.1 System Description

Fig. 6.1 shows the flexible link robot model with a single mode between motor coordinate x_1 and end effector coordinate x_2 . As a result, actuation is now non-collocated for force f and acceleration a_2 feedback. The total inertia is split in two as $m_1 + m_2 = m_r$, connected through structural spring k and damper d . The single mode is assumed underdamped and lies above the haptic performance frequency ω_p . The transfer is derived in app. D.6. To keep the transfer compact, the following notation is used:

$$Z(s) = \frac{V_2(s)}{F(s)} = \frac{(G_a s + Z_2 + \bar{Z}_1)Z_{12} + \bar{Z}_1 Z_2}{(G_f + 1)Z_{12} + \bar{Z}_1}, \quad (6.1)$$

where each impedance $Z_1(s)$, $Z_{12}(s)$ and $Z_2(s)$ corresponds to the coordinate on which it is acting: motor velocity v_1 , end effector velocity v_2 , or the difference between the two:

$$\begin{aligned} Z_1(s) &= m_1 s + d_1 \\ Z_{12}(s) &= d + k s^{-1} \\ Z_2(s) &= m_2 s. \end{aligned}$$

End effector ground damping is neglected for the serial robots considered here. The ideal controller, the continuous-time version of (3.2), is used. Because in this case the effect of $G_{x_1} s^{-1}$ is equivalent to the effect of $Z_1(s)$, they are combined into $\bar{Z}_1(s)$:

$$\bar{Z}_1(s) = Z_1(s) + G_{x_1} s^{-1} = m_1 s + \bar{d}_1 + \bar{k}_1 s^{-1},$$

where the combined damping and stiffness is:

$$\begin{aligned} \bar{d}_1 &= d_1 + G_{x_d}, \\ \bar{k}_1 &= G_{x_p}. \end{aligned}$$

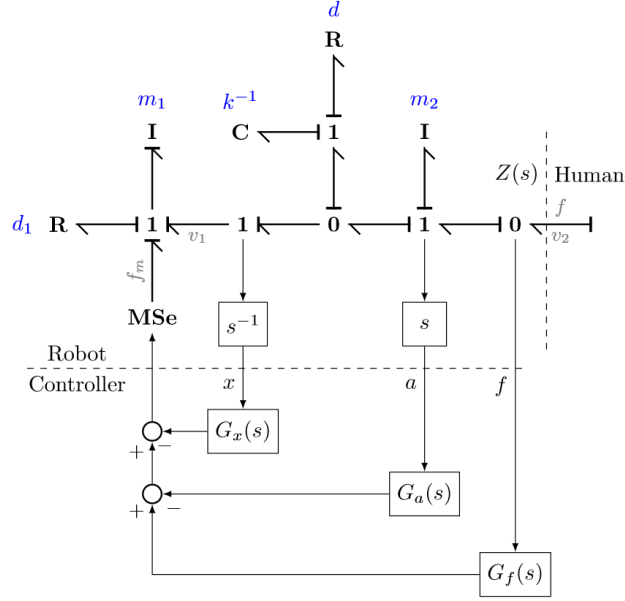


Figure 6.1: Bond graph of the flexible link robot with continuous-time feedback of motor position x_1 , interaction force f and end effector acceleration a_2 .

The full transfer is shown in table 6.1 and is of order four, regardless of feedback. Because the flexible mode is assumed underdamped, the two HF zeros (z_1, z_2) and HF poles (p_1, p_2) are inherently complex conjugate pairs. For the unactuated robot:

$$z_1, z_2 = -\omega_N(\zeta_N \pm i\bar{\zeta}_N) \quad (6.2)$$

$$p_1, p_2 = -\omega_D(\zeta_D \pm i\bar{\zeta}_D), \quad (6.3)$$

where $\bar{\zeta} = \sqrt{1 - \zeta^2}$. Note that ω_N denotes the magnitude of the numerator roots in this chapter, not the Nyquist frequency. The HF poles lie below the zeros on the frequency axis, but above the performance frequency:

$$\omega_N > \omega_D > \omega_p. \quad (6.4)$$

In contrast, the LF zeros (z_3, z_4) lie below the performance frequency such that the transfer of (6.1) can be separated into LF and HF behavior:

$$Z(s) = Z_{LF}(s) \cdot Z_{HF}(s) \propto \frac{(s + z_4)(s + z_3)}{s} \cdot \frac{(s + z_1)(s + z_2)}{(s + p_1)(s + p_2)}. \quad (6.5)$$

Where z_4 is zero if \bar{k}_1 is zero. This form is stated only to to differentiate between behavior above and below ω_p , system parameters still influence the roots above and below. Given this assumption, the LF behavior is the same mass-spring-damper of the ideal case of (4.1):

$$Z_{LF}(s) \approx \frac{G_{a_p} + m_r}{G_{f_p} + 1} s + \frac{\bar{d}_1}{G_{f_p} + 1} + \frac{\bar{k}_1}{G_{f_p} + 1} s^{-1}. \quad (6.6)$$

Fig. 6.2 shows the Bode magnitude plot for the unactuated flexible link system $Z_{flex, u}(s)$ and the target impedance $Z_d(s)$ from (3.4). In general, the goal is to lower apparent LF inertia and damping according to (3.5). What happens to the mode is not important to the user, as long as it remains above ω_p and maintains passivity within the hatched region.

Table 6.1: Terms of the flexible link robot model transfer $Z(s) = Z_N(s)/Z_D(s)$ and approximation for the underdamped system.

	$Z_N(s)$	$\approx Z_N(s)$	$Z_D(s)$	$\approx Z_D(s)$
s^3	$m_1 m_2 + dG_{a_d}$	$m_1 m_2 + dG_{a_d}$		
s^2	$kG_{a_d} + m_2 \bar{d}_1 + d(G_{a_p} + m_r)$	$kG_{a_d} + m_2 \bar{d}_1 + d(G_{a_p} + m_r)$	$m_1 + dG_{f_d}$	$m_1 + dG_{f_d}$
s^1	$k(G_{a_p} + m_r) + m_2 \bar{k}_1 + d\bar{d}_1$	$k(G_{a_p} + m_r)$	$kG_{f_d} + \bar{d}_1 + d(G_{f_p} + 1)$	$kG_{f_d} + \bar{d}_1 + d(G_{f_p} + 1)$
s^0	$d\bar{k}_1 + k\bar{d}_1$	$k\bar{d}_1$	$\bar{k}_1 + k(G_{f_p} + 1)$	$k(G_{f_p} + 1)$
s^{-1}	$k\bar{k}_1$	$k\bar{k}_1$		

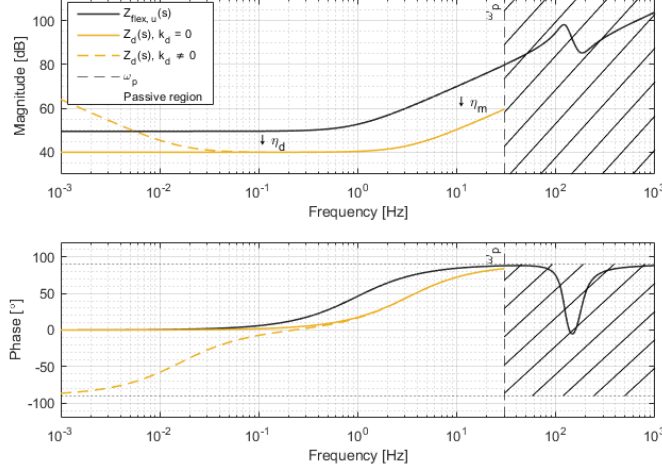


Figure 6.2: Bode plot of the Gable Core unactuated flexible link robot model $Z_{\text{flex},u}(s)$ and the target impedance $Z_d(s)$. The behavior up to ω_p must be reduced by η_d, η_m . The behavior above ω_p must be passive, indicated by the hatched regions, but may otherwise be arbitrary. The flexible mode is assumed to lie above ω_p .

6.2 Safety: Passivity

The passivity conditions of the flexible system are analyzed in three manners: the interpretation of the PE, heuristical reasoning of the effects of feedback, and numerical PRC conditions for the case study. Because the exact passivity conditions for higher order systems quickly become complex, the results derived here vary in effectiveness. Therefore, passivity is best studied numerically in the context of impedance reduction on the case study, done in sec. 6.4.

6.2.1 Physical Equivalence

A PE of the flexible link system is shown in fig. 6.3 and derived in app. D.4. It gives *some* insight into how the system behaves energetically and haptically, although it is difficult to interpret due to its large structure, relative masses (called inerters [69]) and many transmissions. Straightforward passivity conditions from the PE requires that all 15 elements in fig. 6.3 (a) are passive. Where previously, in sec. 4.2, it was possible to quickly obtain passivity conditions from the PE, here it is not, because the parameters are unwieldy. This approach does not lead to compact passivity conditions.

Still, it can be seen that several active (negative parameter) elements can occur as a result of feedback. In fig. 6.3 (b) for example, damping d_1 can cause active elements in the top branch. These active elements can activate the interaction port $Z(s)$ if the generated energy is not internally dissipated. The PE of fig. 6.3 (b) is simple enough to directly give a sufficient but restrictive passivity condition by requiring that every element is passive. For no derivative feedback ($G_{f_d} = G_{a_d} = 0$):

$$\begin{aligned} G_{x_p} &\geq 0 \\ G_{x_d} &\geq -d_r \\ -1 &\leq G_{f_p} \leq \frac{G_{a_p}}{m_2} \end{aligned} \quad (\Omega_{\text{flex, PE b}})$$

This leads to a conservative minimal passive impedance, where G_{f_p} is chosen as the independent parameter over G_{a_p} :

$$\Omega \hat{Z}_{\text{flex, PE b.}}(s) = \left(m_2 + \frac{m_1}{G_{f_p} + 1} \right) s + \frac{\bar{d}_1}{G_{f_p} + 1} + \frac{\bar{k}_1}{G_{f_p} + 1} s^{-1},$$

obtained when substituting the restrictive condition into the LF impedance. For large G_{f_p} the minimal passive impedance is:

$$\Omega \hat{Z}_{\text{flex, PE b.}}(s) = m_2 s.$$

Even though this result is conservative, it agrees with Colgate [3] in that the minimal passive impedance can never be lower than the end effector mass m_2 . Therefore, only adding G_{a_p} does not improve the fundamental inertia reduction limit. For pure force feedback, with $G_{f_d} = G_{a_d} = G_{x_p} = G_{x_d} = d_1 = 0$, the exact result from Colgate [3] is reacquired, as shown in fig. 6.3 (c).

6.2.2 Heuristics

According to the PRC of app. A.1 passivity is attained for this system if numerator $Z_N(s)$ and denominator $Z_D(s)$ are stable and the phase of $Z(s)$ is within $[-\frac{\pi}{2}, \frac{\pi}{2}]$ rad. If (6.5) is a good approximation and all coefficients are assumed to be positive, then both numerator and denominator are stable, because second-order transfers $Z_{LF}(s)$ and $Z_{HF}(s)$ with positive coefficients are always stable. Therefore, any system activity must be due to a violation of the phase requirement.

Additionally, if (6.5) is a good approximation, the phase of $Z(s)$ is $\frac{\pi}{2}$ rad around the performance frequency ω_p , because there must be mass-like behavior. In that case, $Z_{HF}(s)$ may not have any positive phase in order to maintain passivity. The condition for $Z_{HF}(s)$ to not have any positive phase, as shown by app. D.7, is:

$$\frac{\omega_N}{\omega_D} \geq \frac{\zeta_D}{\zeta_N} \geq \frac{\omega_D}{\omega_N}. \quad (6.7)$$

This implies that the condition $\omega_N > \omega_D$ of (6.4) is always required for passivity and thus HF poles before zeros is a necessity for passivity, even after applying feedback. This is because feedback here does not increase the order of the system, but only modifies the roots. The passivity limit is then exact pole-zero cancellation of the HF roots, requiring the same HF pole and zero frequencies ($\omega_N = \omega_D$) and damping ratios ($\zeta_D = \zeta_N$). How proximal the HF root pairs may get to each other on the frequency axis is determined by the ratio of their damping ratios in (6.7).

Fig. 6.4, in combination with table 6.1, show that acceleration and force feedback have similar effects on the HF zeros and poles respectively, due to the symmetry between numerator and denominator. With respect to the HF roots, their most significant effects are:

- Increasing the proportional gains (G_{f_p}, G_{a_p}) increases the magnitudes (ω_D, ω_N) of poles (p_1, p_2) and zeros (z_1, z_2) respectively.
- Increasing the derivative gains (G_{f_d}, G_{a_d}) significantly increases damping (ζ_D, ζ_N) of the inherently underdamped poles (p_1, p_2) and zeros (z_1, z_2) respectively.

Knowing these effects and (6.7), approximate passivity conditions can be derived for two cases.

Undamped Mode

Colgate [3] showed that, for the flexible system with no damping and proportional force feedback only, the passivity condition is:

$$-1 \leq G_{f_p} \leq \frac{m_1}{m_2}. \quad (\Omega_{\text{flex}, [3]})$$

The upper limit is reached because G_{f_p} may move the poles of the system upwards, but only up to pole/zero cancellation ($\omega_N = \omega_D$). Alternatively, the PE of fig. 6.3 (c) yields the same condition. This condition can be extended to include proportional acceleration feedback as done in app. D.8. Without any damping ($d = d_1 = G_{x_d} = 0$), without base stiffness ($G_{x_p} = 0$) and without derivative feedback ($G_{f_d} = G_{a_d} = 0$) the passivity limit is therefore:

$$\begin{aligned} -1 \leq G_{f_p} \leq \frac{m_1 + G_{a_p}}{m_2} \\ G_{a_p} \geq -m_1 \end{aligned} \quad (\Omega_{\text{flex}, \text{n.d.}})$$

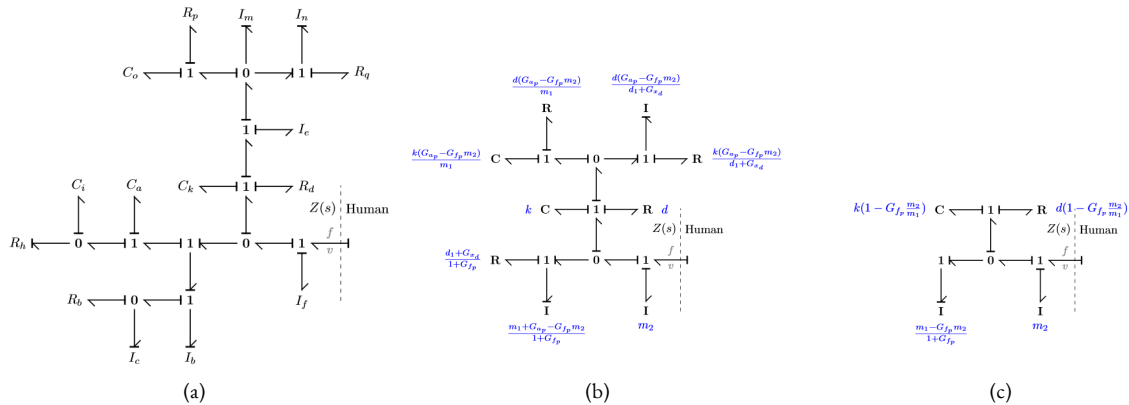


Figure 6.3: PE of the flexible link continuous-time controller system with position, force, and acceleration PD feedback (a). The parameters of (a) are unwieldy and are shown in app. D.5. This reduces to the middle PE for $G_{f_d} = G_{a_d} = 0$ in (b) and the undamped system of [3] with additionally $G_{a_d} = G_{x_d} = G_{x_p} = d_1 = 0$ in (c).

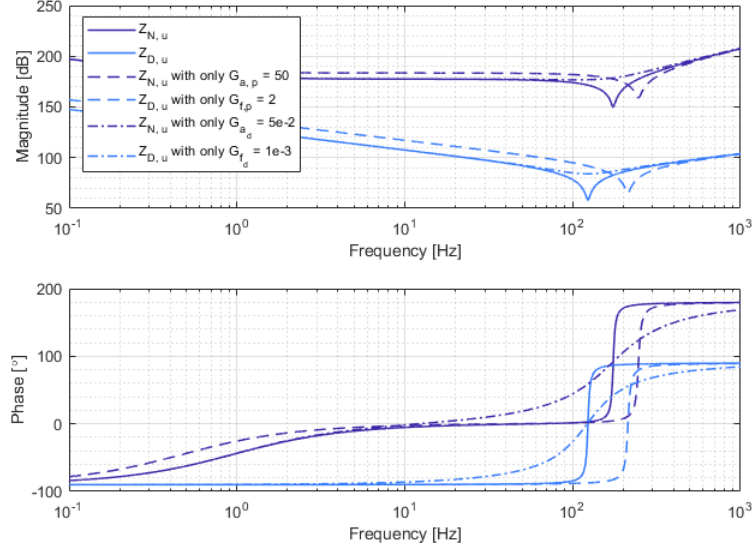


Figure 6.4: Visualization of most significant effects of varying the controller gains on the apparent impedance for the underdamped system: proportional gains modify locations of the roots and derivatives modify damping.

When exactly on the limit, during pole-zero cancellation ($\omega_N = \omega_D$), the simple condition $G_{a_d} = G_{f_d} m_2$ must be added. This equalizes the damping ratios of (6.7), because the derivatives are the only sources of damping in the system.

Underdamped Mode

If damping is added, the HF roots are not equally damped any more in general, and (6.7) is not an equality. Because proportional gains (G_{f_p}, G_{a_p}) are related to the magnitudes of the roots (ω_D, ω_N), they are now limited in how close they may get to the ideal undamped condition of $\Omega_{\text{flex, n.d.}}$. The condition including damping is then more generally:

$$\begin{aligned}
 G_{x_p} &\geq 0 \\
 G_{x_d} &\geq -d_1 \\
 -1 &\leq G_{f_p} \leq \frac{G_{a_p} + m_1}{m_2} - \epsilon, \quad \epsilon \geq 0 \\
 G_{a_p} &\geq -m_1.
 \end{aligned} \tag{\Omega_{\text{flex, u.d.}}}$$

Here, ϵ is an unspecified function of all parameters, evaluated in sec. 6.4. When damping ratios are equal, this difference is zero ($\epsilon = 0$), for example in the undamped case. Alternatively, it was noted that derivative gains G_{f_d} and G_{a_d} can modify the poles and zeros damping ratios. Therefore, exact tuning of gains can equalize the damping ratios.

6.2.3 Positive Real Condition

The exact passivity conditions of the flexible link model, utilizing all feedback, are derived from the PRC in sec. D.9. The three conditions are approximately:

$$\begin{aligned}
 G_{f_p} + 1 &\geq G_{f_d} \frac{\bar{k}_1}{\bar{d}_1} \\
 G_{a_p} + m_1 + G_{a_d} \frac{k}{\bar{d}} &\geq m_2 \left(G_{f_p} + G_{f_d} \frac{k}{\bar{d}} \right)
 \end{aligned} \tag{\Omega_{\text{flex}}}$$

See D.9 for the third condition.

The first condition restricts how negative G_{f_p} can be, similar to $G_{f_p} > -1$ from the rigid case of Ω_{ideal} . The second contains the fundamental limit $\Omega_{\text{flex, u.d.}}$, now apparently relaxed by negative G_{f_d} and positive G_{a_d} . The third condition, obtained due to this being a fourth order system, is unwieldy even after approximation.

Because it contains all eleven (six controller and five system) parameters it is hard to compare the effect of each respective parameter with another. Instead, the amount of parameters to investigate is significantly limited when considering its effect on the attainable inertia and damping reduction. Therefore, the passivity conditions are only studied in context with impedance reduction of the case study system in the following sec. 6.4, visualized numerically.

6.3 Performance: Impedance Shaping

Given the assumption of (6.6), the flexible mode acts above the haptic performance frequency ω_p . The LF impedance can thus be assumed to be equal to that of the LF approximation of ch. 4. Therefore, the same controller parameterization Ψ_{ideal} can be used to shape the LF impedance. Additionally, to not influence the mass-spring-damper behavior, Ψ_p must be used as well. In short, the shaping conditions do not change with respect to the ideal robot, only the passivity properties.

6.4 Passive/Stable Impedance Reduction

The shaping conditions of Ψ_{ideal} and Ψ_p are used to reduce the LF impedance, while passivity conditions Ω_{flex} guarantee safety. Using these rules, there are then three DOF left out of the six feedback parameters. Due to the fundamental passivity limit of $\Omega_{flex, u.d.}$, the minimal passive inertia will be limited. Therefore, it is worth investigating whether stable shaping allows more inertia reduction. Either is discussed in the following sections.

6.4.1 Passive Reduction

Substituting the exact passivity conditions Ω_{flex} into the apparent impedance of (6.6) does not have a compact solution, given that the conditions are unwieldy. Instead, substituting the more general passivity conditions $\Omega_{flex, u.d.}$, obtained by understanding the role of feedback, into (6.6) gives a comprehensible minimal passive impedance:

$$\Omega_{\hat{Z}_{flex}}(s) = m_2 \frac{m_1 + m_2}{m_1 + m_2(1 - \varepsilon)} s + \frac{d_1}{\eta_d}. \quad (6.8)$$

Here, ε is a function of all system and control parameters. This function is shown in fig. 6.5 (a) as a function of damping reduction η_d for the Gable Core case study system. At each point in the figure, the inertia and damping reductions (η_m, η_d) are achieved, with $G_{f_p}, G_{f_d}, G_{a_d}$ considered the free parameters.

The figure shows the tradeoff between inertia and damping reduction. It is seen that damping may be reduced completely ($\eta_d = \infty$), but nonzero ε causes a tradeoff with passive inertia reduction to be limited. The maximum achievable inertia reduction is $\eta_m = 1 + m_1 m_2^{-1}$. This always maintaining the end effector inertia m_2 in 6.8, such that only the actuator inertia m_1 is masked. The limit of $\Omega_{flex, u.d.}$ must thus be respected, which agrees with the result from Colgate [3]. In this case of equal inertia ratio, the maximum passive inertia reduction is $\eta_m = 2$.

Only in the equal damping ratio case can this limit be achieved exactly, such that $\varepsilon = 0$. This is achieved in three cases: for the undamped system of $\Omega_{flex, n.d.}$, when artificially there is no damping ($\eta_d = \infty$), or when tuning G_{f_d}, G_{a_d} . The former was already discussed in sec. 6.2.2.

Artificially removing all damping such that ($\eta_d = \infty$), is not a realistic option. This does reiterate that, perhaps surprisingly, damping d_1 is the most significant cause of the reduced limit $\Omega_{flex, u.d.}$. This is because it unequalizes the damping ratios of the HF roots.

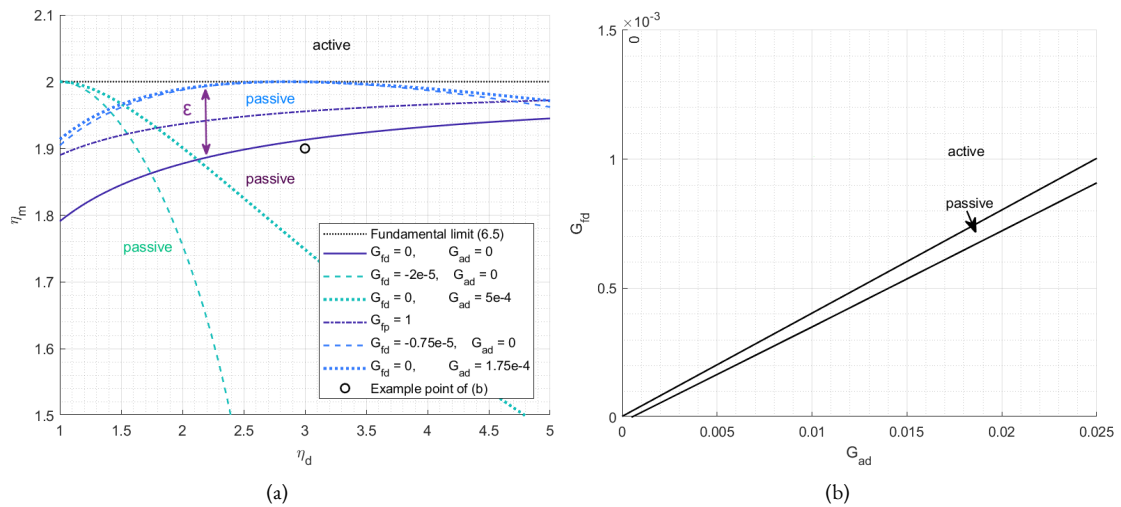


Figure 6.5: (a) Passive reduction ratio tradeoff for Gable Core case study using the shaping of Ψ_{ideal} . Green and blue are tuned to be able to reach $\eta_m = 2$ for $\eta_d = 1$ and $\eta_d = 3$ respectively. The marked point is shown in (b), which shows the range for G_{f_d}, G_{a_d} in which $\eta_m = 1.9, \eta_d = 3$ can be passively achieved.

Because derivative feedback (G_{fd}, G_{ad}) can compensate for differences in relative damping ratios, $\varepsilon = 0$ can be reached if the derivatives are properly tuned. Therefore, for every damping ratio (η_d), there exist derivative gains (G_{fd}, G_{ad}) that allows reaching the limit $\eta_m = 1 + m_1 m_2^{-1}$.

In fig. 6.5 (a) this is shown for reaching $\eta_d = 1$ and $\eta_d = 3$ for the Gable Core. These curves only clip $\eta_m = 2$ exactly at one point, which indicates that the derivative gains (G_{fd}, G_{ad}) must be *exact* values.

Below the limit of $\eta_m = 2$, passivating gains (G_{fd}, G_{ad}) lie in a range, as seen in fig. 6.5 (b). If the limit is reached exactly this range is a single line. At the limit, the method is implicitly equivalent to stable pole/zero cancellation, which cancels the excess phase introduced by the mode. This essentially removes the flexible mode, which is not practical because it requires exact tuning and is thus not robust to errors in parameter estimates.

Colgate [3] claimed that base damping of the flexible link system does not influence the achievable passive inertia reduction much. Indeed, this is seen to reduce the maximum inertia reduction by about 10% at worst when using only force feedback in fig. 6.5. Even though this 10% can be reclaimed in theory, it is not robust in practice. If instead of damping reduction a damping increase is desired ($\eta_d < 1$), for example for training purposes, the maximum inertia reduction lowers more.

6.4.2 Stable Reduction

As shown, passive inertia reduction can be inadequate due to a fundamental limit in inertia reduction. Therefore, stability conditions might be considered instead. The loop gain of the flexible link model with a human is the product of the apparent impedance and the human admittance:

$$L_{\text{flex}}(s) = Z(s)Y_h(s).$$

When violating the PRC by reducing more inertia, a phase above $\frac{\pi}{2}$ rad occurs near the zero pair (z_1, z_2). If all system damping is low, the maximum phase of $Z(s)$ as a result of violation can be at most $\frac{3}{2}\pi$ rad. This means that a scaling of $Z(s)$ is enough to encircle -1 and destabilize the system by the Nyquist criterion. The interpretation then is that purely real $Y_h(s)$, a pure damper in addition to a pure spring, can destabilize the system.

This is an undesirable property, because end effector damping is assumed to be negligible for decoupled serial robots. It is thus important to reduce the maximum phase to below π rad, such that only a stiff spring can destabilize the coupled system. The case study system is damped enough by itself, as seen in e.g. fig. 6.2, such that there is no danger of a destabilizing environmental damper.

The amount of the phase violation can be reduced by increasing the damping ratios of either numerator or denominator: by adding damping \bar{d}_1 or by the derivatives feedbacks (G_{fd}, G_{ad}). Due to their large effect on increasing damping ratio, only a small amount of the latter two is necessary.

For any robot violating the PRC, the loop gain is guaranteed to cross the negative real axis on a Nyquist plot, when connected to a spring. The magnitude at that point is:

$$|L_{\text{flex}}(i\omega_\pi)| = \left| Z(i\omega_\pi) \frac{\omega_\pi}{k_h} \right|,$$

where ω_π is the frequency at which crossing happens. The marginally stable spring \hat{k}_h , which causes the marginally stable loop gain $|L_{\text{flex}}(i\omega_\pi)| = 1$, is then found by finding the crossing frequency. The stability condition, assuming a spring to be the only destabilizing environment, is:

$$k_h < Z(i\omega_\pi)\omega_\pi. \quad (\Lambda_{\text{flex}, k_h})$$

6.5 Noise Sensitivity

The noise transfers for the flexible link system are derived in app. D.6 to be

$$W_{n,\text{flex}}(s) = \frac{Z_{12}(s)G_n(s)M_n(s)\sigma_n}{Z_1(s) + G_x(s)s^{-1} + Z_{12}(s)(1 + G_f(s))}.$$

At LF, this is unsurprisingly similar to the ideal noise transfers $W_{n,\text{ideal}}(s)$ because the terms with $Z_{12}(s)$ dominate the LF range. But in the HF range the additional terms of $Z_1(s) + G_x(s)s^{-1}$ in the denominator add roll-off to all transfers. Therefore, all noise sources are inherently band limited due to the additional mode. However, the addition of $Z_{12}(s)$ in the numerator can increase noise in the middle frequency range.

6.6 Design: Gable Core

The minimal passive inertias shown in sec. 6.4 yield that any damping reduction target can be achieved passively, and thus also the minimal target of $\eta_d = 3$. In the best case however, the inertia can be reduced to m_2 during perfect stable pole/zero cancellation, only masking m_1 . For this system the limit is $\eta_m = 2$, which is not enough to obtain the target inertia reduction of $\eta_m = 10$. Therefore, the reduction target can not be achieved passively. Stable shaping was described by sec. 6.4 to be promising.

For stable reduction the design problem can be defined as in (3.8): a tradeoff between the noise sensitivity and stability margin, assuming a pure environmental spring. This section studies in-depth how to obtain an optimal trade-off between noise sensitivity and robustness. The results derived here are largely similar to those of ch. 5. However, because chapters are readable on their own, this section contains the full description as well.

The optimization, subjected to shaping rules Ψ_{ideal} , Ψ_p and stability condition $\Lambda_{\text{flex}, k_h}$, is:

$$\min \left(\alpha \|W_{\text{flex}}(s)\|_2 + \frac{1 - \alpha}{\hat{k}_h} \right), \quad \alpha \in [0, 1],$$

where \hat{k}_h is the marginally stable spring following from the stability conditions and α is a linear tradeoff between costs.

There are three DOF remaining in the controller, these are chosen to be G_{fp} , G_{fd} , G_{ad} . The first is a the free parameter from Ψ_{ideal} , which determines how large G_{xd} , G_{ap} will be. Derivative gains G_{fd} , G_{ad} are limited to a fifth of their limit in Ψ_p . Because any optimization follows these shaping rules, their LF impedance errors are equally low.

The stability condition $\Lambda_{\text{flex}, k_h}$ is best evaluated numerically due to the order of the system.

Numerical Analysis Fig. 6.7 (a) shows an example of noise versus gain margin tradeoffs for varying gain sets, with derivatives as a fraction of their allowable limit. It is seen that increasing G_{ad} is derogatory for both noise and gain margins in any case. Increasing G_{fd} on the other hand is always beneficial for both, at least within the plotted gain ranges.

Fig. 6.6 (a) and fig. 6.7 show the effects of varying the DOF on the noise norm and marginally stable spring. The curves trace $G_{fp} = [2, 40]$ with G_{xd} , G_{ap} linearly following Ψ_{ideal} , starting at the top-right of every curve. The derivatives are varied as fractions of their allowed limit in Ψ_p , to illustrate which is beneficial.

Fig. 5.6 (a) shows that increasing G_{fd} is beneficial in both lowering noise norm and increasing marginally stable stiffness, whereas G_{ad} is detrimental. This holds true for any of the tested reduction sets (η_m, η_d) in fig. 5.7.

In fig. 5.6 (a) and fig. 5.7 there is a clear optimal point for each curve to minimize the amount of noise: the point where $G_{fp} = \eta_m - 1$. At that parametrization, no acceleration feedback is necessary $G_{ap} = 0$. However, increasing the gain of Ψ_{ideal} , visualized by following the curves left and up, increases robustness.

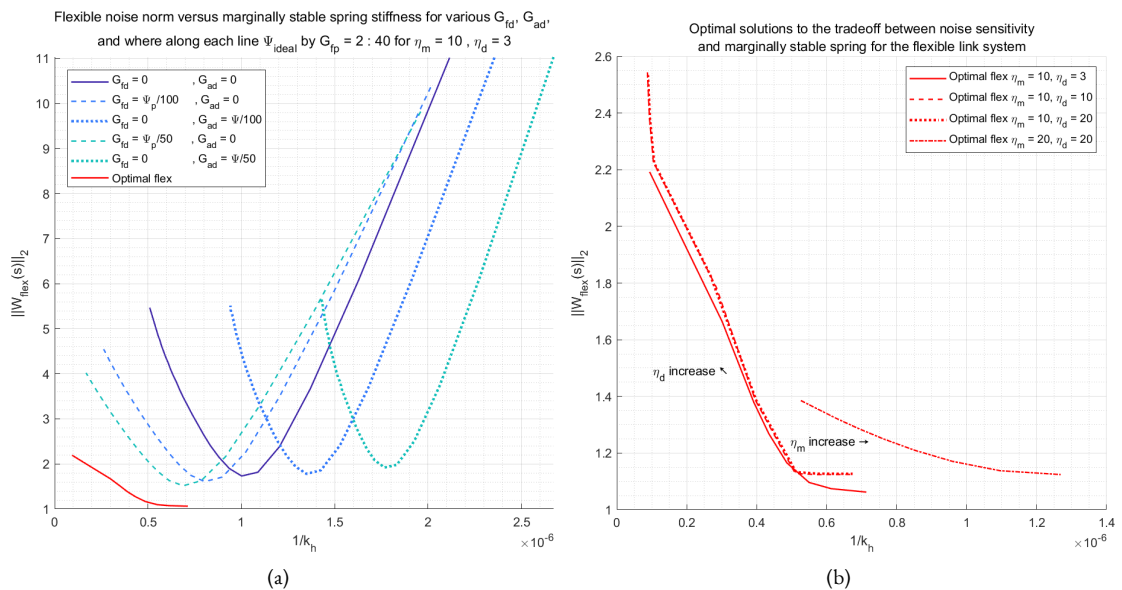


Figure 6.6: Noise norms versus marginally stable stiffness, for varying gains. The stiffness axis is inverted such that the bottom and left is more desirable. (a) shows an example of the effect of increasing G_{ad} , G_{fd} . (b) is the combination of optimal curves derived from the graphs of fig. 6.7.

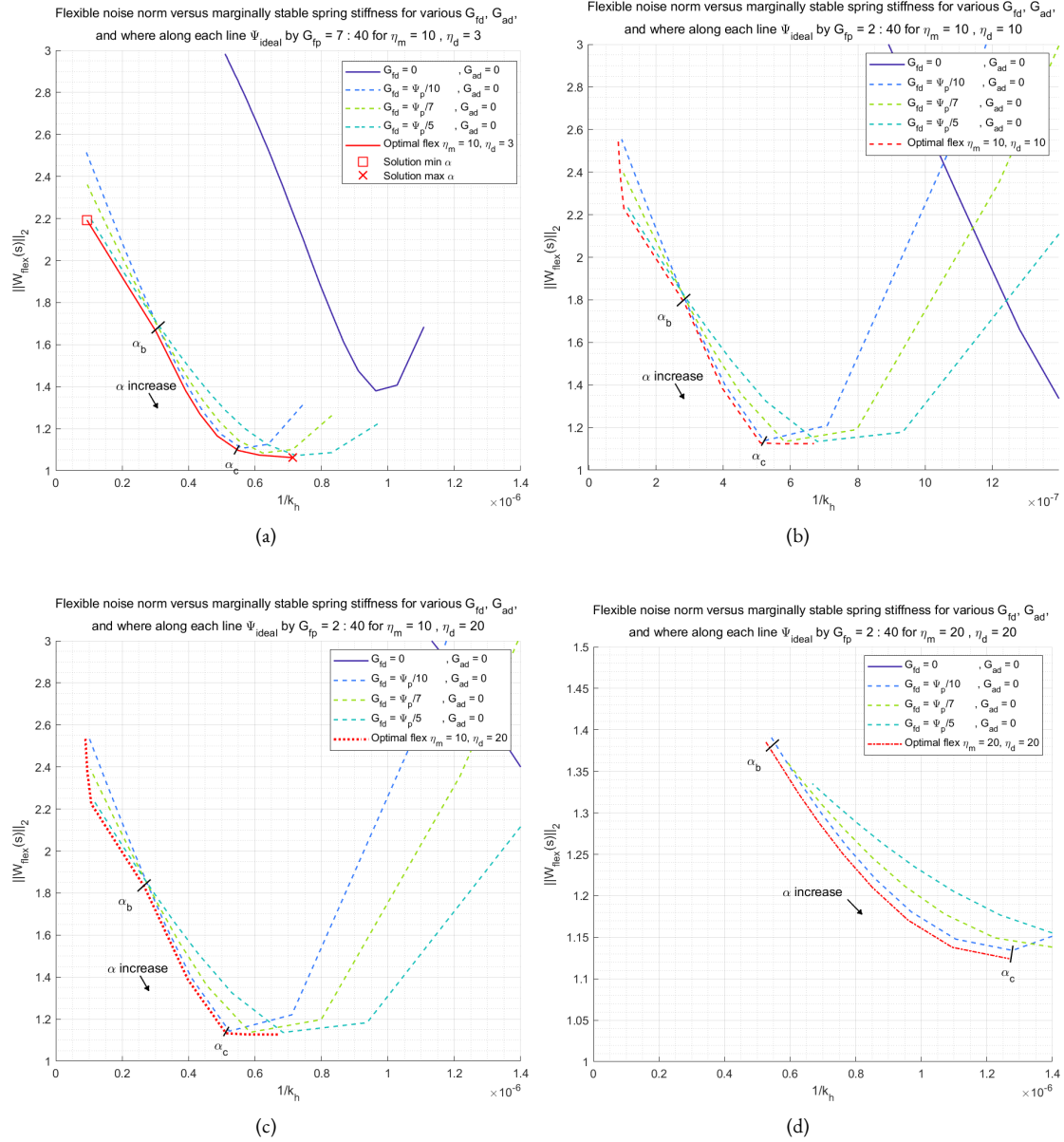


Figure 6.7: Noise norms versus destabilizing stiffness for varying G_{fp}, G_{fd}, G_{ad} and four different η_m, η_d . Optimal paths are obtained by following the bottom-most and left-most curves, and are shown slightly offset for visibility reasons. Note that (d) has half the y-axis. The two marked solutions in (a) are shown in fig. 6.8.

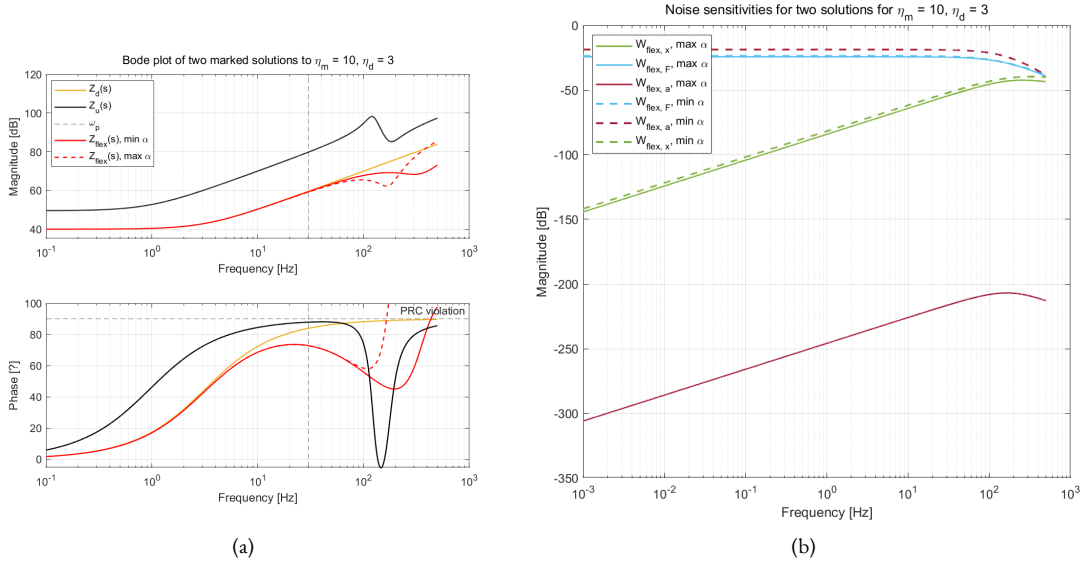


Figure 6.8: Frequency responses (a) and noise transfers (b) of two marked optimal solutions to the case study design problem chosen in fig. 6.7 in comparison with unactuated- $Z_r(s)$ and target $Z_d(s)$ impedance. Only the magnitude of the noise transfers are shown because the phase is not relevant for random noise.

Optimal Design To obtain the optimal controller designs of this system, fig. 6.7 shows the four reduction sets (η_m, η_d) with increasing G_{fd} up to its allowable limit. The optimal paths, as a function of tradeoff α , then trace the bottom-leftmost points. These optimal paths are estimated from the three fractions of G_{fd} , by piecing their bottom-leftmost points together.

The optimal paths for these four reduction sets are shown in fig. 6.6 (b). It is seen that requiring twice the inertia reduction more than halves the robustness. Decreasing the required damping reduction shifts the optimal curve to slightly lower noise, while increasing does not shift the curve much.

This graph does not directly say anything about the gains used along the curves, nor what α exactly is, only what the best reachable tradeoff is. Gain information can be derived from fig. 6.7, when varying α from small (more emphasis on robustness) to big (more emphasis on noise attenuation).

There is a corner tradeoff α_c at $G_{fp} = \eta_m - 1$ and related gains of Ψ_{ideal} , where medium allowable G_{fd} is optimal. Below α_c , along the left of the optimal curves, the optimal G_{fp} and the related gains of Ψ_{ideal} increase while G_{fd} increases. Above α_c , along the bottom of the optimal curves, the optimal G_{fp} and the related gains of Ψ_{ideal} are fixed at $G_{fp} = \eta_m - 1$ while G_{fd} increases.

For minimum noise thus, G_{fp} and the related gains of Ψ_{ideal} must be $G_{fp} = \eta_m - 1$. Increasing G_{fd} then increases robustness. For even larger robustness, but increased noise sensitivity, G_{fp} and the related gains of Ψ_{ideal} must be increased, while G_{fd} decreases, but only up to α_b . Below α_b (upwards in the graphs), a higher G_{fd} increases robustness.

The region of the curve that is slightly concave, around α_b , is never reached for the optimization used here. For the linear cost tradeoff by α , the optimal parametrization can be interpreted as lying somewhere on a line tangent to the origin, of which the angle is determined by α . In such a case, another section of the curve always touches this line before α_b does. These concave points have to either be manually chosen, or using another cost tradeoff, such as a quadratic function. Fig. 6.7 (d) contains this concave section as well, although above the considered gains.

As an example, fig. 6.8 shows the two marked optimal solutions of 6.7 (a), at opposing ends of the optimal curve for allowed gains. Both are seen to have negligible LF impedance error up to ω_p due to Ψ_{ideal} and Ψ_p . The more robust solution (min α) crosses the negative real axis at a higher frequency and at a lower gain, resulting in a stiffer marginally stable spring. This means that increasing G_{fp} and the related gains of Ψ_{ideal} push the flexible mode towards higher frequency. The tradeoff is that the noise sensitivities are much higher, because there is acceleration feedback required for this solution.

Table 6.2: Optimal parameters for the minimization of $\|W_{flex}(s)\|_2$ for the case study system, assuming the flexible link robot model, of the two example points in fig. 6.7 (a).

η_m	η_d	Constraints	α	$\ W_{flex}\ _2$ [N]	\hat{k}_h [$\frac{N}{m}$]	G_{x_p} [$\frac{N}{m}$]	G_{x_d} [$\frac{Ns}{m}$]	G_{f_p} [-]	G_{f_d} [s]	G_{a_p} [kg]	G_{a_d} [kgs]
10	3	$\Lambda_{flex}, \Psi_{Ideal}, \Psi_p$	min	2.202	$9.632 \cdot 10^6$	0	$3.8 \cdot 10^3$	40	0.0435	155	0
10	3	$\Lambda_{flex}, \Psi_{Ideal}, \Psi_p$	max	1.067	$1.337 \cdot 10^6$	0	700	9	0.0106	0	0

6.7 Discussion and Conclusion

This chapter attempts to derive the passive impedance reduction of the flexible model: a flexible link robot with continuous-time controller. However, the higher order of the model quickly complicates analytical manageability, leading to the necessity of numerical analysis instead. Regardless, it was found that inertia reduction is fundamentally limited for the underdamped system. Therefore, stable design must be considered for the case study system of the Gable Core. The main findings in short are described at the beginning of this chapter.

Passive Reduction Passivity analysis was done in three manners with varying success. A novel PE was found to be too unwieldy to directly lead to passivity conditions when considering all feedback options. The fourth order system results in a PRC of relatively simple quadratic-quadratic order polynomial. The extend of its coefficients however, nonlinear in system parameters, are hard to interpret directly. Still, both the numerical evaluation of the PRC for the case study system and a reasoning based on the underdamped system approximation leads to a fundamental limit in inertia reduction ($\eta_m = 1 + m_1 m_2^{-1}$).

This extends the findings of Colgate [3] to include damping, derivative force, PD position and acceleration feedback. However, the fundamental inertia reduction limit remains. For the underdamped system, perhaps counterintuitively, base damping was found to limit inertia reduction to further below this fundamental limit. Still, the fundamental inertia limit can be reached exactly for any damping reduction, but requires exact tuning of derivative gains (G_{f_d}, G_{a_d}). To allow different damping reduction (η_d) during runtime then requires gain scheduling of G_{f_d} and/or G_{a_d} to maintain the limit inertia reduction (η_m).

Passive Pole/Zero Cancellation The described tuning to reach arbitrary η_d is implicitly the same as stable pole/zero cancellation. Here, the target is cancelling additional phase due to a mismatching HF pole and zero pairs. This passive pole/zero cancellation is not robust for small deviations, since there is only a single passivating solution that exactly cancels the phase. This is analogous to why, in control engineering in general, unstable pole/zero cancellation is not practically possible.

Stable Optimal Design Due to the limited passive inertia reduction, stable design must be considered for the case study design. It was shown that, while derivatives G_{f_d}, G_{a_d} do not in practice contribute much to maintaining passivity of the underdamped system, they do contribute to closed loop stability. Their added damping on the flexible mode can dampen the naturally underdamped mode, lowering the amount of phase that violates the PRC. This can remove the existence of a destabilizing environmental damper, stabilizing the robot when uncoupled from a human.

Because any solution to the stable reduction problem already has destabilizing stiffness far above human stiffness, it is recommended to focus on noise reduction. Furthermore, equal reduction of inertia and damping is recommended such that only force feedback is necessary at $G_{f_p} = \eta_m - 1$ for minimal noise. There exists a single optimal G_{f_d} , best evaluated numerically, that provides the highest robustness. The optimal curves are shown to not be completely reachable by a linear tradeoff in cost.

Part IV

Conclusions

Chapter 7

Comparison and Discussion

This chapter compares and discusses the main findings of each chapter, their limitations and possible future work. For in-depth discussion, the reader is referred to the individual chapters.

The previous chapters (ch. 4, ch. 5, ch. 6) analyzed the passive and stable impedance reduction capabilities of the ideal (rigid robot continuous-time controller), hybrid (rigid robot discrete-time controller) and flexible (flexible link robot continuous-time controller) system models respectively according to the structure described in sec. 1.4. Two main comparisons between system models are discussed: on passive impedance reduction in sec. 7.1 and on stable impedance reduction in sec. 7.2. Afterwards, general conclusions are drawn in ch. 8.

7.1 Passivity Analysis

The derived analytical passivity conditions and the corresponding minimal passive impedances of each chapter are shown in table 7.1. Three different methods of passivity analysis were used: the PE, PRC and closed loop stability given an arbitrary passive environment.

Comparison The three system models allow for complete passive damping reduction ($\eta_d = \infty$) by damping compensation. This is indicated in the table by each model having a minimal passive impedance that does not have a damping term. The maximum ideal model passive reduction is infinite, meaning that any combination of η_d, η_m can be achieved passively. In contrast, the passive inertia reductions η_m of both hybrid and flexible systems are severely limited.

The flexible system's lowest passive inertia is limited to that of the end effector regardless of feedback options, masking only the actuator inertia. The addition of more feedback options thus does not improve the best passive reduction found by Colgate [3]. Where base damping causes this limit to be harder to reach, the derivatives of force and/or acceleration make this limit always attainable. Any damping reduction can thus be achieved while maintaining the limit inertia reduction and the reductions are thus uncoupled in theory. Reaching this limit exactly however, is not a practical option due to uncertainty in passive pole/zero cancellation.

System	Condition	Reduction of	Max reduction	Minimal passive impedance $\Omega, \Lambda \hat{Z}(s)$	Remarks
Ideal (4)	Ω_{ideal}	η_m, η_d	∞, ∞	0	-
Hybrid (5)	$\Omega_{hybrid, x, [i]}$	η_d	∞	$m_r s$	Damping compensation
	$\Omega_{hybrid, a}$	η_m	4	$\frac{m_r}{4} s + d_r$	Inertia compensation, scales badly
	$\Omega_{hybrid, f}$	$\eta_m = \eta_d$	0	$m_r s + d_r$	None allowed
	Ω_{hybrid}	η_m, η_d	$\frac{1}{1 - \frac{3}{4\eta_d}}, \eta_d$	$m_r(1 - \frac{3}{4\eta_d})s + \frac{d_r}{\eta_d}$	Trade-off, scales badly
	$\Lambda_{hybrid, f, damped}$	$\eta_m = \eta_d$	∞	0	-
	Λ_{hybrid, f, k_h}	$\eta_m = \eta_d$	$1 + \frac{2d_r}{T k_h}$	$\frac{m_r s + d_r}{1 + \frac{2d_r}{T k_h}}$	Scales well
Flexible (6)	$\Omega_{flex, u.d.}$	η_m, η_d	$1 + \frac{m_1}{m_2}, \infty$	$m_2 s$	Pole/zero cancellation

Table 7.1: Analytically derived passivity (Ω) and stability (Λ) conditions, safe reduction ratios and minimal safe impedances. Equal reduction ($\eta_m = \eta_d$) means that reduction can only be done by the same amount, while unequal (η_m, η_d) means decoupled.

The hybrid system on the surface appears more promising in reducing inertia two- to fourfold. However, this reduction is based on inertia compensation, which scales very disadvantageously with sample time and damping. As a result, modern robots barely allow any passive inertia reduction. In theory, the hybrid model always has a tradeoff between the reduction of damping versus inertia.

Hybrid reduction can directly be compared with flexible reduction, but both must only use position and acceleration feedback. Because the hybrid model does not allow force feedback, force feedback must be omitted from the flexible system reduction for a fair comparison. The maximum reduction ratios are shown numerically in fig. 7.1. In theory, the hybrid model can achieve at least as much inertia reduction as the flexible system, but is barely allowed for the Gable Core. Damping reduction is not the limiting factor, both allowing infinitely much if any inertia reduction is acceptable.

Neither system model can achieve the Gable Core target reduction ($\eta_m = 10, \eta_d = 3$) passively.

Validation All conditions for passivity have at least heuristically been validated. However, as noted in sec. 5.7, they cannot strictly be verified in simulation. This would require evaluation of passivity for *every* input signal, due to aliasing as a result of the sampler, for the hybrid system. However, there is still value in validation by simulation, because this can indicate how restrictive the derived passivity conditions are. If in simulation activity is shown close to the derived passivity condition, that passivity condition is close to the real condition. Because the conditions are only derived to be sufficient, it is currently unclear how restrictive they are.

Physical Equivalent Uniqueness Colgate [3] noted that a PE is not necessarily unique, which opens the possibility that different PE exist for the ideal and flexible systems derived here. Although the passivity conditions for two PE of one system will be the same, one PE can more conveniently lead to the true passivity conditions. This is because obtaining passivity conditions from a PE, by requiring all elements are positive, is potentially restrictive. A different PE may have less restrictive conditions because its elements have different parameters.

In this work, PEs were derived manually, by manually checking decompositions of a transfer for a physical realization. Even after finding a consistent method for derivation, this requires laborious trial and error even for the ideal system. The PE of the ideal system was noted to have at least one other physical interpretation, consisting of one less element but with much more complicated parameters. For the larger system of the flexible link model, the amount of elements grow rapidly, and thus the uniqueness of the PE is not checked. More advanced network synthesis methods, rather than manual labor, may lead convenient derivations of PEs and may confirm their uniqueness.

Impedance Shaping A useful and relatively straightforward addition to this work is the consideration of full impedance shaping rather than solely reduction. A robot that is solely impedance reduced is not yet a functional PHRI robot, in general. Including the shaping of an apparent stiffness or damping increase greatly benefits the functionality of such

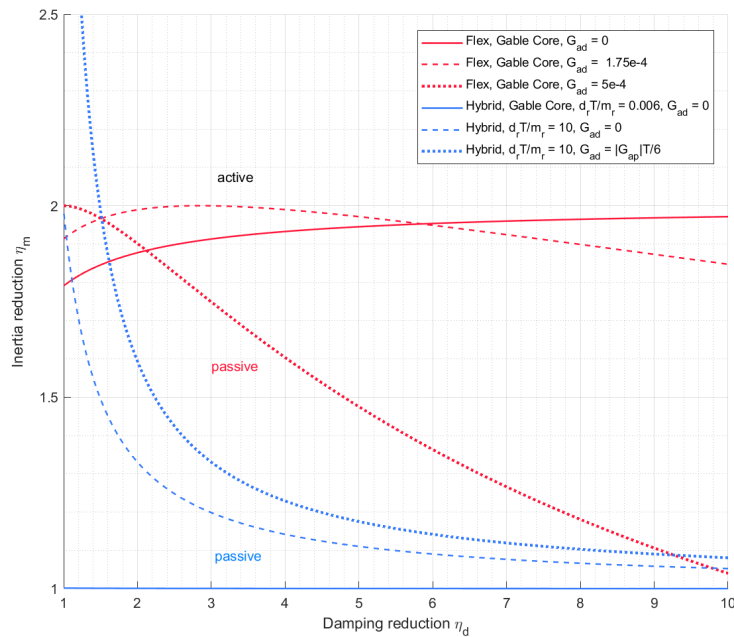


Figure 7.1: Maximum passive reduction of the hybrid system versus the flexible link system, both using only acceleration and position feedback. Systems are passive below the curves. The ideal system spans the entire positive plane. The hybrid Gable Core boundaries practically lie on the x-axis.

robots, allowing resistance training. Position feedback has been included in all passivity conditions, but was omitted as soon as impedance reduction was considered. However, the damping compensation by discrete-time position feedback is known to be limited by the rendered stiffness $\Omega_{\text{hybrid},x,[1]}$. An interesting extension is therefore how this property extends to the flexible system.

Context App. D.10 shows how the ideal and hybrid system models of this work relate to publications by Ott [25] and Albu-Schaeffer [24]. Where this work attempts impedance reduction of the total flexible link inertia, theirs only reduce motor impedance and leave link side inertia unchanged. In the context of the flexible model of this work, any flexibility between rotor and load sensing limits passive motor reduction, although unlikely to be noticeable. In the context of the hybrid model, this work studies the discrete-time controller version of their motor reduction loop. Because no force feedback is passively allowed according to this work, their passive motor reduction is fundamentally not allowed.

With regard to the SEA paradigm, a mathematical equivalence between the SEA and the feedback methods of flexible link robots in this work are shown in app. D.10, although not practically interchangeable. The SEA considers a different impedance as the boundary between robot and environment, where its purpose is never to reduce the end effector inertia. Because SEA literature considers the end effector inertia part of the environment, mechanical SEA design minimizes end effector inertia by design, to avoid this problem entirely. Therefore, the inertia reduction in this work is of a different nature.

Sensor Bandwidth A point of discussion that applies to both the passivity and stability work is the assumption of unlimited sensor bandwidth. Sensor bandwidths were assumed to only influence noise sensitivity, but not passivity and stability. This assumption was made to simplify analytical analysis, whereas including more dynamics in numerical analysis is not hard. Even though it has been illustrated in sec. 3.5 why noise itself does not influence passivity, it has long been known that LP filtering severely influences stability and passivity. This shown by Colgate [3] in short on continuous-time force feedback filtering.

Where absolute position sensing is known to have a large bandwidth, the same cannot be said for force and acceleration sensing, whose outputs are known to be LP filtered by design. This was confirmed in the identification of sec. 3.6. Therefore, any results for position feedback are likely more valid than those for force and acceleration feedback in practice.

This is another reason for limiting the size of force and acceleration derivative gains done in Ψ_p , because the effects of derivative gains are in the HF range, where true bandwidth is unmodeled.

7.2 Stability Analysis

The target passive impedance reductions of ($\eta_m = 10, \eta_d = 3$) for both the hybrid and flexible models were found to be unachievable for the Gable Core. Reaching this reduction thus violates the passivity conditions. Therefore, passivity was forfeit and analysis was extended with the less restrictive stability property. For the case study this means that there exists a destabilizing environmental impedance: a pure spring.

Because passivity was forfeit, all feedback was included and reduction done by solving for Ψ_{ideal} and limited by Ψ_p . Given these constraints, three DOF remain in the controller in general. These are used to optimize a tradeoff between noise sensitivity and robustness in the definition of the optimization (3.11).

Mixed System To complete the comparison between the system models studied in this work, the mixed model is added. This model fully contains both the flexible link and the discrete-time controller. Because analytical analysis is unlikely to be fruitful, given the separate model complexity, no chapter is dedicated to this model. However, numerical stability analysis can still be done, combining the approaches of ch. 5 and ch. 6. Using the same method as sec. 5.6, described in app. C.9, the marginally stable spring can be numerically found when approximating the sampled loop gain to a high order. This is described in short in app. E.1, to be included in the following comparison.

Comparison For each of the system models: ideal, hybrid, flexible and mixed, the optimal tradeoff between destabilizing spring and noise spectra were derived in sec. 4.6, sec. 5.6, sec. 6.6 and app. E.1 respectively. These results are combined in fig. 7.2. The ideal model, has infinite destabilizing spring stiffness because it is stable for any passive environment.

All optimal curves consist of no acceleration derivative feedback ($G_{a,d} = 0$), but varying force derivative feedback ($G_{f,d}$). The bottom of all optimal curves use $G_{f,p} = \eta_m - 1$ for minimal noise. For all models and curves in this graph, larger gains increase the noise sensitivity, but increase robustness, visualized when tracing to the top-left. This reasoning does not continue forever in general, but is the case on these optimal curves for these reduction ratios. The interpretation for the flexible system is that larger gains suppress the flexible mode more, lessening its effect on stability.

From fig. 7.2, three rankings can be made based on required tradeoff: pure robustness, pure noise attenuation, and a tradeoff between the two.

For pure system model robustness, neglecting noise, the ideal model is unsurprisingly the most robust, followed by the flexible, hybrid and mixed models. However, if any noise suppression is desired, the hybrid system becomes more robust than the flexible system. This is indicated by the crossing of their curves at the upper-left of the graph.

For pure system model noise attenuation, neglecting robustness, the ranking is as follows: hybrid, ideal, flex and mixed. The ideal model having higher noise sensitivity than the hybrid system is because of two reasons: added roll-off due to the ZOH and limited evaluation up to the Nyquist frequency, both of which are discussed in the following paragraphs.

Note that all optimal destabilizing stiffnesses for the case study system, seen in the graph, are far above stiffnesses renderable by humans. Approximate destabilizing stiffnesses of the hybrid system at $5 \cdot 10^6 \text{ Nm}^{-1}$ has double the marginally stable stiffness of the flexible link system at $2.5 \cdot 10^6 \text{ Nm}^{-1}$, which has one and a half times the marginally stable stiffness of the mixed system at $1.6 \cdot 10^6 \text{ Nm}^{-1}$. It can therefore be argued that in this case, any tradeoff between noise sensitivity and robustness should favor noise sensitivity, because the system is already robust for human interaction.

Locked Output Noise Estimation All noise sensitivity analyses assume a locked output robot, meaning that the environment is considered to have infinite impedance. The choice for a locked output problem is made to avoid the inclusion of estimated human dynamics in the noise spectra in general. This way, human dynamics need not be estimated or evaluated over an uncertain range. This is thus not a prediction for experienced noise, since humans are dynamical systems and not infinitely rigid. A more realistic prediction of noise perception should include human dynamics and a model of frequency dependent proprioceptive sensitivity. Still, this method allows a fair comparison between systems models, such that conclusions about relative noise sensitivities can be drawn.

The argument can be made that the performance charts of fig. 7.2 already assume a human environment, although unrealistically high, which can be included in the noise sensitivities. However, including the human spring would not allow for comparison with the ideal system, because there no spring is destabilizing. Moreover, including pure stiffnesses was found not to be numerically robust. Due to their high stiffness the noise spectra themselves have very underdamped roots. These underdamped roots require impractically large frequency resolution for numerical estimation of the H_2 norm, which integrates the area under the spectra.

Nyquist Frequency-Bound Evaluation In fact, limited numerical frequency resolution is also one of the two reasons why the noise sensitivities are only evaluated up to the Nyquist frequency. The ZOH in the hybrid noise transfers, both in numerator and denominator, also create underdamped roots occurring at every integer of the sampling frequency. These roots were found to require impractically high resolution, increasing computation time drastically during the optimization of finding the marginally stable springs. The other reason is that, as mentioned in sec. 5.5, the effect of sampling cannot be included in the noise sensitivity of these types of hybrid systems. Therefore, the noise transfers are not considered accurate near and after the Nyquist frequency. To avoid both these issues, the noise transfers are evaluated up to the Nyquist frequency only. As a result, any noise sensitivity underestimates the true locked output noise norm. In addition, it is unclear whether sampling positively or negatively influences the experienced noise.

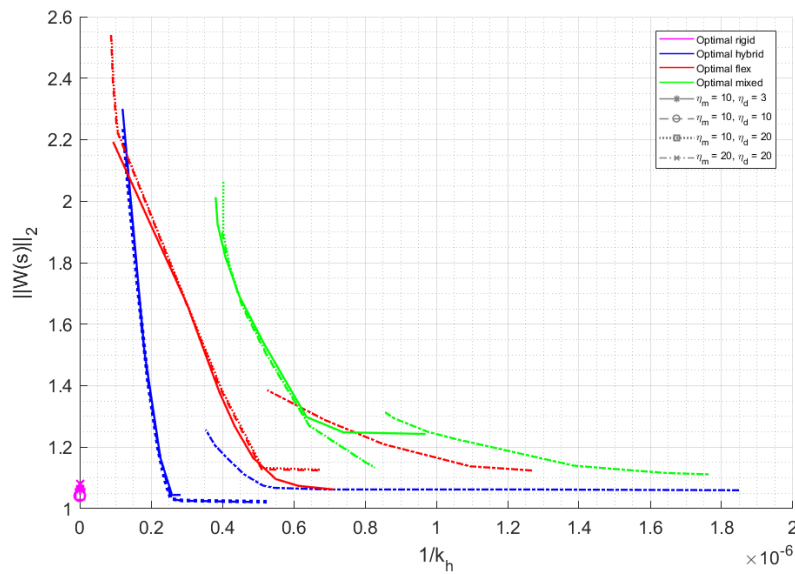


Figure 7.2: Optimal solutions to the minimization problems of (3.11), using gains determined by Ψ_{ideal} and limited by Ψ_P to achieve inertia and damping reduction (η_m, η_d) . Passive solutions lie on the y-axis, represented by a single mark, because there are no destabilizing springs. Stable solutions form a tradeoff curve between noise sensitivity and destabilizing spring stiffness. Bottom-left is considered better.

Hybrid and Mixed Stability Approximations The destabilizing effects of discrete-time acceleration feedback can be less accurate than discrete-time position and force feedback. Where the loop gains of position (5.4) and force (5.5) have large roll-off due to s^{-2} , acceleration (5.6) does not. The stability approximation of app. C.9 approximate the discrete-time loop gain by adding $n = 100$ frequency transposed versions of the same loop. Large roll-off means that when adding transposed loop gains, the effect of adding neighboring loop gains is not as large. Position and force feedback are therefore less affected by sampling than acceleration feedback. Thus, the discrete-time loop gain approximation of acceleration feedback may result in over or underestimated stability margins.

Moreover, the loop gain addition of app. C.9 is based on the superposition principle of linear systems. It can easily be verified for LTI systems that parallel loops may be added in this manner. For the time varying systems studied here, which are not invariant to input delays, this principle is not proven.

However, the stability estimates have seen limited validation in the mixed system of app. E.1 by simulation in Matlab's Simulink and Controllab's 2osim. This showed good fit, suggesting that the loop gain superposition holds for hybrid systems, and that stability of acceleration feedback is accurate enough for order $n = 100$.

Noise Norm Validation Validation of noise norms directly in simulations was found to be cumbersome, because converting the used models to locked output systems spoil preferred simulation causality. As a result algebraic loops occur, which in both simulation engines are solved by including an additional delay. These delays rendered the locked output simulations to noise unstable. To obtain simulations of the locked output systems thus requires rewriting of the models, which is a straightforward step towards further validation.

Instability as a result of a single delay also begs the question how stable these models are to additional delays, not included here. For example, Colgate [3] found that no delays may be introduced to the flexible link system using force feedback to maintain passivity. This agrees with the findings here, although for a different transfer, in that even small delays can severely limit stability and thus passivity. Because any discrete system has computation delay, a straightforward extension of this work should study these effects.

Piecewise Optimal Solutions The optimal curves shown in charts such as fig. 7.2 are piecewise segments obtained from the curves of e.g. fig. 5.6. The same discrete gain sets were chosen for each model, and then the approximate optimal curves pieced together. The true optimal curves can *in theory* be found by numerical optimization.

However, finding the destabilizing stiffness as defined in app. C.9 for hybrid and mixed models is already defined as an optimization problem. Numerical optimization of the true optimal curves thus requires nested optimization, finding the destabilizing stiffness for each trial gain set. Such nested optimization increases computation time extensively, which is avoided in this work. Therefore, the optimal solutions to the hybrid and mixed system models are not truly optimized and the definition of tradeoff factor α is only symbolic. The flexible link system does allow fully automated optimization, because it does not require optimization to find the marginally stable spring. As such, its solutions can give an idea of how close the found curves are to the true optimal curves.

Optimizations are thus in part done manually, which has the potential of finding local rather than global minima.

Stability Analysis Context Where the literature review of ch. 2 includes extensive literature on passive interaction control, the passivity target is forfeit in both chapters with derogatory effects. The optimal stability analyses are therefore not rooted in literature, in contrast to the passivity analyses, but more so in the desire to find working solutions to the case study problem. As a result, there is a lack of context for the latter part of this work. Here, it was found that the flexible model is more derogatory than the hybrid model for the Gable Core. Interesting future work could consider varying system parameters to observe the effects on this comparison. Such research can lead to important design recommendations.

Identification The identified case study of sec. 3.7 shows that the single flexible mode model of ch. 6 decently fits the spectral data in the HF range. Estimation of the masses was confirmed by the robot's Solidworks source material to be within a couple kg. However, the middle frequency range identification of base damping appears magnitudes higher than is haptically present in the physical system. There are two main explanations for this mismatch between practice and measurement. First, physical damping is nonlinear in nature especially for smaller actuation, which does not fit with the assumed linear models and can severely mismatch the identification data. A coherence analysis can confirm these nonlinearities, which is not performed here. Second, dynamics missed in the fitted model, such as base stiffness of the robot identification setup and end effector damping. End effector damping in particular of the case study system is likely significant, because of linear bearings in the extending sleeve of fig. 3.4. The models in this work, neglecting end effector damping, are thus possibly not sufficient for this case study. To keep the system models simple, the inclusion of these added dynamics was avoided. Therefore, the LF behavior was measured ad hoc and fit to be compatible with the more accurate HF fit.

Chapter 8

Conclusions

This work studied several knowledge gaps on the interaction control of physical human-robot interaction systems. Namely, safely improving the human experience of inherent robot dynamics, referred to as impedance reduction. As a case study for a system requiring impedance reduction the Gable Core rehabilitation platform, introduced in 1.1, was studied.

To facilitate safe impedance reduction, the first priority was set on passive impedance reduction, limiting interaction energy to that generated by the human. Where passivity was found to be too restrictive, coupled stability was considered instead. Passivity analysis was done analytically, while stability analysis was mainly done numerically.

The literature study of ch. 2 found that passive impedance reduction using impedance control is underrepresented in modern literature. This is the case especially when applied to hybrid and flexible link systems. Moreover, force and acceleration feedback is rarely applied in this context, in addition to common position feedback.

To address these issues, the reduction of three system models was considered: the ideal, the hybrid and the flexible link system. Each system was studied through a consistent structure defined in sec. 1.5. The impedance controller was considered to linearly add PD position, interaction force and end-effector acceleration, resulting in six feedback paths. Ch. 3 describes the impedance reduction goals, methods to analyze passivity and modern optimal design using a tradeoff between noise sensitivity and robustness.

The ideal system model, a rigid robot with continuous-time control, of ch. 4 expands upon Colgate [3] from proportional force feedback to include all six feedback paths. Novel passivity conditions were found by a physical equivalent, and the system was shown to be passively reducible to any impedance. This states the benefit of this method of impedance reduction, especially considering force feedback, lowering even nonlinear parasitic dynamics.

The hybrid system model, a rigid robot with discrete-time control, of ch. 5 expands upon Colgate [1] by adding discrete-time PD force and acceleration feedback. It was found that the hybrid system does not allow any force feedback passively. Therefore, any reduction must be due to acceleration and position feedback. Although promising in theory, in practice the achievable passive inertia reduction is negligible, while damping reduction is fully allowed.

The flexible system model, an underdamped flexible link robot with continuous-time control, of ch. 6 expands upon the undamped system of Colgate [3] by including damping and all six feedback paths. Regardless, the same fundamental inertia reduction limit of only masking the actuator inertia must be respected. At the same time, full damping reduction is allowed. To reach this inertia masking exactly, derivative feedback of force or acceleration must be included, because base damping lowers the limit otherwise. This requires exact tuning of the derivative gains, which is not realistic in practice.

Both derogatory systems have been shown to be severely limited in passive inertia reduction in ch. 7.1. Therefore, the case study system must consider stability, rather than passivity, to achieve its reduction targets. This underlines the restrictiveness of passive interaction control, adding to the old but ongoing discussion.

Even though passivity was forfeit, the stability conditions of the case study system were inherently acceptable for pure human interaction. Optimal design for all models, balancing noise sensitivity and robustness, is best focused on noise reduction. To this end, all systems prefer the use of solely force feedback and its derivative, minimizing feedback complexity. Ch. 7.2 shows that with respect to stability and noise sensitivity, the hybrid system model is the least derogatory, followed by the flexible link system model, and finally the combined hybrid and flexible system model. This is in contrast to passive design, which found the hybrid system model to be more derogatory than the flexible link system model.

Part V

Appendix

Appendix A

Appendix to Chapter 3

A.1 Definition: LTI Frequency Passivity

Colgate [3] showed that the transfer function $Z(s)$ of a one-dimensional LTI system is passive if and only if it is a positive real function:

$$\operatorname{Re}\{Z(s)\} \geq 0 \quad \forall \sigma \geq 0, \quad \omega \in \mathbb{R}. \quad (\text{A.1})$$

This is referred to as the positive real condition (PRC), and demands that the Nyquist plot of $Z(s)$ is in the RHP. The requirement can be split into three sub-requirements which are often more easily checked:

1. $Z(s)$ has no poles in the right half plane.
2. Any imaginary poles of $Z(s)$ are simple, and have positive real residues.
3. $\operatorname{Re}\{Z(i\omega)\} \geq 0$.

The first requirement is stability, the second is pole simplicity (no identical imaginary poles), and the last requirement is simply the purely complex part of the Nyquist contour. The first and second take care of the infinite radius semicircular arc of tracing the Nyquist contour.

Alternatively, the second and third requirements can be combined into one:

1. $Z(s)$ has no poles in the right half plane.
2. $Z(s)$ has a Nyquist plot that lies in the right half plane.

As a result of these conditions, it must follow that all zeros and poles of $Z(s)$ are stable.

A.2 Definition: Nyquist Criterion

For a feedback loop with characteristic equation $1 + L(s)$, with P_{OL} amount of unstable open-loop poles of $L(s)$, the Nyquist criterion is

$$Z_{CL} = N_{CW} + P_{OL}. \quad (\text{A.2})$$

Where N_{CW} is the number of clockwise encirclements of -1 by $L(s)$ when tracing the Nyquist contour \mathcal{D} , and Z_{CL} is the number of unstable roots of the characteristic equation. Consequently, for stability the number of unstable poles Z_{CL} of the closed-loop system must be zero.

Thus, for every unstable open-loop pole P_{OL} of $L(s)$ there must be one counter-clockwise encirclement of -1 by $L(s)$.

The Nyquist contour \mathcal{D} is the following path, in polar coordinates (r, ϕ) , starting at $(0, 0)$:

- Traveling up the imaginary axis: $(0 \rightarrow \infty, \pi)$.
- Rotating along a positive real semicircle: $(\infty, \pi \rightarrow -\pi_+)$, approaching $(\infty, -\pi)$ from the right side.
- Returning to zero from the negative infinite imaginary axis: $(\infty \rightarrow 0, -\pi)$.

A.3 Real and Imaginary Parts of a Complex Ratio

Any complex ratio $Z = Z_N/Z_D$ can be written as the following split parts real and imaginary:

$$Z = \frac{Z_N}{Z_D} = \frac{P_R + iP_I}{\text{Re}\{Z_D\}^2 + \text{Im}\{Z_D\}^2},$$

where

$$\begin{aligned} P_R &= \text{Re}\{Z_N\} \text{Re}\{Z_D\} + \text{Im}\{Z_N\} \text{Im}\{Z_D\} \\ P_I &= \text{Im}\{Z_N\} \text{Re}\{Z_D\} - \text{Re}\{Z_N\} \text{Im}\{Z_D\}. \end{aligned}$$

The denominator is always positive because of the squares, such that the signs of the real and imaginary parts are determined only by P_R and P_I respectively. This is useful because for example the dissipative part P_R can then be used to test the PRC:

$$\text{Re}\{Z(i\omega)\} > 0 \iff P_R(\omega) > 0.$$

A.4 Manual Physical Equivalent Synthesis

This section states some rules for rewriting transfers to separate into passively realizable parts manually. The difference in order of a transfer to be split as a PE is at most one. In addition, the denominator must have an equal or fewer number of terms. If a transfer cannot be split as such, it must be inverted.

The simplest transfer can be trivially split into two elements as follows:

$$\begin{aligned} \frac{as + b}{c} &= \frac{as}{c} + \frac{b}{c} \\ \frac{as + b}{cs} &= \frac{a}{c} + \frac{b}{cs}. \end{aligned}$$

A lead-lag equivalent can be split in two ways:

$$\frac{as + b}{cs + d} = \frac{as}{cs + d} + \frac{b}{cs + d} = \frac{a}{c} + \frac{(b - da/c)}{cs + d}.$$

Its derivative only has one option:

$$\frac{as^2 + bs}{cs + d} = \frac{as}{c} + \frac{s(b - da/c)}{cs + d}.$$

The following has two options:

$$\frac{as^2 + bs + c}{ds^2 + es} = \frac{a}{d} + \frac{s(b - ae/d) + (c)}{ds^2 + es} = \frac{as}{ds + e} + \frac{bs + c}{ds^2 + es}.$$

When adding a denominator term there is only one option:

$$\frac{as^2 + bs + c}{ds^2 + es + f} = \frac{a}{d} + \frac{s(b - ae/d) + (c - af/d)}{ds^2 + es + f}.$$

And for their derivatives:

$$\begin{aligned} \frac{as^3 + bs^2 + cs}{ds^2 + es} &= \frac{as}{d} + \frac{s^2(b - ae/d) + s(c)}{ds^2 + es} = \frac{as^2 + bs}{ds + e} + \frac{c}{ds + e} \\ \frac{as^3 + bs^2 + cs}{ds^2 + es + f} &= \frac{as}{d} + \frac{s^2(b - ae/d) + s(c - af/d)}{ds^2 + es + f}. \end{aligned}$$

And with added numerator term:

$$\frac{as^3 + bs^2 + cs + d}{es^2 + fs + g} = \frac{as}{e} + \frac{s^2(b - af/e) + s(c - ag/e) + d}{es^2 + fs + g}.$$

The general rule for this type of partial fraction decomposition is:

$$\frac{a_n s^n + \dots + a_0}{b_{n-1} s^{n-1} + \dots + b_0} = \frac{a_n s}{b_{n-1}} + \frac{\sum_{m=1}^n s^{m-1} (a_{m-1} - a_n b_{m-2}/b_{n-1})}{b_{n-1} s^{n-1} + \dots + b_0}.$$

Appendix B

Appendix to Chapter 4

B.1 Rigid Robot Continuous-Time Controller PRC Without Derivatives

If $Z(s)$ is the impedance

$$Z(s) = \frac{(m_r + G_{a_p})s + d_r + G_{x_d} + G_{x_p}s^{-1}}{G_{f_p} + 1}$$

then according to A.1, the real part of $Z(s)$ must be larger than or equal to zero on the Nyquist contour. In this case it is convenient to check directly for $s = i\omega + \sigma$ instead of the more common three individual properties of the PRC. Substituting $s = i\omega + \sigma$ and using app. A.3 yields:

$$\operatorname{Re}\{Z(i\omega + \sigma)\} = \frac{d_r + G_{x_d} + (m_r + G_{a_p})\sigma + G_{x_p}/(\omega^2 + \sigma^2)}{G_{f_p} + 1} \geq 0, \quad \forall \sigma \geq 0, \quad \forall \omega.$$

With more general notation

$$\operatorname{Re}\{Z(i\omega + \sigma)\} = d(\omega^2 + \sigma^2) + m\sigma(\omega^2 + \sigma^2) + k \geq 0,$$

where d, m, k are defined below. Setting $\omega = \sigma = 0$ requires that $k \geq 0$, because then

$$\operatorname{Re}\{Z(i\omega + \sigma)\} \propto k.$$

Setting $\sigma = 0, \omega \neq 0$ requires $d \geq 0$, because then

$$\operatorname{Re}\{Z(i\omega + \sigma)\} \propto d\omega^2 + k.$$

Setting $\sigma \neq 0, \omega = 0$ requires that $m \geq 0$, because then

$$\operatorname{Re}\{Z(i\omega + \sigma)\} \propto d\sigma^2 + m\sigma^3 + k.$$

For the PRC to hold at these extreme points, all three coefficients of the polynomial must be positive. As a result, the original polynomial is then positive real for all ω and $\sigma \geq 0$. The conditions are then:

$$\begin{aligned} d &= \frac{d_r + G_{x_d}}{G_{f_p} + 1} \geq 0 \\ m &= \frac{m_r + G_{a_p}}{G_{f_p} + 1} \geq 0 \\ k &= \frac{G_{x_p}}{G_{f_p} + 1} \geq 0. \end{aligned}$$

B.2 Rigid Robot Continuous-Time Controller PRC Including Derivatives

The apparent impedance for the ideal system with all feedback is:

$$Z(s) = \frac{G_{a_d}s^3 + (m_r + G_{a_p})s^2 + (d_r + G_{x_d})s + G_{x_p}}{G_{f_d}s^2 + (1 + G_{f_p})s}.$$

Following the two requirements of the PRC of app. A.1:

1. Stability demands that:

$$\frac{1 + G_{f_p}}{G_{f_d}} \geq 0.$$

2. A positive real gain at DC requires that

$$Z(0) = \frac{G_{x_p}}{1 + G_{f_p}} \geq 0.$$

Then $1 + G_{f_p}$ must be the same sign as G_{x_p} , which must be positive to emulate passive springs. As a result of the stability condition, then G_{f_d} must be positive too. A positive real gain at positive infinite s requires that the highest term of $Z(s)$ is positive:

$$Z(\infty) = \frac{G_{a_d}}{G_{f_d}} \geq 0.$$

Because the sign of G_{f_d} must be positive, so must G_{a_d} . This yields the first four requirements:

$$\begin{aligned} G_{x_p} &\geq 0 \\ G_{f_p} + 1 &\geq 0 \\ G_{f_d} &\geq 0 \\ G_{a_d} &\geq 0. \end{aligned}$$

Substituting $s = i\omega$ and using app. A.3, the complex part is proportional to:

$$\text{Re}\{Z(i\omega)\} \propto \omega^4 (G_{f_d}(m_r + G_{a_p}) - G_{a_d}(1 + G_{f_p})) + \omega^2 ((1 + G_{f_p})(d_r + G_{x_d}) - G_{f_d}G_{x_p}) \geq 0.$$

For this polynomial to be positive real, both coefficients of the polynomial in ω must be positive:

$$(1 + G_{f_p})(d_r + G_{x_d}) - G_{f_d}G_{x_p} \geq 0$$

$$G_{f_d}(m_r + G_{a_p}) - G_{a_d}(1 + G_{f_p}) \geq 0.$$

All terms except $(d_r + G_{x_d})$ in the first requirements are known to be positive, which fixes $(d_r + G_{x_d})$ to be positive as well. The same logic can be applied to $(m_r + G_{a_p})$ in the second requirement. All requirements combined are then:

$$\begin{aligned} G_{x_p} &\geq 0 \\ G_{x_d} &\geq -d_r \\ G_{a_p} &\geq -m_r \\ G_{f_p} &\geq -1 \\ \frac{(d_r + G_{x_d})(G_{f_p} + 1)}{G_{x_p}} &\geq G_{f_d} \geq 0 \\ \frac{(m_r + G_{a_p})G_{f_d}}{G_{f_p} + 1} &\geq G_{a_d} \geq 0. \end{aligned}$$

Note that the two last conditions imply the second and third, given the other conditions. However, these are still explicitly included for clarity on all individual feedback terms.

B.3 Rigid Robot Continuous-Time Controller PE

The transfer is

$$Z(s) = \frac{G_{a_d}s^3 + (m_r + G_{a_p})s^2 + (d_r + G_{x_d})s + G_{x_p}}{G_{f_d}s^2 + (1 + G_{f_p})s}.$$

The general forms of app. A.4 are shown here to give options for splitting. Black boxed equations are the retrieved simple physical elements (mass, spring or damper), as impedance (Z) or admittance (Y). The transfer is of type

$$\frac{as^3 + bs^2 + cs + d}{es^2 + fs + g} = \boxed{\frac{sa}{e}}^{Z_1} + \frac{s^2(b - af/e) + s(c - ag/e) + d}{es^2 + fs + g},$$

where

$$a = G_{a_d}, \quad b = m_r + G_{a_p}, \quad c = d_r + G_{x_d}, \quad d = G_{x_p}, \quad e = G_{f_d}, \quad f = G_{f_p} + 1, \quad g = 0.$$

The right-hand ratio is of type

$$\frac{As^2 + Bs + C}{Ds^2 + Es} = \frac{A}{D} + \frac{s(B - AE/D) + C}{Ds^2 + Es} = \frac{As}{Ds + E} + \frac{Bs + c}{Ds^2 + Es},$$

where

$$A = b - af/e, \quad B = c, \quad C = d, \quad D = e, \quad E = f.$$

Choosing the right-hand equality leads to a simpler PE, although with one more element. The first element of the right-hand side are two other elements:

$$\frac{Ds + E}{As} = \boxed{\frac{D}{A}}^{Y_2} + \boxed{\frac{E}{As}}^{Y_3}.$$

The second element of the right hand-side can be inverted and is then of form

$$\frac{Ds^2 + Es}{Bs + c} = \boxed{\frac{Ds}{B}}^{Y_4} + \frac{s(E - DC/B)}{Bs + C}.$$

Of which the right-hand can be inverted again to give

$$\boxed{\frac{B}{E - DC/B}}^{Z_5} + \boxed{\frac{C}{s(E - DC/B)}}^{Z_6}.$$

All these element impedances and admittances are shown in fig. B.1, substituting the system parameters then obtains the PE of fig. 4.2.

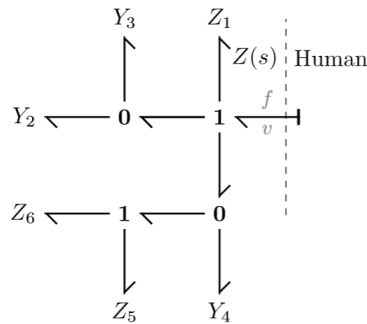


Figure B.1: Bond graph used when deriving the PE of the rigid robot continuous-time controller with unevaluated parameters.

B.4 Inertia Cancellation of the Rigid Robot Continuous-Time Controller by G_{fd}

Instead of considering G_{fd}, G_{ad} to be detrimental and introducing a less convenient physical interpretation in fig. 4.2 (a), there is one case where the interpretation is simple and beneficial. If $G_{xp} = G_{ad} = 0$, the transfer becomes a lead-lag compensator:

$$Z(s) = \frac{(m_r + G_{ap})s + (d_r + G_{xd})}{G_{fd}s + (1 + G_{fp})}.$$

The inertia behavior can be completely annihilated ($m_d = 0, \eta_m = \infty$), resulting in a pure damper d_d equivalence, by setting the pole and root equal. Conditions that result in a pure damper d_d are:

$$\begin{aligned} G_{xp} &= 0 \\ G_{ad} &= 0 \\ \frac{d_r + G_{xd}}{1 + G_{fp}} &= d_d \\ \frac{G_{fd}}{1 + G_{fp}} &= \frac{m_r + G_{ap}}{d_r + G_{xd}}. \end{aligned}$$

This cancels the HF zero of (4.1) with its pole, which is allowed because both numerator and denominator have stable roots for positive coefficients. Because this cancellation occurs around zero phase delay, the passivity of the system is robust against parameter estimation errors.

Appendix C

Appendix to Chapter 5

C.1 Definition: Starred Transform

The definition of the starred transform as given by Jury [68] is the infinite sum of transfers transposed by the sample frequency ω_s :

$$[H(s)]^* = \frac{1}{T} \sum_{n=-\infty}^{+\infty} H(s + i\omega_s n), \quad \omega_s = \frac{2\pi}{T}. \quad (\text{C.1})$$

Splitting the sum into a numerator $N(s)$ and denominator $D(s)$ shows that the resulting transfer has infinitely many of the original poles, but transposed. This is illustrated for two terms of the infinite series:

$$\sum_{n=-\infty}^{+\infty} H(s + i\omega_s n) = \frac{N(s)}{D(s)} + \frac{N(s + i\omega_s)}{D(s + i\omega_s)} + \dots, \quad D(s) = K(s - p_1)(s - p_2)\dots$$

The starred transform in a single fraction is thus

$$\frac{N(s + i\omega_s)D(s) + N(s)D(s + i\omega_s) + \dots}{D(s)D(s + i\omega_s)\dots},$$

which has poles

$$D(s)D(s + i\omega_s)\dots = (K(s - p_1)(s - p_2)\dots)(K(s + i\omega_s - p_1)(s + i\omega_s - p_2)\dots)$$

The real parts of the poles are unchanged, and therefore stability is maintained. This is also an implicit result from C.8, because if the starred transform preserves passivity then it preserves stability as well.

C.2 Rigid Robot With Discrete-Time Controller Transfer

Fig. 5.1 can be rewritten to the block diagram in fig. C.1, from which attempting to determine the transfer from $F(s)$ to $V(s)$ is more obvious:

$$V(s) = Y_r(s)F(s) - Y_r(s)\tilde{D}(z) [N(s)V(s)]^* \quad (\text{C.2})$$

Multiply both sides by $N(s)$ and star-transform each side

$$[N(s)V(s)]^* = [N(s)Y_r(s)F(s)]^* - [N(s)Y_r(s)]^* \tilde{D}(z)[N(s)V(s)]^*$$

Solving for $[N(s)V(s)]^*$:

$$[N(s)V(s)]^* = \frac{[N(s)Y_r(s)F(s)]^*}{1 + [N(s)Y_r(s)]^* \tilde{D}(z)}$$

Substitute back into the right hand side of (C.2) gives the result

$$V(s) = Y_r(s)F(s) - Y_r(s) \frac{\tilde{D}(z) [N(s)Y_r(s)F(s)]^*}{1 + \tilde{D}(z) [N(s)Y_r(s)]^*}$$

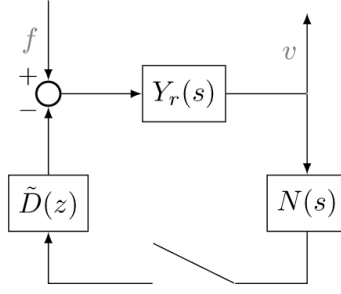


Figure C.1: Fig. 5.1 rewritten to a simple feedback loop to attempt to determine the relationship between f and v .

C.3 Rigid Robot Discrete-Time Position Feedback Passivity (Alternative to [1])

The loop gain of discrete-time position feedback is:

$$L_x(s) = \tilde{D}_x(z)[H_x(s)]^* = \tilde{D}_x(z) \left[\frac{1}{s^2} \frac{1}{Z_h(s) + Z_r(s)} \right]^*.$$

Define the admittance as $Y_{hr}(s)$:

$$Y_{hr}(s) = \frac{1}{Z_h(s) + Z_r(s)}.$$

Colgate [1] recognized that for arbitrary passive $Z_h(s) \in \mathbf{Z}_0$ in the RHP this admittance is bound to a frequency independent complex region for every frequency, here denoted by \mathbf{Y}_{hr} :

$$Y_{hr}(s) \in \mathbf{Y}_{hr}.$$

This region is always a disk from the origin to $1/d_r$ as shown in fig. C.2. Using (C.5), the loop gain can be shown to lie in:

$$L_x(s) \in \mathbf{L}_x(s) = \tilde{D}_x(z) \left[\frac{1}{s^2} \right]^* \mathbf{Y}_{hr}.$$

And the starred transform of the double integrator can be found to be [70]:

$$\left[\frac{1}{s^2} \right]^* = \frac{1}{2} \frac{T}{\cos(\omega T) - 1}.$$

The loop gain is then contained in:

$$\mathbf{L}_x(s) = \tilde{D}_x(z) \frac{1}{2} \frac{T}{\cos(\omega T) - 1} \mathbf{Y}_{hr}.$$

This is visualized in fig. C.2 as the product of the left-hand side with the circular region of the right-hand side. The unambiguously worst-case scenario to contain -1 is when $\mathbf{L}_x(s)$ is purely real and the most negative. This occurs when $\tilde{D}_x(z) \left[\frac{1}{s^2} \right]^*$ is most negative, because \mathbf{Y}_{hr} is a static circular region.

Let $\overline{\text{Re}}\{\cdot\}$ denote the *purely* real part of a function, where $\text{Im}\{\cdot\} = 0$. From fig. C.2 it is seen that after multiplying both parts the left bound is:

$$\min \overline{\text{Re}}\{\mathbf{L}_x(s)\} = -\frac{G_{x_p} T/2 + G_{x_d}}{d_h}, \quad G_{x_d} \geq 0$$

$$\min \overline{\text{Re}}\{\mathbf{L}_x(s)\} = -\frac{G_{x_p} T/2 - G_{x_d}}{d_h}, \quad G_{x_d} \leq 0$$

Regardless of the sign of G_{x_d} , the minimum is the following, which must be larger than -1 for Nyquist stability:

$$\min \overline{\text{Re}}\{\mathbf{L}_x(s)\} = -\frac{G_{x_p} T/2 + |G_{x_d}|}{d_h} \geq -1$$

Rearranging gives the known result:

$$d_h \geq G_{x_p} \frac{T}{2} + |G_{x_d}|, \quad G_{x_p} > 0$$

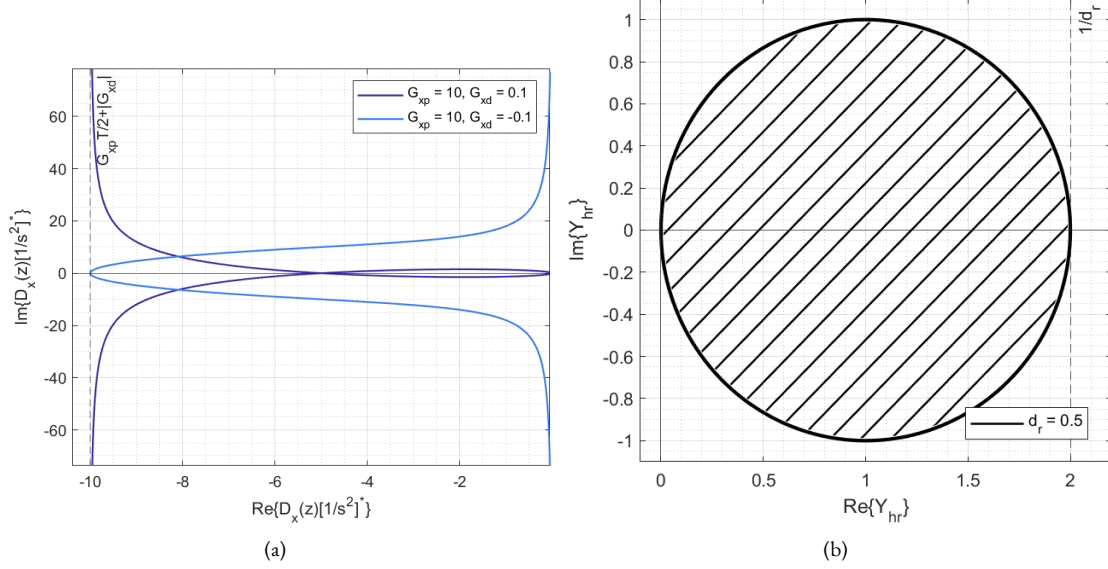


Figure C.2: The two multiplied parts (a) and (b) of the discrete-time position feedback loop gain $\mathbf{L}_x(s)$ in the complex plane. Note that changing the sign of G_{x_d} swaps part of the left locus but leaves the same bounds.

C.4 Rigid Robot Discrete-Time Force Feedback Passivity

The loop gain of discrete-time force feedback is:

$$L_f(s) = \tilde{D}_f(z)[H_f(s)]^* = \tilde{D}_f(z) \left[\frac{1}{s} \frac{Z_h(s)}{Z_h(s) + Z_r(s)} \right]^*.$$

Define the impedance ratio as $A(s)$:

$$A(s) = \frac{Z_h(s)}{Z_h(s) + Z_r(s)}.$$

Given that the human impedance spans the RHP ($Z_h(s) \in \mathbf{Z}_0$), this is a division of the numerator RHP with an offset RHP in the denominator. This offset is determined by $Z_r(i\omega) = i\omega m_r + d_r$, where ω may be anything. The offset is thus a constant d_r along the real axis and may be anything along the imaginary axis. The division of a RHP by another RHP arbitrarily shifted along $i\omega$ spans the entire complex plane, because any point in the RHP may be rotated by $[-\frac{\pi}{2}, \frac{\pi}{2}]$. Consequently, the division of a RHP by another RHP arbitrarily shifted along $i\omega m_r + d_r$ spans the entire complex plane except for the purely real negative strip.

Excluding of the negative real strip can be illustrated by substituting the worst-case environment for spanning as far left as possible: a purely imaginary element $Z_h(s) = iy_h(\omega)$ which can be arbitrary large. Substituting leads to:

$$A(s) = \frac{y_h(\omega)(m_r\omega + y_h(\omega)) + id_r y_h(\omega)}{d_r^2 + (m_r\omega + y_h(\omega))^2}.$$

On the negative real strip the imaginary part is zero, which is only when $y_h(\omega) = 0$, for assumed nonzero d_r . However, for $y_h(\omega) = 0$ the real part is always zero and thus $A(s)$ can not be negative purely real. In contrast, on the positive real strip the imaginary part is zero too, but this can be attained for $y_h(\omega) = \infty$ for e.g. a spring at DC frequency.

Because $A(s)$ spans the complex plane (except the purely real negative strip) any rotation of $A(s)$ by $1/s$ or $\tilde{D}_f(z)$ will include -1 , meaning that there always exists a destabilizing $Z_h(s)$. This means the system is active and there is no non-zero $\tilde{D}_f(z)$ and thus force feedback gain that maintains passivity.

Assumptions must be made about the environment $Z_h(s)$ to get insight into stability. Two cases are shown here, which together give sufficient stability conditions for the environment having simple parallel form:

$$Z_h(s) = m_h s + d_h + k_h/s.$$

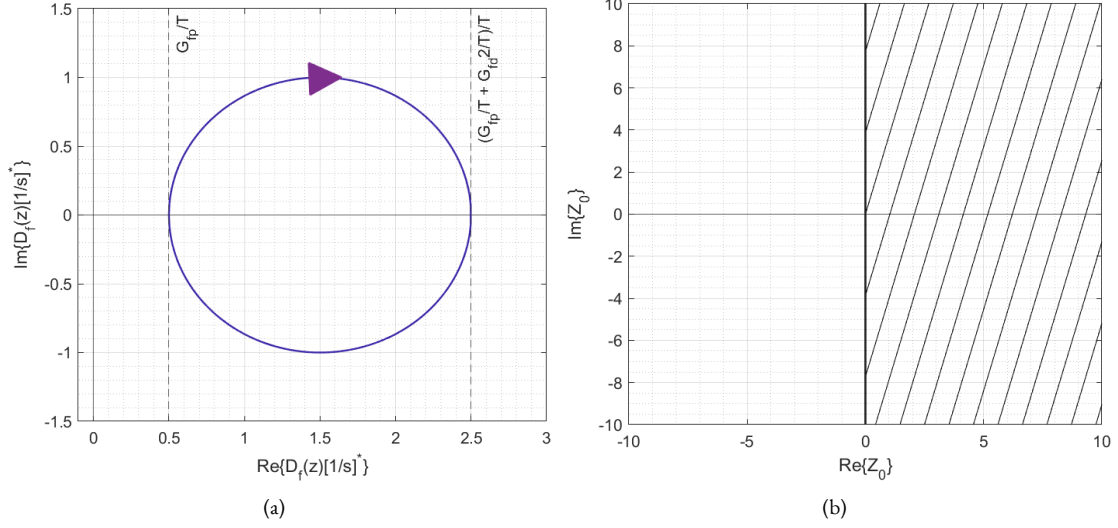


Figure C.3: The two multiplied parts (a) and (b) of the discrete-time force feedback loop gain $\mathbf{L}_f(s)$ in the complex plane if $Z_h(s)$ is sufficiently damped.

C.4.1 Limited Resonance

If the parallel form has sufficient damping:

$$d_h(d_h + d_r) \geq k_h(2m_h + m_r),$$

then the impedance ratio $A(s)$ is positive real according to app. C.5 and is in the RHP:

$$A(s) \in \mathbf{Z}_0.$$

Using (C.5) the loop gain is contained in:

$$L_f(s) \in \mathbf{L}_f(s) = \tilde{D}_f(z) \left[\frac{1}{s} \right]^* \mathbf{Z}_0.$$

And the starred transform of the single integrator is:

$$\left[\frac{1}{s} \right]^* = \frac{1}{1 - e^{-sT}} = \frac{1}{\bar{h}(z)T},$$

which cancels out with the finite difference in $\tilde{D}_f(z)$. The loop gain is then contained in:

$$\mathbf{L}_f(s) = \frac{G_{f_p} + \bar{h}(z)G_{f_d}}{T} \mathbf{Z}_0.$$

This product is visualized in fig. C.3. The only way for $\mathbf{L}_f(s)$ with positive G_{f_p} to contain -1 is when the left part becomes negative real. reveals that for positive G_{f_p} the condition for to never touch -1 is:

$$0 < G_{f_p} \frac{T}{2} + G_{f_d}, \quad G_{f_p} \geq 0$$

Thus, for any positive control parameters the system should be stable, although G_{f_d} may be negative.

C.4.2 Pure Environmental Stiffness

If the environment is assumed to be a pure spring

$$Z_h(s) = k_h s^{-1},$$

substituting into (5.5) reveals that the problem becomes analogous to the discrete-time position feedback problem in C.3, because the continuous-time part of the loop gain is then:

$$H_f(s) = \frac{1}{s^{-1} + k_h^{-1} Z_r(s)} s^{-2},$$

which is analogous to the position feedback continuous-time part:

$$H_x(s) = \frac{1}{Z_h(s) + Z_r(s)} s^{-2}.$$

Such that now the human $Z_h(s)$ is replaced by an integrator and the robot dynamics are scaled by k_h . Then, a sufficient stability condition is analogous too and can be substituted directly as:

$$\frac{d_r}{k_h} > \frac{G_{f_p} T}{2} + |G_{f_d}|, \quad G_{f_p} \geq 0.$$

C.5 Lemma: Positive Realness Condition of $A(s)$

Starting with the impedance ratio

$$\frac{Z_h(s)}{Z_h(s) + Z_r(s)},$$

and evaluating numerator and denominator for $s = i\omega$ with the parallel environment $Z_h(s) = m_h s + d_r + k_h/s$:

$$Z_h(i\omega) = d_h + i(m_h \omega - k_h/\omega)$$

$$Z_h(i\omega) + Z_r(i\omega) = d_h + d_r + i((m_h + m_r)\omega - k_h/\omega).$$

The sign of the real part, according to app. A.3, is determined by:

$$d_h(d_h + d_r) + m_h(m_h + m_r)\omega^2 + \frac{k_h^2}{\omega^2} - k_h(2m_h + m_r).$$

Given that the polynomial terms of ω are always positive because they are squared, a sufficient condition for this function to be positive regardless of ω is:

$$d_h(d_h + d_r) \geq k_h(2m_h + m_r).$$

In that case the impedance ratio is guaranteed positive real:

$$\text{Re} \left\{ \frac{Z_h(s)}{Z_h(s) + Z_r(s)} \right\} \geq 0.$$

C.6 Minimal Passive Impedance for Combined Discrete-Time Position and Acceleration Feedback

For discrete-time position feedback the passivity condition using the conceptually split robot is:

$$(1 - \mu)d_r > G_{x_p} \frac{T}{2} + |G_{x_d}|, \quad G_{x_p} \geq 0.$$

When impedance reduction is the target, negative G_{x_d} can compensate inherent damping d_r and the rewritten condition is:

$$G_{x_d} > G_{x_p} \frac{T}{2} - (1 - \mu)d_r, \quad G_{x_p} \geq 0, G_{x_d} < 0.$$

And discrete-time negative acceleration feedback, when using approximate condition ($\Omega_{\text{hybrid},a}$), results in:

$$G_{a_p} \leq 0, \quad G_{a_d} \leq |G_{a_p}| \frac{T}{6},$$

$$G_{a_p} + G_{a_d} \frac{2}{T} > -\mu \frac{m_r}{2} (1 - e^{-\frac{d_r}{2m_r} T}).$$

The combination of these condition can be denoted $\Omega_{\text{hybrid},x,a}$. For maximum inertia reduction, G_{a_p} should be minimized, using maximum allowed positive G_{a_d} :

$$G_{a_p} \leq 0, \quad G_{a_d} = |G_{a_p}| \frac{T}{6},$$

After substitution the condition is:

$$G_{a_p} + |G_{a_p}| \frac{1}{3} > -\frac{m_r}{2} (1 - e^{-\frac{d_r}{2m_r} T}).$$

Which, due to $G_{a_p} < 0$, results in:

$$G_{a_p} > -\mu \frac{3m_r}{4} (1 - e^{-\frac{d_r}{2m_r}T}).$$

Substituting both conditions:

$$Z_{\text{hybrid, x, a, min}}(s) = m_r \left(1 + \mu \frac{3}{4} \left(e^{-\frac{d_r}{2m_r}T} - 1 \right) \right) s + \left(\mu d_r + \frac{G_{x_p}T}{2} \right) + \mu G_{x_p} s^{-1}.$$

Here, the apparent inertia, damping and rendered stiffness are all tradeoffs of μ . For impedance reduction, typically no spring rendering is required and thus G_{x_p} is set to zero.

C.7 Discrete-Time Part of Loop Gains

The general discrete-time part $\tilde{D}_n(z)$ of each loop gain is:

$$\tilde{D}_n(z) = \bar{h}(z)(G_{n_p} + G_{n_d}\bar{h}(z)).$$

This function is periodic and has the following two properties, using positive G_{n_p} :

If

$$|G_{n_d}| \leq G_{n_p} \frac{T}{2} \quad \textcircled{1},$$

the function is positive real:

$$\min \text{Re}\{\tilde{D}_n(z)\} = 0.$$

If

$$G_{n_d} \geq -G_{n_p} \frac{T}{6} \quad \textcircled{2},$$

the positive real maximum of the function is

$$\max \text{Re}\{\tilde{D}_n(z)\} = \left(G_p + G_d \frac{2}{T} \right) \frac{2}{T}.$$

In these two cases the cycloid is in a predictable rectangle in the complex plane bounded by 0 and this maximum real value. These conditions are shown visually in fig. C.4. The multiplication of $\tilde{D}_n(z)$ with other complex functions have easily predictable consequences if both of these conditions are true.

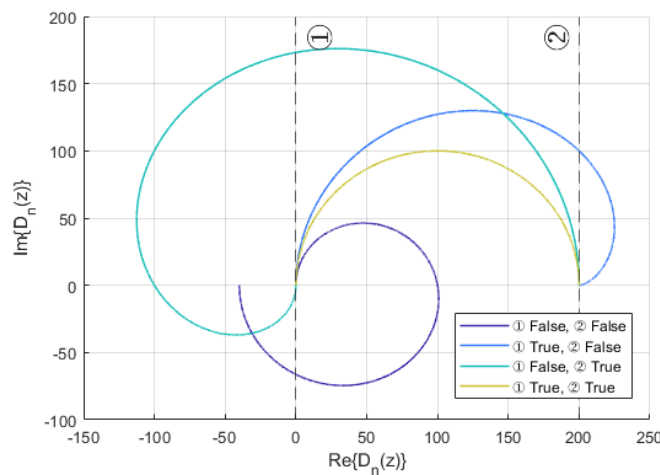


Figure C.4: The shape of $\tilde{D}_n(z)$ when violating conditions (1) and (2).

C.8 Lemma: Sampling of RHP Passive and RHP Offset Systems

Sampling a function is by the definition of app. C.1 an infinite sum of the same function transposed over complex frequency.

Intuitively, summing complex functions that lie to the right of a positive real value (such as passive systems according to the PRC) will always result in the summed function moving to the right of that plane. The analogue holds for complex functions that lie to the left of a negative real value as well. Therefore, sampling a positive real (passive) transfer function maintains passivity. A more exact proof is as follows.

Any complex function of the Laplace variable can be split up into its real and imaginary part:

$$Z_0(s) = x_0(\omega, \sigma) + iy_0(\omega, \sigma),$$

and let the real part always be larger than some positive value γ ,

$$x_0(\omega, \sigma) \geq \gamma \geq 0, \quad \sigma \geq 0 \quad (\text{C.3})$$

for all ω and positive σ . The function $Z_0(s)$ thus lies completely to the right of this value. Then the real part of the sampled function, using (C.1), is the infinite series of only the real parts:

$$\text{Re}\{[Z_0(s)]^*\} = \sum_{n=-\infty}^{\infty} x_0(\omega + n\omega_s, \sigma).$$

This is a summation of arguments all larger than γ for all ω , for all $n\omega_s$ and positive σ by assumption of (C.3):

$$x_0(\omega + n\omega_s, \sigma) \geq \gamma, \quad \sigma \geq 0.$$

Summing values which are all larger than γ surely results in a value larger than γ . Thus, if the unsampled system is contained in some RHP with positive offset γ , so is its sampled version:

$$\begin{aligned} \text{Re}\{Z(s)\} \geq \gamma &\Rightarrow \text{Re}\{[Z(s)]^*\} \geq \gamma \\ &\forall \omega, \quad \sigma \geq 0 \end{aligned}$$

The definition of a passive system from (A.1) is a single case of this statement ($\gamma = 0$), and therefore output sampling a passive system yields a passive system.

C.9 Combined Hybrid and Mixed Loop Marginal Stability for Spring Environments

Because the hybrid system is still linear, although not time-invariant, the parallel loop gains of fig. 5.2 can be added to obtain the combined loop gain. From the combined system loop gain then, stability margins can be derived given an environment model. Adding the separate loop gains defined in (5.3), explicitly defining as a function of k_h :

$$L(s, k_h) = L_x(s, k_h) + L_f(s, k_h) + L_a(s, k_h)$$

The k_h that makes $L(s, k_h)$ pass through -1 is then the marginally stable spring. Even though it is unlikely that there exist a compact analytical solution when solving for k_h due to the sampling infinite sum, numerically the lowest k_h that touches critical point can be found. Because the loops gains contain the starred transform, this numerically requires approximating the definition of C.1, in this work done up to order $n = 100$. The approximate marginally stable spring is numerically found by increasing the spring from zero up to where the loop gain is purely real -1 :

$$\hat{k}_h = \min k_h \quad \text{such that} \quad L(i\omega, k_h) = -1 \quad \forall \omega = [0, \omega_N]$$

And because the loop gain is periodic, even though the apparent impedance is not periodic, it only has to be evaluated up to the Nyquist frequency. This is implemented in Matlab as a one dimensional search problem that minimizes the following cost:

$$\hat{k}_h = \arg \min_{k_h} J, \quad J = \begin{cases} k_h^{-1}, & \text{if } \min \overline{\text{Re}}\{L(i\omega, k_h)\} > -1 \\ k_h, & \text{if } \min \overline{\text{Re}}\{L(i\omega, k_h)\} < -1 \end{cases} \quad \forall \omega = [0, \omega_N]$$

Where $\min \overline{\text{Re}}\{\cdot\}$ is the minimum purely real part, such that $\text{Im}\{\cdot\} = 0$, the used function interpolates where this crossing happens since numerically $\text{Im}\{\cdot\} = 0$ and -1 are never exactly reached. If the currently tested k_h leads to an stable loop (the top case), the cost is lowered by increasing the candidate stiffness. If the currently tested k_h leads to an unstable loop (the bottom case), the cost is lowered by lowering the candidate stiffness. This finds where the negative real axis is crossed for smallest k_h , converging from both sides.

C.10 Complex Region Product Sampling

If some complex term u_n is bound to a corresponding complex region \mathbf{U}_n :

$$u_n \in \mathbf{U}_n \subseteq \mathbb{C}$$

Then an arbitrary series of u_n is bounded as well as:

$$\sum_n u_n \in \sum_n \mathbf{U}_n$$

Where the right-hand summation of regions is the complex Minkowski sum. This results in another region consisting of all combinations of elements in all \mathbf{U}_n . For two elements for example the Minkowski sum is:

$$\mathbf{C} = \mathbf{A} \oplus \mathbf{B} = \{a + b \mid a \in \mathbf{A}, b \in \mathbf{B}\}$$

The same must hold when both are functions as well, if

$$u_n(\omega) \in \mathbf{U}_n(\omega) \quad \forall \omega,$$

then their sums are:

$$\sum_n u_n(\omega) \in \sum_n \mathbf{U}_n(\omega) \quad \forall \omega. \quad (\text{C.4})$$

These functions can be chosen as follows:

$$u_n(\omega) = X(\omega + n\omega_s)Y(\omega + n\omega_s)$$

$$\mathbf{U}_n(\omega) = X(\omega + n\omega_s) \odot \mathbf{Y},$$

where the latter operation is defined as

$$\mathbf{C}(\omega) = A(\omega) \odot \mathbf{B} = \{A(\omega)b \mid b \in \mathbf{B}\}.$$

This results in a region $\mathbf{U}_n(\omega)$ as a function of ω , due to the multiplication of frequency independent region \mathbf{Y} scaled and rotated by the complex function $X(\omega + n\omega_s)$.

Evaluating (C.4) with the chosen functions gives:

$$\sum_{n=-\infty}^{\infty} X(\omega + n\omega_s)Y(\omega + n\omega_s) \in \sum_{n=-\infty}^{\infty} X(\omega + n\omega_s) \odot \mathbf{Y},$$

which is equal to

$$[X(\omega)Y(\omega)]^* \in [X(\omega)]^* \odot \mathbf{Y} \quad \forall \omega. \quad (\text{C.5})$$

Where the left-hand side is the starred transform of the functions' product and the right-hand side is the multiplication of region \mathbf{Y} scaled and rotated by the complex function $[X(\omega)]^*$.

The direct reasoning for (C.5) used by [1] is that sampling $X(\omega) \odot \mathbf{Y}$ does not affect \mathbf{Y} , because it is not dependent on frequency, and therefore

$$[X(\omega) \odot \mathbf{Y}]^* = [X(\omega)]^* \odot \mathbf{Y}.$$

In the rest of this work the \odot operation is implied when multiplying a region in boldface with another function, and is omitted in notation.

C.II Physical Interpretation of Uncoupled Pure Inertia Robot Acceleration Feedback

Using (C.7) with the uncoupled robot $Z_h(s) = 0$, solely robot inertia $Z_r(s) = m_r s$, and proportional feedback G_{a_p} only, results in the simple loop gain:

$$[L_a(s)]^* = \bar{h}(z) G_{a_p} \left[\frac{1}{s} \frac{s}{m_r s} \right]^*$$

Using the definition of the starred transform C.1 gives:

$$\left[\frac{1}{s} \frac{s}{m_r s} \right]^* = \sum_{n=-\infty}^{\infty} \frac{1}{m_r (s + i\omega_s n)}$$

Each positive and negative term of n , its complex conjugate, can be combined as follows:

$$\frac{1}{m_r (s + i\omega_s n)} + \frac{1}{m_r (s - i\omega_s n)} = \frac{(s - i\omega_s n)}{m_r (s + i\omega_s n)(s - i\omega_s n)} + \frac{(s + i\omega_s n)}{m_r (s - i\omega_s n)(s + i\omega_s n)} = \frac{2s}{m_r s^2 + m_r \omega_s^2 n^2}$$

Such that, after extracting $n = 0$ from the sum, the other terms can be added as follows:

$$\left[\frac{1}{m_r s} \right]^* = \frac{1}{m_r s} + \sum_{n=1}^{\infty} \frac{2}{m_r s + m_r \omega_s^2 n^2 s^{-1}}$$

The terms in the sum can be interpreted as the admittances of masses with mass $m_r/2$ with springs with stiffness $m_r \omega_s^2 n^2/2$. The interpretation is shown in fig. C.5. Note that this is not a PE, only a partly physical interpretation of the effect of the sampler.

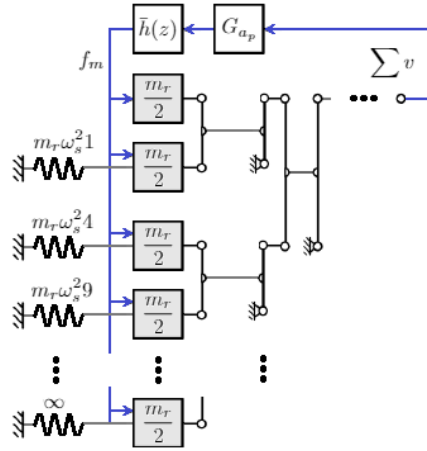


Figure C.5: Physical interpretation of discrete acceleration feedback with the uncoupled robot $Z_h(s) = 0$, solely robot inertia $Z_r(s) = m_r s$, and proportional feedback G_{a_p} . Levers linearly add velocities, dots indicate infinite sum of adding elements.

C.12 Positive Discrete-Time Acceleration Feedback Passivity

The loop gain of discrete-time acceleration feedback is:

$$L_a(s) = \tilde{D}_a(z)[H_a(s)]^* = \tilde{D}_a(z) \left[\frac{1}{Z_h(s) + Z_r(s)} \right]^*. \quad (\text{C.6})$$

For arbitrary human impedance in the RHP $Z_h(s) \in \mathbf{Z}_0$, following the same logic as app. C.3 and [1] yields that $\mathbf{H}_a(s)$ always lies in a disk from the origin to $1/d_r$ as shown in fig. C.2. Because sampling itself does not influence the positive realness of a function according to app. C.8, the sampled version of the continuous-time dynamics then lies in the RHP as well:

$$[\mathbf{H}_a(s)]^* \in \mathbf{Z}_0(s)$$

As seen in app. C.7, the discrete-time part $\tilde{D}_a(z)$ cannot rotate the RHP of $[\mathbf{H}_a(s)]^*$ more than $\pm \frac{\pi}{2}$ rad if:

$$|G_{a_d}| \leq G_{a_p} \frac{T}{2}.$$

In that case, $L_a(s)$ can never include the critical point -1 , because it cannot be negative purely real.

C.13 Negative Discrete-Time Acceleration Feedback Passivity

The following derivation is first done for proportional acceleration feedback only, after which adding the derivative is slightly easier.

Proportional feedback The loop gain of discrete-time acceleration feedback is:

$$L_a(s) = \tilde{D}_a(z)[H_a(s)]^* = \bar{h}(G_{a_p} + \bar{h}G_{a_d}) \left[\frac{1}{s} \frac{s}{Z_h(s) + Z_r(s)} \right]^*. \quad (\text{C.7})$$

The area-loci argument of sec. 5.2.1 cannot be used here, such that the worst-type environment assumption must be used. The worst type of environment is assumed to be captured in a mass, spring and damper:

$$Z_h(s) = m_h s + d_h + k_h s^{-1}.$$

The continuous-time dynamics are then of the form

$$H_a(s) = \frac{1}{Z_h(s) + Z_r(s)} = \frac{1}{m_a} \frac{s}{s^2 + 2\zeta\omega_0 s + \omega_0^2}.$$

Where

$$m_a = m_r + m_h, \quad d_a = d_r + d_h, \quad \zeta = \frac{d_a}{2m_a\omega_0}, \quad \bar{\zeta} = \sqrt{1 - \zeta^2}, \quad \omega_0 = \sqrt{\frac{k_h}{m_a}}.$$

This has the following starred transform [71]:

$$[H_a(s)]^* = -\frac{T}{m_a \bar{\zeta}} \frac{-\bar{\zeta} + z^{-1} e^{-\zeta\omega_0 T} \sin(\bar{\zeta}\omega_0 T + \cos^{-1}(\zeta))}{1 - 2z^{-1} e^{-\zeta\omega_0 T} \cos(\bar{\zeta}\omega_0 T) + z^{-2} e^{-2\zeta\omega_0 T}}, \quad z = e^{sT}.$$

The loop gain is then:

$$L_a(s) = G_{a_p} \frac{1 - z^{-1}}{m_a \bar{\zeta}} \frac{\bar{\zeta} - z^{-1} e^{-\zeta\omega_0 T} \sin(\bar{\zeta}\omega_0 T + \cos^{-1}(\zeta))}{1 - 2z^{-1} e^{-\zeta\omega_0 T} \cos(\bar{\zeta}\omega_0 T) + z^{-2} e^{-2\zeta\omega_0 T}},$$

which is a function of combined inertia m_a , combined damping d_a , environmental stiffness k_h and sample time T , linearly scaled by G_{a_p} , which is negative for inertia compensation.

Because this loop gain is always open-loop stable, for the same reasoning described in sec. 5.2, encirclement of -1 must be the cause of instability. Let $\min \overline{\text{Re}\{\cdot\}}$ denote the minimum *purely* real gain of a function, thus where $\text{Im}\{\cdot\} = 0$. This is a useful value, because this is where the Nyquist plot crosses the negative real axis at minimum value. Thus the Nyquist stability criterion requires, given that the open loop gains themselves are stable, that the critical point is never encircled:

$$\min \overline{\text{Re}\{L_a(s)\}} \geq -1.$$

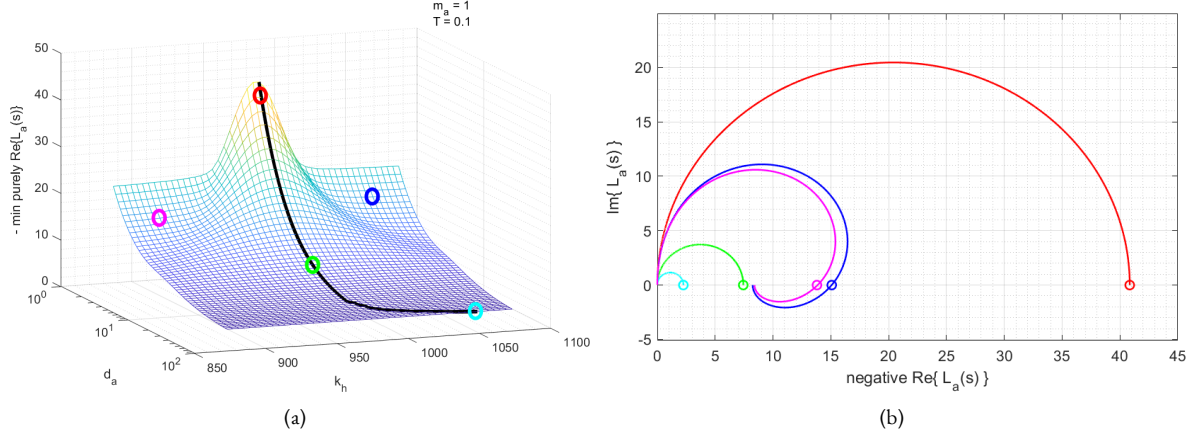


Figure C.6: Numerical surface of minimum purely real (the inverse of the gain margin) value of $L(s)$ in (a) and select points with their corresponding Nyquist loci (b) plotted up to the Nyquist frequency. For $G_{ap} = -1, G_{ad} = 0, m_r = 1, T = 0.1$. The black curve traces the worst-case gain, because k_h may be anything. Loci lying on the black curve always have their minimum purely real value, indicated in (b) by the open circles, at the Nyquist frequency.

This function is the inverse of the gain margin, because for minimal purely real gain this is where the system is closest to instability.

The value of $\min \overline{\text{Re}}\{L_a(s)\}$ is best investigated numerically, as done in fig. C.6 (a) and fig. C.7. Note that the z-axis is negative here, to visualize minima better, appearing as maxima in the figure. Each point on such a surface corresponds to the minimum purely real gain for the loop gain at some choice of parameters. What these loop gains look like or at which frequency the gain margin occurs is not visible in these surfaces, but shown for select points in fig. C.6 (b).

A wider view in fig. C.7 (a) reveals local minima (appearing as maxima) when the combined system natural frequency is at the Nyquist frequency:

$$\omega_0 = (1 + 2n)\omega_N, \quad n \in \mathbb{Z}.$$

and for each set of parameters, the global minimum purely real is at the first peak, at the particular stiffness

$$k_h = m_r \omega_N^2. \quad (\text{C.8})$$

This tunes the combined systems natural frequency to lie on the Nyquist frequency. This is the same worst-case environment found by Colgate [1] for discrete-time position feedback.

The minimum purely real gain $\min \overline{\text{Re}}\{L_a(s)\}$ is a function of m_a, k_h, d_a, T . Of these variables, m_a and d_a are lower bound to m_r and d_r respectively, but may get infinitely large. In contrast, stiffness k_h may be any positive number.

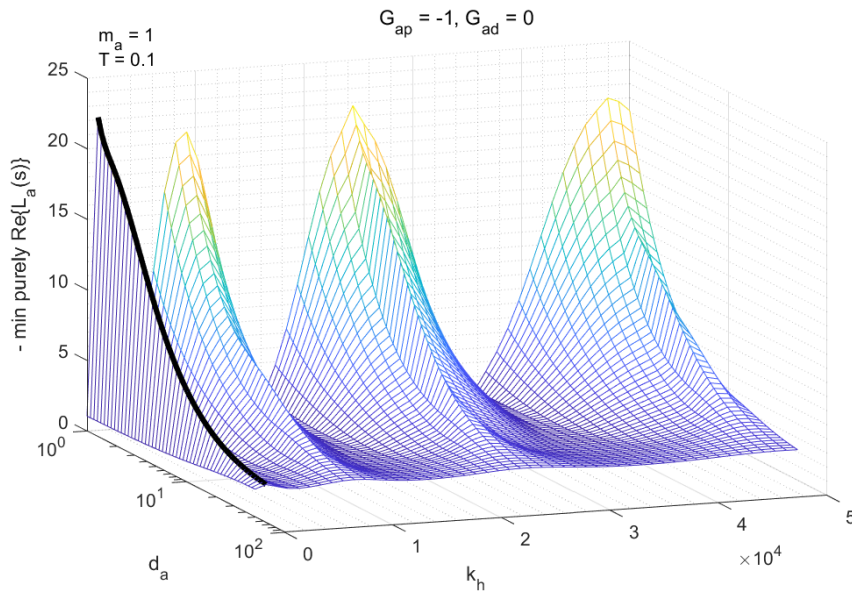


Figure C.7: A wider view of fig. C.6 (a), revealing returning peaks at springs tuned to integers of the Nyquist frequency as (C.8).

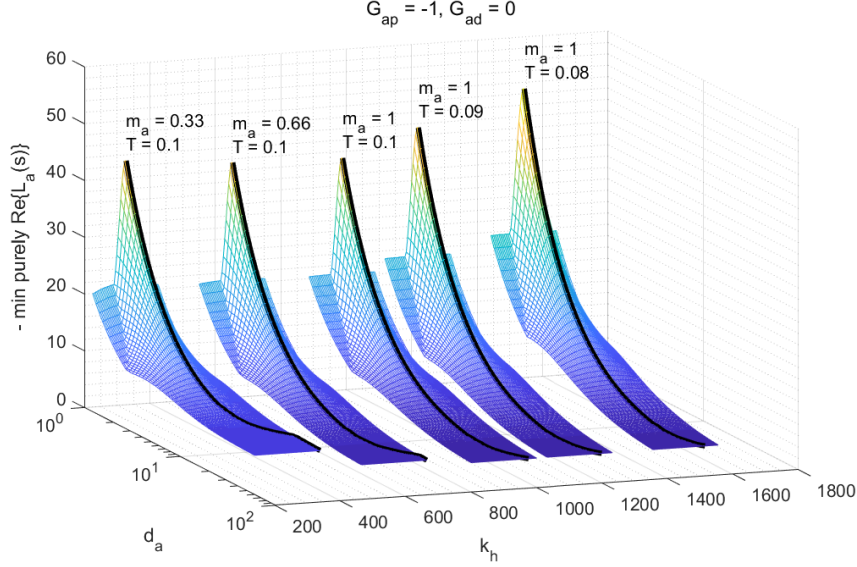


Figure C.8: Minimum purely real gain when varying m_a, T , each surface represents one of these combinations plotted on the same axes system.

Therefore, figures here shows the maximum gain as a function of d_a by the black curve, because k_h may be anything. For low damping, the black curve is at spring stiffness tuned to (C.8) while for higher damping, the black curve requires larger stiffness. Regardless, minimal $d_a = d_r$ yields the worst case gain if k_h adjusts to always be on the black curve. The additional surfaces of fig. C.8 show that lower T and m_a increase the black curve monotonically.

The loci that lie on these black curves all have the property that their maximum purely real function occurs when the complex frequency is the Nyquist frequency $\omega = \omega_N$, shown in fig. C.6 This property is useful because at the Nyquist frequency, the minimum purely real gain is simplified.

Combining these conditions (spring $k_h = m_r \omega_N^2$, minimal damping $d_a = d_r$, minimal inertia $m_a = m_r$, and at the Nyquist frequency $\omega = \omega_N$), the worst-case loop gain simplifies to:

$$\min \overline{\text{Re}}\{L_a(s)\} = \min \overline{\text{Re}}\{L_a(i\omega_N)\} = G_{a_p} \frac{2}{m_r \bar{\zeta}_N} \frac{\bar{\zeta}_N + e^{-\zeta_N \pi} \sin(\bar{\zeta}_N \pi + \cos^{-1}(\zeta_N))}{1 + 2e^{-\zeta_N \pi} \cos(\bar{\zeta}_N \pi) + e^{-2\zeta_N \pi}},$$

for negative G_{a_p} and where

$$\bar{\zeta}_N = \sqrt{1 - \zeta_N^2}, \quad \zeta_N = \frac{d_r T}{2m_r \pi}.$$

The right-hand side equation is denoted \mathcal{R} , where d_r and T only occur in multiplication, such that $d_r T$ behaves as a single variable:

$$\mathcal{R}(m_r, d_r T) = \frac{2}{m_r \bar{\zeta}_N} \frac{\bar{\zeta}_N + e^{-\zeta_N \pi} \sin(\bar{\zeta}_N \pi + \cos^{-1}(\zeta_N))}{1 + 2e^{-\zeta_N \pi} \cos(\bar{\zeta}_N \pi) + e^{-2\zeta_N \pi}}. \quad (\text{C.9})$$

An approximation when damping ratio is low ($\zeta \approx 0, \bar{\zeta} \approx 1$) is:

$$\mathcal{R}(m_r, d_r T) \approx \mathcal{R}_1(m_r, d_r T) = \frac{2}{m_r} \frac{1}{1 - e^{-\frac{d_r T}{2m_r}}}.$$

According to app. C.13.1, a conservative (with respect to \mathcal{R}_1 and the true condition) but simpler and less accurate approximation is:

$$\mathcal{R}(m_r, d_r T) \approx \mathcal{R}_2(m_r, d_r T) = \frac{2}{m_r} \left(1 + \frac{2m_r}{d_r T}\right).$$

Both approximations are shown in fig. C.10. The approximate passivity condition is then:

$$\min \overline{\text{Re}}\{L_a(s)\} = G_{a_p} \mathcal{R}(m_r, d_r T) \geq -1, \quad G_{a_p} \leq 0$$

Addition of Derivative Feedback The entire surfaces of minimum purely real gains scale linearly with G_{a_p} , but the large peaks at (C.8) can be reduced by opposite sign G_{a_d} , as seen in fig. C.9 (a) and (b). However, when G_{a_d} becomes too large, the maximum trajectory on the default right-hand side is replaced by a left-hand trajectory at lower k_h , as seen in fig. C.9 (c). This might seem favorable in increasing gain margin, but the default curve had relatively simple form and approximation (C.9) because loci on that curve are maximized at $\omega = \omega_N$, shown in fig. C.9 (d). Moreover, the addition of G_{a_d} to the worst-case loop gains is simple when $\omega = \omega_N$ is the worst case frequency, because in that case the derivative term is simple:

$$G_{a_d} \bar{h}(e^{i\omega_N T}) = G_{a_d} \frac{2}{T}.$$

Thus, when the worst-case curve is the right curve, the minimum purely real values are simply:

$$\min \overline{\text{Re}}\{L_a(s)\} = \min \overline{\text{Re}}\{L_a(i\omega_N)\} = \left(G_{a_p} + \frac{2}{T}G_{a_d}\right) \mathcal{R}(m_r, d_r T)$$

Here, it is conjectured, but not proven¹, that

$$G_{a_d} \geq -|G_{a_p}| \frac{T}{6}, \quad (\text{C.10})$$

is a sufficient condition for the minimum curve $\min \overline{\text{Re}}\{L_a(s)\}$ to follow the predictable right-hand peak.

A sufficient stability condition for the worst-case environment, and thus passivity condition, for negative G_{a_p} is then:

$$-\left(G_{a_p} + \frac{2}{T}G_{a_d}\right) \mathcal{R}(m_r, d_r T) \geq -1, \quad G_{a_p} \leq 0, \quad 0 \leq G_{a_d} \leq |G_{a_p}| \frac{T}{6}$$

¹A proof, if it exists, is likely based on fractions such as $\frac{T}{2}$, $\frac{T}{4}$, $\frac{T}{6}$, because they all have geometrical interpretations for the general discrete controller as shown in C.7. Therefore, $\frac{T}{6}$ is chosen to be on the safe side, to give a safe sufficient condition.

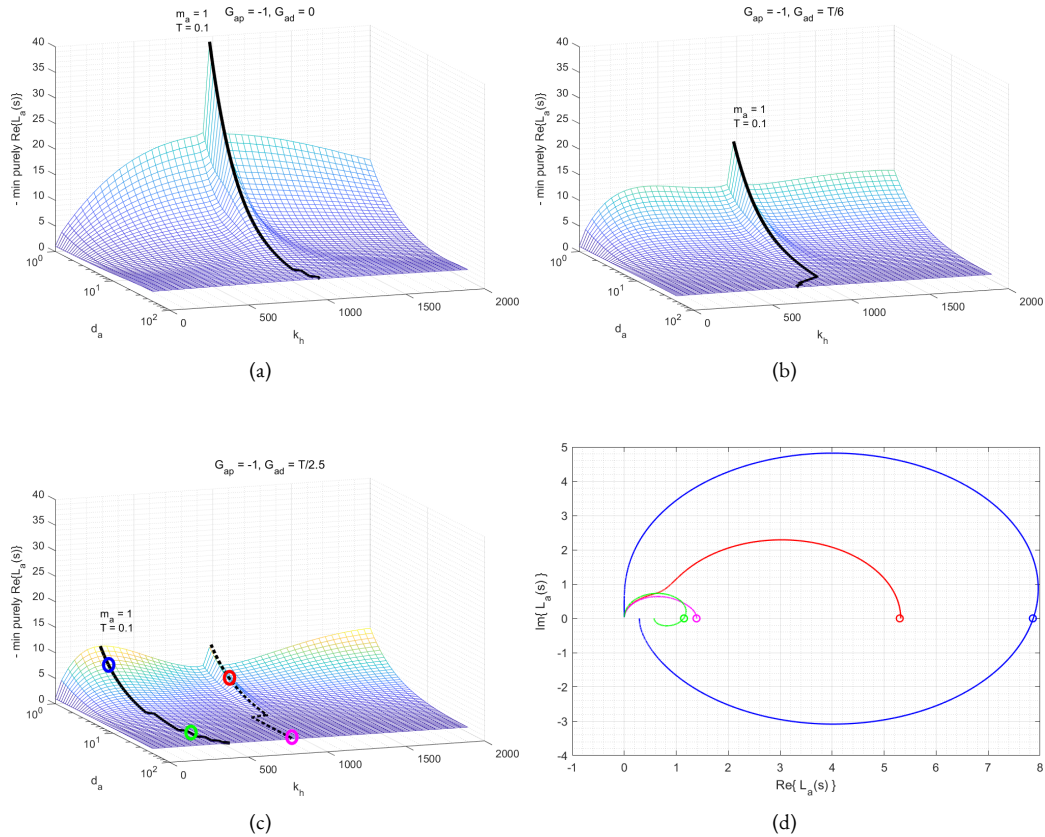


Figure C.9: Maximum purely real loop gains for negative discrete-time acceleration feedback of G_{a_p} , and increasing positive G_{a_d} for (a), (b) and (c). The original peak completely vanishes for $G_{a_d} = -|G_{a_p}|T/2$. In (c) the maximum curve is the left black curve instead of the original dotted right curve. Points on either curve of (c) are shown in (d) up to the Nyquist frequency. The loci on the dotted curve are maximized at the Nyquist frequency.

C.13.1 Lemma: Conservative Approximation

The proposed inequality

$$\frac{1}{1 - e^{-x}} \leq 1 + \frac{1}{x}$$

can be manipulated into

$$1 + x \leq e^x,$$

which is proven conveniently for positive x by the series definition of e :

$$e^x := 1 + x + \frac{x^2}{2!} + \frac{x^3}{3!} + \dots$$

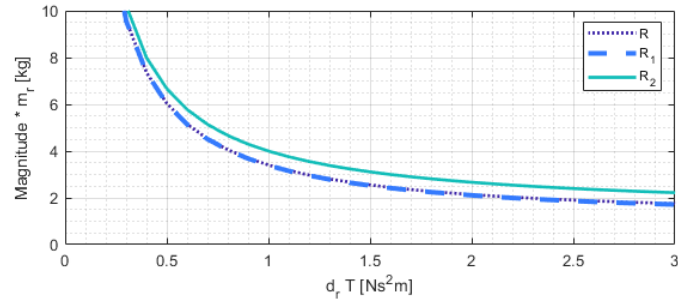


Figure C.10: Function \mathcal{R} of (C.9); inverse of the gain margin for proportional feedback. Plotted as a function of damping and sampling $d_r T$ and robot inertia m_r for the exact condition and two approximations $\mathcal{R}_1, \mathcal{R}_2$.

Appendix D

Appendix to Chapter 6

D.1 Root Separation

If for a polynomial

$$P(s) = A_n s^n + \dots + A_0$$

subsequent factors of coefficients are decreasing in magnitude sufficiently

$$\left| \frac{A_{n-1}}{A_n} \right| \gg \left| \frac{A_{n-2}}{A_{n-1}} \right| \gg \dots \gg \left| \frac{A_k}{A_{k+1}} \right| \gg \left| \frac{A_{k-1}}{A_k} \right| \gg \dots \gg \left| \frac{A_0}{A_1} \right|$$

then the roots of the polynomial are approximately those factors themselves:

$$P(s) \propto \left(s - \frac{A_{n-1}}{A_n} \right) \left(s - \frac{A_{n-2}}{A_{n-1}} \right) \dots \left(\frac{A_{k+1}}{A_{k-1}} s^2 + \frac{A_k}{A_{k-1}} s + 1 \right) \dots \left(s - \frac{A_0}{A_1} \right).$$

The factors for which the separation by magnitude is untrue, the roots cannot be separated. If such a single pair is the other way around:

$$\dots \gg \left| \frac{A_k}{A_{k+1}} \right| \ll \left| \frac{A_{k-1}}{A_k} \right| \gg \dots$$

then that pair of roots is a complex conjugate pair (z_1, z_1^*) with much larger imaginary part:

$$\operatorname{Re}\{z_1\} \approx -\frac{A_k}{2A_{k+1}} \ll \operatorname{Im}\{z_1\} \approx \sqrt{\frac{A_{k-1}}{A_{k+1}}},$$

according to the quadratic equation.

D.2 Flexible Link Robot Numerator Root Separation

Applying the theory of D.1 to the $Z_N(s)$ terms of order 1,2 and 3 in table 6.1:

$$\frac{k(G_{a2p} + m_r)}{kG_{a2d} + m_2\bar{d}_1 + d(G_{a2p} + m_r)} \gg \frac{\bar{d}_1}{(G_{a2p} + m_r)}.$$

This yields that due to naturally large k the numerator can be written as two second-order polynomials:

$$Z_N(s) \propto (n_2 s^2 + n_1 s + 1)(N_2 s^2 + N_1 s + 1).$$

D.3 Quadratic-Quadratic Polynomial

For a fourth-order real and even polynomial

$$p(x) = a_2x^4 + a_1x^2 + a_0 \geq 0$$

to be purely positive real requires that its leading- and lowest order coefficient are positive and that there are no purely real roots, these conditions are:

$$\begin{aligned} a_0 &> 0 \\ a_2 &> 0 \\ a_1 &> -\sqrt{4a_0a_2}. \end{aligned} \tag{D.1}$$

The first two requirements are straightforward for the polynomial to be positive at zero and infinity, the third requires some explanation. This condition for the non-existence of purely real roots is found easiest when inverting the condition for all roots to be purely real.

The four zeros of the polynomial are the square roots of the quadratic formula solutions:

$$z = \pm \sqrt{\frac{-a_1 \pm \sqrt{\Delta}}{2a_2}}, \quad \Delta = a_1^2 - 4a_0a_2.$$

At least one of z is purely real if and only if the content of the outer square root is purely positive real, because the square root of any complex or negative number is complex. Given that the second requirement of D.1 must hold, the numerator must then be purely positive real. For a purely positive real numerator, the content of the inner square root must surely be positive:

$$\Delta > 0.$$

And for all roots to be purely real, both of the numerator roots must be purely positive real. Because purely positive real Δ is always smaller than a_1 for the first and second requirement of D.1, the only way for this to be positive purely real for all roots is

$$a_1 < 0.$$

Rewriting the former requirement

$$|a_1| > \sqrt{4a_0a_2},$$

and requiring that a_1 is negative

$$a_1 = -|a_1|$$

Yields

$$a_1 < -\sqrt{4a_0a_2}.$$

The condition for the non-existence of purely real roots is then the inverse of this requirement, shown in D.1.

D.4 Flexible Link Robot Continuous-Time Controller PE Without Derivatives

The flexible link PE for proportional force and acceleration feedback is derived in a number of steps by the rules of app. A.4. Black boxed equations are the retrieved simple physical elements (mass, spring or damper), as impedance (Z) or admittance (Y) in the structure of fig. D.1. Top-right notation names these transfers.

1 The transfer of 6.1 can immediately be split into two impedances, of which one is the end effector mass:

$$Z(s) = \frac{(G_{a_2}s + \bar{Z}_1 + Z_2)Z_{12} + \bar{Z}_1Z_2}{(G_f + 1)Z_{12} + \bar{Z}_1} = \boxed{Z_2} + \frac{(G_{a_2}s + \bar{Z}_1 - G_fZ_2)Z_{12}}{(G_f + 1)Z_{12} + \bar{Z}_1} Z_A$$

2 The right side impedance inverted Z_A is

$$Y_A = \frac{(G_f + 1)Z_{12} + \bar{Z}_1}{(G_{a_2}s + \bar{Z}_1 - G_fZ_2)Z_{12}} = \frac{G_f + 1}{G_{a_2}s + \bar{Z}_1 - G_fZ_2} Y_B + \frac{\bar{Z}_1}{(G_{a_2}s + \bar{Z}_1 - G_fZ_2)Z_{12}} Y_C$$

Of which the left side Y_B has the following parallel mass and damper impedance

$$Z_B = \frac{G_{a_2}s + \bar{Z}_1 - G_fZ_2}{G_f + 1} = \boxed{\frac{\bar{d}_1}{G_f + 1}}^{Z_{B1}} + \boxed{\frac{G_{a_2} + m_1 - G_fm_2}{G_f + 1} s}^{Z_{B2}}$$

D.5 Flexible Link Robot Continuous-Time Controller PE with Derivatives

Finding a PE for the flexible link robot with all feedback is done by extending the PE of app. D.4 to include $(G_{f_d}, G_{a_d}, G_{x_p})$. This is done by assuming fig. D.1 and extending those found parameters to include the added feedback, rather than starting from scratch with a PE derivation. From those parameters Z_2, Z_{12} remain the same, but new Z_{B_1}, Z_{B_2}, Z_D of which Z_D is the entire top branch. These new transfers including $(G_{f_d}, G_{a_d}, G_{x_p})$ are marked with an apostrophe. Black boxed equations are the retrieved simple physical elements (mass, spring or damper), given names are in the top-right corner of each transfer. The extended PE is shown in fig. 6.3 (a).

- 1 Extending the spring-damper of Z_{B_1} to include the new parameters gives three elements:

$$Z'_{B_1} = \frac{\bar{d}_1 + G_{x_p}/s}{G_{f_p} + G_{f_d}s + 1} = \boxed{\frac{G_{x_p}}{s(G_{f_p} + 1)}}^{C_a} + \frac{\bar{d}_1 - (G_{f_d}G_{x_p})/(G_{f_p} + 1)Z^\beta}{G_{f_p} + G_{f_d}s + 1}$$

$$Y^\beta = \frac{G_{f_p} + G_{f_d}s + 1}{\bar{d}_1 - (G_{f_d}G_{x_p})/(G_{f_p} + 1)} = \boxed{\frac{G_{f_p} + 1}{\bar{d}_1 - (G_{f_d}G_{x_p})/(G_{f_p} + 1)}}^{R_h} + \boxed{\frac{G_{f_d}s}{\bar{d}_1 - (G_{f_d}G_{x_p})/(G_{f_p} + 1)}}^{C_i}$$

- 2 Extending the mass of Z_{B_2} to include the new parameters gives three elements:

$$Z'_{B_2} = \frac{s(G_{a_p} + m_1 + G_{a_d}s - m_2(G_{f_p} + G_{f_d}s))}{G_{f_p} + G_{f_d}s + 1} = \boxed{\frac{s(G_{a_d} - G_{f_d}m_2)}{G_{f_d}}}^{I_b} + \frac{s(G_{a_p} + m_1 - G_{f_p}m_2 - ((G_{f_p} + 1)(G_{a_d} - G_{f_d}m_2))/(G_{f_d}))Z^\delta}{G_{f_p} + G_{f_d}s + 1}$$

$$Y^\delta = \frac{G_{f_p} + G_{f_d}s + 1}{s(G_{a_p} + m_1 - G_{f_p}m_2 - ((G_{f_p} + 1)(G_{a_d} - G_{f_d}m_2))/(G_{f_d}))} = \boxed{\frac{G_{f_p} + 1}{s(G_{a_p} + m_1 - G_{f_p}m_2 - ((G_{f_p} + 1)(G_{a_d} - G_{f_d}m_2))/(G_{f_d}))}}^{I_c} + \boxed{\frac{G_{f_d}s}{s(G_{a_p} + m_1 - G_{f_p}m_2 - ((G_{f_p} + 1)(G_{a_d} - G_{f_d}m_2))/(G_{f_d}))}}^{R_b}$$

- 3 Extending the top branch of Z_D to include the new parameters first retrieves an inertia:

$$Z'_D = \frac{s((G_{a_d}d - G_{f_d}dm_2)s^2 + (G_{a_p}d + G_{a_d}k - G_{f_p}dm_2 - G_{f_d}km_2)s + (G_{a_p}k - G_{f_p}km_2))}{(G_{x_p} + \bar{d}_1s + m_1s^2)} = \boxed{\frac{(s(G_{a_d}d - G_{f_d}dm_2))}{m_1}}^{I_e} + \frac{(G_{a_p}dm_1 - G_{a_d}d\bar{d}_1 + G_{a_d}km_1 + G_{f_d}d\bar{d}_1m_2 - G_{f_p}dm_1m_2 - G_{f_d}km_1m_2)s^2 + (G_{a_p}km_1 - G_{a_d}G_{x_p}d + G_{f_d}G_{x_p}dm_2 - G_{f_p}km_1m_2)s}{m_1^2s^2 + (\bar{d}_1m_1)s + G_{x_p}m_1}^{Z_\kappa}$$

The latter is split into two branches, in the top of fig. 6.3.

$$\begin{aligned}
Y_\kappa &= \frac{m_1^2 s^2 + (\bar{d}_1 m_1) s + G_{x_p} m_1}{(G_{a_p} \dot{d} m_1 - G_{a_d} d \bar{d}_1 + G_{a_d} k m_1 + G_{f_p} d m_1 m_2 - G_{f_d} d \bar{d}_1 m_2 - G_{f_p} d m_1 m_2 - G_{f_d} k m_1 m_2) s^2 + (G_{a_p} k m_1 - G_{a_d} G_{x_p} d + G_{f_d} G_{x_p} d m_2 - G_{f_p} k m_1 m_2) s} \\
&= \frac{Y_\xi}{(G_{a_p} d m_1 - G_{a_d} d \bar{d}_1 + G_{a_d} k m_1 + G_{f_p} d m_1 m_2 - G_{f_d} d \bar{d}_1 m_2 - G_{f_p} d m_1 m_2 - G_{f_d} k m_1 m_2) s} + \frac{Y_\lambda}{(\bar{d}_1 m_1) s + G_{x_p} m_1} \\
&= \frac{Y_\lambda}{(G_{a_p} d m_1 - G_{a_d} d \bar{d}_1 + G_{a_d} k m_1 + G_{f_p} d m_1 m_2 - G_{f_d} d \bar{d}_1 m_2 - G_{f_p} d m_1 m_2 - G_{f_d} k m_1 m_2) s}
\end{aligned}$$

4 The left top branch is:

$$\begin{aligned}
Z_\xi &= \frac{(G_{a_p} d m_1 - G_{a_d} d \bar{d}_1 + G_{a_d} k m_1 + G_{f_p} d m_1 m_2 - G_{f_d} d \bar{d}_1 m_2 - G_{f_p} d m_1 m_2 - G_{f_d} k m_1 m_2) s^2 + (G_{a_p} k m_1 - G_{a_d} G_{x_p} d + G_{f_d} G_{x_p} d m_2 - G_{f_p} k m_1 m_2) s}{m_1^2 s^2} \\
&= \frac{(G_{a_p} \dot{d} m_1 - G_{a_d} d \bar{d}_1 + G_{a_d} k m_1 + G_{f_p} d m_1 m_2 - G_{f_d} d \bar{d}_1 m_2 - G_{f_p} d m_1 m_2 - G_{f_d} k m_1 m_2) s^2}{m_1^2 s^2} + \frac{R_p}{(G_{a_p} k m_1 - G_{a_d} G_{x_p} d + G_{f_d} G_{x_p} d m_2 - G_{f_p} k m_1 m_2) s} \\
&= C_o
\end{aligned}$$

5 The middle-top branch consists of an inertia attached to the top zero junction, and another inertia damper on an attached one junction.

$$\begin{aligned}
Y_\lambda &= \frac{(\bar{d}_1 m_1) s + G_{x_p} m_1}{(G_{a_p} d m_1 - G_{a_d} d \bar{d}_1 + G_{a_d} k m_1 + G_{f_p} d m_1 m_2 - G_{f_d} d \bar{d}_1 m_2 - G_{f_p} d m_1 m_2 - G_{f_d} k m_1 m_2) s^2 + (G_{a_p} k m_1 - G_{a_d} G_{x_p} d + G_{f_d} G_{x_p} d m_2 - G_{f_p} k m_1 m_2) s} \\
&= \frac{-(G_{x_p} m_1) / (s(G_{a_d} G_{x_p} d - G_{a_p} k m_1 - G_{f_d} G_{x_p} d m_2 + G_{f_p} k m_1 m_2))}{-(s(\bar{d}_1 m_1 - (G_{x_p} m_1)(G_{a_d} d \bar{d}_1 - G_{a_p} d m_1 - G_{a_d} k m_1 - G_{f_p} d m_1 m_2 + G_{f_d} d \bar{d}_1 m_2 - G_{f_p} d m_1 m_2 - G_{f_d} k m_1 m_2)) / (G_{a_d} G_{x_p} d - G_{a_p} k m_1 - G_{f_d} G_{x_p} d m_2 + G_{f_p} k m_1 m_2))} Y_\nu \\
&= \frac{s^2(G_{a_d} d \bar{d}_1 - G_{a_p} d m_1 - G_{a_d} k m_1 - G_{f_p} d m_1 m_2 + G_{f_d} d \bar{d}_1 m_2 - G_{f_p} d m_1 m_2 - G_{f_d} k m_1 m_2) + s(G_{a_d} G_{x_p} d - G_{a_p} k m_1 - G_{f_d} G_{x_p} d m_2 + G_{f_p} k m_1 m_2)}{-(s(\bar{d}_1 m_1 - (G_{x_p} m_1)(G_{a_d} d \bar{d}_1 - G_{a_p} d m_1 - G_{a_d} k m_1 - G_{f_p} d m_1 m_2 + G_{f_d} d \bar{d}_1 m_2 - G_{f_p} d m_1 m_2 - G_{f_d} k m_1 m_2)) / (G_{a_d} G_{x_p} d - G_{a_p} k m_1 - G_{f_d} G_{x_p} d m_2 + G_{f_p} k m_1 m_2))} \\
&= \frac{s^2(G_{a_d} d \bar{d}_1 - G_{a_p} d m_1 - G_{a_d} k m_1 - G_{f_p} d m_1 m_2 + G_{f_d} d \bar{d}_1 m_2 - G_{f_p} d m_1 m_2 - G_{f_d} k m_1 m_2)}{-(s(\bar{d}_1 m_1 - (G_{x_p} m_1)(G_{a_d} d \bar{d}_1 - G_{a_p} d m_1 - G_{a_d} k m_1 - G_{f_p} d m_1 m_2 + G_{f_d} d \bar{d}_1 m_2 - G_{f_p} d m_1 m_2 - G_{f_d} k m_1 m_2)) / (G_{a_d} G_{x_p} d - G_{a_p} k m_1 - G_{f_d} G_{x_p} d m_2 + G_{f_p} k m_1 m_2))} \\
&= \frac{s(G_{a_d} G_{x_p} d - G_{a_p} k m_1 - G_{f_d} G_{x_p} d m_2 + G_{f_p} k m_1 m_2)}{-(s(\bar{d}_1 m_1 - (G_{x_p} m_1)(G_{a_d} d \bar{d}_1 - G_{a_p} d m_1 - G_{a_d} k m_1 - G_{f_p} d m_1 m_2 + G_{f_d} d \bar{d}_1 m_2 - G_{f_p} d m_1 m_2 - G_{f_d} k m_1 m_2)) / (G_{a_d} G_{x_p} d - G_{a_p} k m_1 - G_{f_d} G_{x_p} d m_2 + G_{f_p} k m_1 m_2))} \\
&= R_q
\end{aligned}$$

D.6 Flexible Link Continuous-Time Controller (Noise) Transfer

The force balance on either inertia in the Laplace domain, from fig. 6.1, is:

$$Z_1 V_1 - Z_{12}(V_2 - V_1) - F_m = 0$$

$$Z_2 V_2 - Z_{12}(V_1 - V_2) - F = 0,$$

Here, the dependence on s in notation is omitted. The motor force is the linear addition of signals and their noise sources:

$$F_m = G_f(F + \bar{\Xi}_f) + G_{x_1}(s^{-1}V_1 + \bar{\Xi}_x) + G_a(sV_2 + \bar{\Xi}_a),$$

where the noise is defined in sec. 3.5 as $\bar{\Xi}_n = M_n \sigma_n \Xi_n$. Substituting to obtain the system equation between end effector velocity V_2 and force F :

$$V_2 Z_N = F Z_D + Z_{12}(G_f \bar{\Xi}_f + G_x \bar{\Xi}_x + G_a \bar{\Xi}_a), \quad (\text{D.2})$$

where

$$Z_N = (G_a s + Z_2 + \bar{Z}_1) Z_{12} + \bar{Z}_1 Z_2$$

$$Z_D = (G_f + 1) Z_{12} + \bar{Z}_1.$$

The signs of $\bar{\Xi}_n$ do not matter because they are random signals, and are therefore chosen positive. The apparent impedance from (D.2) is thus:

$$\frac{F}{V_2} = \frac{Z_N}{Z_D} = \frac{(G_a s + Z_2 + \bar{Z}_1) Z_{12} + \bar{Z}_1 Z_2}{(G_f + 1) Z_{12} + \bar{Z}_1},$$

where

$$\bar{Z}_1 = Z_1 + G_x s^{-1}.$$

The noise transfers, defined in sec. 3.5 for a locked output $V_2 = 0$ are then from (D.2):

$$W_{n,\text{flex}} = \frac{F}{\bar{\Xi}_n} = \frac{Z_{12} G_n M_n \sigma_n}{Z_1 + G_x s^{-1} + Z_{12}(1 + G_f)}.$$

D.7 Second Order Transfer Phase Requirement

For a numerator and denominator that are both second order systems, the general description is:

$$Z(s) = \frac{s^2 + 2\zeta_n \omega_n s + \omega_n^2}{s^2 + 2\zeta_d \omega_d s + \omega_d^2}.$$

The condition for the phase to never be larger than zero is the same as checking that

$$\text{Im}\{Z(s)\} \leq 0,$$

of which it is shown in A.3 that it is sufficient and necessary to check

$$P_I(\omega) \leq 0.$$

Substituting $s = i\omega$ here is equal to:

$$P_I(\omega) = (\omega_n^2 - \omega^2)(2\zeta_d \omega_d \omega) - (\omega_d^2 - \omega^2)(2\zeta_n \omega_n \omega)$$

$$P_I(\omega) = 2\omega^3(\zeta_n \omega_n - \zeta_d \omega_d) + 2\omega(\zeta_n \omega_n \omega_d^2 - \zeta_d \omega_d \omega_n^2).$$

Then both coefficients must be purely positive for the polynomial to be positive for positive ω . These conditions can respectively be rewritten to:

$$\frac{\zeta_n}{\zeta_d} \geq \frac{\omega_d}{\omega_n}$$

$$\frac{\omega_n}{\omega_d} \geq \frac{\zeta_n}{\zeta_d}$$

Which can be combined into

$$\frac{\omega_n}{\omega_d} \geq \frac{\zeta_n}{\zeta_d} \geq \frac{\omega_d}{\omega_n}$$

D.8 Flexible Link Robot HF PRC

The flexible mode in the HF is approximated by:

$$Z(s) = \frac{s^2 + 2\zeta_n\omega_n s + \omega_n^2}{s^2 + 2\zeta_d\omega_d s + \omega_d^2},$$

where

$$\zeta_n = \frac{kG_{a_d} + m_2\bar{d}_1 + d(G_{a_p} + m_r)}{2\sqrt{(m_1m_2 + dG_{a_d})(G_{a_p} + m_r)k}}, \quad \zeta_d = \frac{kG_{f_d} + \bar{d}_1 + d(G_{f_p} + 1)}{2\sqrt{(m_1 + dG_{f_d})(G_{f_p} + 1)k}}$$

$$\omega_n = \sqrt{\frac{(G_{a_p} + m_r)k}{m_1m_2 + dG_{a_d}}}, \quad \omega_d = \sqrt{\frac{(G_{f_p} + 1)k}{m_1 + dG_{f_d}}}.$$

Here, $m_r = m_1 + m_2$. Passive pole/zero cancellation requires that $\omega_n = \omega_d$ and $\zeta_n = \zeta_d$.

Undamped In the case that there is no damping ($\zeta_n = \zeta_d = 0$), the equalized magnitudes are:

$$\sqrt{\frac{(G_{a_p} + m_r)k}{m_1m_2}} = \sqrt{\frac{(G_{f_p} + 1)k}{m_1}}.$$

Which, when solving yields

$$G_{f_p} = \frac{G_{a_p} + m_1}{m_2}.$$

Underdamped In the case that there is damping, the only condition that equalizes both $\omega_n = \omega_d$ and $\zeta_n = \zeta_d$ is:

$$G_{a_d} = G_{f_d}m_2.$$

This can be verified by substitution.

D.9 Flexible Link Robot with Continuous-Time Controller PRC

As shown in A.3, an equivalent but simpler condition for the PRC is:

$$P_R(\omega) > 0.$$

For the fourth order system of 6.1 this results in a fourth order even polynomial as a function of ω :

$$P_R(i\omega) = a_2\omega^4 + a_1\omega^2 + a_0.$$

Thus, the three conditions of D.1 obtain the PRC. These conditions are found to be:

$$G_{f_p} + 1 > G_{f_d} \frac{\bar{k}_1}{\bar{d}_1}$$

$$G_{a_p} + m_1 + G_{a_d} \frac{k}{d} > m_2 \left(G_{f_p} + G_{f_d} \frac{k}{d} \right)$$

$$(d\bar{d}_1^2 + d^2\bar{d}_1 - 2d\bar{k}_1m_1) - G_{f_p}(G_{a_d}k^2 + \bar{d}_1km_2) + G_{f_d}k^2(G_{a_p} + m_1 + m_2) + G_{a_p}\bar{d}_1k - G_{a_d}k^2 >$$

$$-\sqrt{(\bar{d}_1k^2(G_{f_p} + 1) - G_{f_d}k^2\bar{k}_1)(dm_1^2 - G_{f_p}dm_1m_2 - G_{f_d}km_1m_2 + G_{a_p}dm_1 + G_{a_d}km_1)}.$$

First condition $a_0 > 0$ The constant coefficient condition is:

$$a_0 = (\bar{k}_1 + k(G_{f_p} + 1))(d\bar{k}_1 + \bar{d}_1k) - k\bar{k}_1(\bar{d}_1 + G_{f_d}k + d(G_{f_p} + 1)) > 0.$$

Expanding this simplifies to:

$$d\bar{k}_1^2 + \bar{d}_1k^2(G_{f_p} + 1) > G_{f_d}k^2\bar{k}_1.$$

When assuming large k this is approximated by:

$$\bar{d}_1k^2(G_{f_p} + 1) > G_{f_d}k^2\bar{k}_1.$$

Rewriting then yields the approximate first condition:

$$G_{f_p} + 1 > G_{f_d} \frac{\bar{k}_1}{\bar{d}_1}.$$

Second condition $a_2 > 0$ The higher order coefficient and condition are:

$$a_2 = (G_{f_d}d + m_1)(G_{a_d}k + \bar{d}_1m_2 + d(G_{a_p} + m_1 + m_2)) - (G_{a_d}d + m_1m_2)(G_{f_d}k + \bar{d}_1 + d(G_{f_p} + 1)) > 0.$$

Collecting by feedback gains:

$$a_2 = dm_1^2 - G_{f_p}(G_{a_d}d^2 + dm_1m_2) + G_{f_d}(G_{a_p}d^2 + d^2m_1 + d^2m_2 + d\bar{d}_1m_2 - km_1m_2) + G_{a_p}dm_1 + G_{a_d}(km_1 - d^2 - d\bar{d}_1).$$

When assuming large k this is approximated by:

$$a_2 = dm_1^2 - G_{f_p}dm_1m_2 - G_{f_d}km_1m_2 + G_{a_p}dm_1 + G_{a_d}km_1.$$

Rewriting then yields the approximate second condition:

$$G_{a_p} + m_1 + G_{a_d}\frac{k}{d} > m_2 \left(G_{f_p} + G_{f_d}\frac{k}{d} \right).$$

Evaluate a_1 Before the third condition can be evaluated a_1 must be determined:

$$\begin{aligned} a_1 = & (d\bar{d}_1 + \bar{k}_1m_2 + k(G_{a_p} + m_1 + m_2))(\bar{d}_1 + G_{f_d}k + d(G_{f_p} + 1)) - \\ & (\bar{k}_1 + k(G_{f_p} + 1))(G_{a_d}k + \bar{d}_1m_2 + d(G_{a_p} + m_1 + m_2)) - \\ & (d\bar{k}_1 + \bar{d}_1k)(m_1 + G_{f_d}d). \end{aligned}$$

Rewritten

$$\begin{aligned} a_1 = & (d\bar{d}_1^2 + d^2\bar{d}_1 - 2d\bar{k}_1m_1) + \\ & G_{f_p}(d^2\bar{d}_1 + d\bar{k}_1m_2 - G_{a_d}k^2 - \bar{d}_1km_2) + \\ & G_{f_d}(k^2(G_{a_p} + m_1 + m_2) - d^2\bar{k}_1 + k\bar{k}_1m_2) + \\ & G_{a_p}(\bar{d}_1k - d\bar{k}_1) - \\ & G_{a_d}(k^2 + k\bar{k}_1). \end{aligned}$$

Assuming large k

$$a_1 = (d\bar{d}_1^2 + d^2\bar{d}_1 - 2d\bar{k}_1m_1) - G_{f_p}(G_{a_d}k^2 + \bar{d}_1km_2) + G_{f_d}k^2(G_{a_p} + m_1 + m_2) + G_{a_p}\bar{d}_1k - G_{a_d}k^2.$$

Third condition The approximate third condition is then, using the approximate a_0, a_1, a_2 is:

$$\begin{aligned} & (d\bar{d}_1^2 + d^2\bar{d}_1 - 2d\bar{k}_1m_1) - G_{f_p}(G_{a_d}k^2 + \bar{d}_1km_2) + G_{f_d}k^2(G_{a_p} + m_1 + m_2) + G_{a_p}\bar{d}_1k - G_{a_d}k^2 > \\ & -\sqrt{(d\bar{k}_1k^2(G_{f_p} + 1) - G_{f_d}k^2\bar{k}_1)(dm_1^2 - G_{f_p}dm_1m_2 - G_{f_d}km_1m_2 + G_{a_p}dm_1 + G_{a_d}km_1)}. \end{aligned}$$

Because all parameters are both in and outside of the square root, solving for any parameter requires solving the quadratic equation again, leading to very cumbersome solutions.

D.10 Flexible Link Robot Literature Comparison

The systems of publications by Ott. et al. [25], Albu-Schaeffer et al. [24] at the german aerospace center (DLR) and general SEA structure of [72] are compared to the systems of this work in D.2. For clarity, these figures only include inertia and stiffness.

D.10.1 DLR

The DLR inner torque loop is used to reduce motor inertia, where a deflecting harmonic drive is used as the torque sensor. This loop is equivalent to the rigid systems studied in ch. 4 and ch. 5. Even though link compliance and passive cartesian impedance control is considered in their work, those elements are part of the environment in fig. D.2 (a). Their reduction is thus limited to motor inertia, and link compliance is outside of the DLR reduction scope.

In contrast, fig. D.2 (c) corresponding to ch. 6 attempts inertia reduction over a structure including compliance. If there were additional compliance between the motor and harmonic drive, the model of ch. 6 applies. In practice however this is designed to be a much more rigid connection than the harmonic drive. Thus, the model of ch. 6 is likely not limiting in the DLR inner torque loop.

However, the model of ch. 5 is relevant because most practical controllers are discrete-time controllers. The results of that chapter thus apply directly. This work can therefore be seen as a subset the DLR motor inertia reduction. It explains why the DLR inner torque loop might be fundamentally limited due to unaccounted gear flexibility, but most likely by discrete-time control.

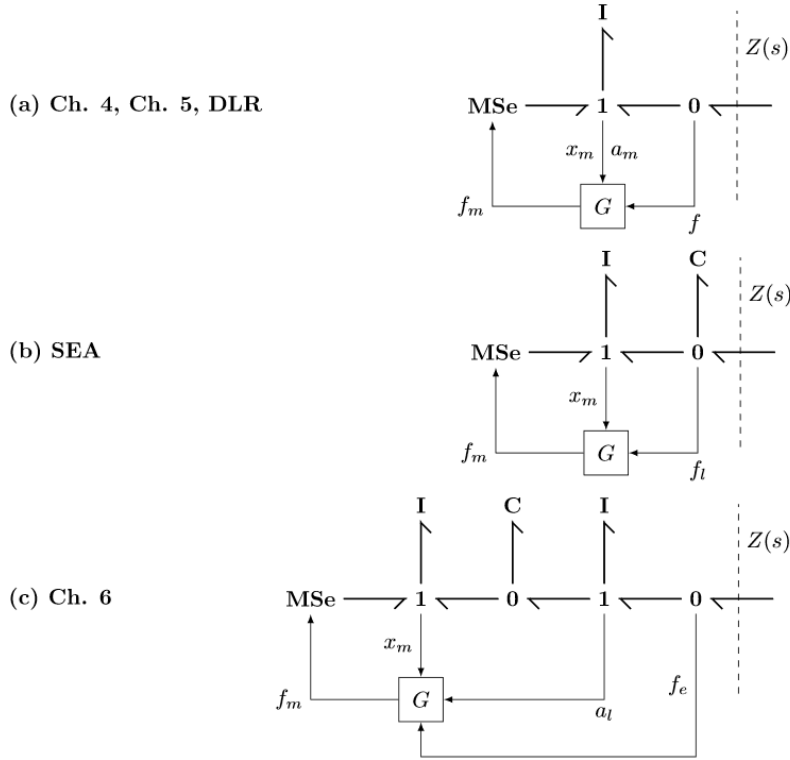


Figure D.2: Comparison of the systems studied in this work in ch. 4, ch. 5, ch. 6, the work of the DLR [25], [24], and the SEA structure [72]. Here, the SEA structure is assumed to measure force directly over the compliance.

D.10.2 SEA

A SEA robot assumes that motor and end effector positions can be measured on either side of a compliance. After calibration, the measured interaction force is then controlled by position control of the motor, driving the measured force to a desired force. This is a key difference in design philosophies: the SEA focuses on minimizing a force error in real time, in addition to impedance reduction.

Although the measuring principle is the same as a load cell, a load cell is considered practically rigid. In contrast, the SEA with higher compliance is a design element, rather than a derogatory feature. This causes the difference between models fig. D.2 (a) and (b): the former ignores the compliance because it is much lower. Still, inertia reduction by force feedback lowers the LF apparent robot impedance of both.

The work in ch. 6 considers serial robots that cannot accurately measure end effector position. This means that the internal force is not measured explicitly in the same way as a SEA. Instead, force sensing is done *after* the internal compliance, seen in fig. D.2 and (c). Additionally, the load cell is considered rigid.

The very general controller of a SEA [72] is shown in fig. D.3 in comparison to the controller of ch. 6. SEA literature often considers torque tracking of a desired torque τ_d , whereas this work does not. To compare control strategies, a torque command τ_d must be generated for the SEA. Here, this is assumed to be done with the target impedance $Z_d(s)$. The resulting apparent impedances $Z(s)$ can then be compared directly. The conceptual difference is that the SEA in real-time tries to enforce $Z_d(s)$ by the force error explicitly. In contrast, in this work impedance shaping is implicit. This results in a much simpler control scheme, but does not minimize any error in real time.

It can be seen that the second inertia is not included in the SEA model. However, because the end effector only experiences inertia (no damping) and acceleration, forces are related through:

$$\begin{aligned}\tau_e &= m_2 a_l + \tau_l \\ \tau_l &= k(\theta_l - \theta_m).\end{aligned}\tag{D.3}$$

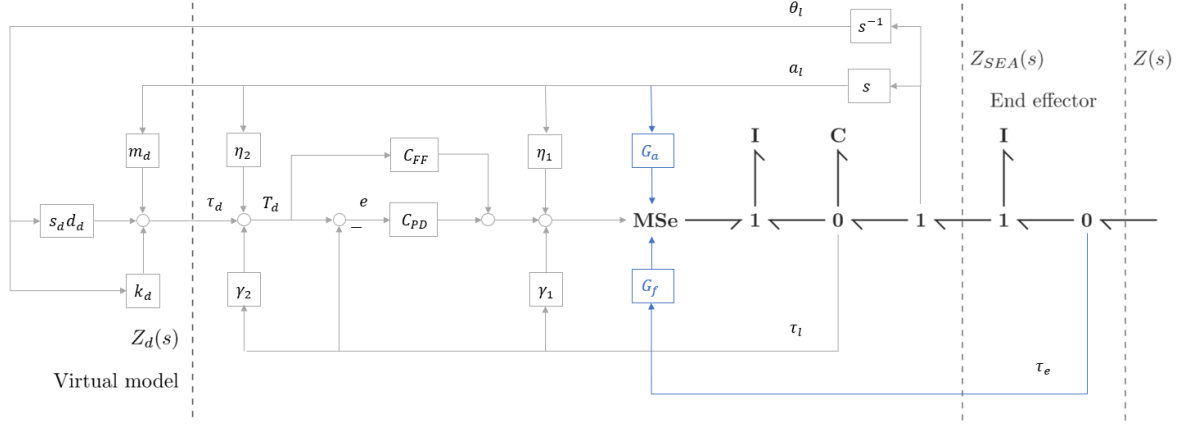


Figure D.3: The general SEA controller from [72] in grey, feeding back interaction force τ_l , end effector position θ_l and acceleration a_l . The latter two are used in a virtual model to obtain τ_d . Acceleration and force are fed back either before or after the PD and feedforward controller by η, γ . In blue is the controller used in ch. 6. System boundaries are different; the SEA at $Z_{SEA}(s)$ does not consider the end effector to have inertia, while this work does at $Z(s)$.

App. D.II finds that the equivalence between these controllers is:

$$\begin{aligned} G_{a_2} &= (\eta_1 + C_{FF}(\eta_2 + m_d) + C_{PD}(\eta_2 + m_d) - \bar{m}_2(\gamma_1 + C_{FF}\gamma_2 + C_{PD}(\gamma_2 - 1) + 1/\bar{k}(C_{FF} + C_{PD})(k_d + d_d s_d))) \\ G_f &= \gamma_1 + C_{FF}\gamma_2 + C_{PD}(\gamma_2 - 1) + 1/\bar{k}(C_{FF} + C_{PD})(k_d + d_d s_d) \\ G_{x_1} &= (C_{FF} + C_{PD})(k_d + d_d s_d). \end{aligned}$$

There are then multiple parametrizations that lead to equivalent solutions for the low-frequency shaping of Ψ_{ideal} . If the controllers C_{PD}, C_{FF} only include a proportional and derivative gain (e.g. no filtering), these equivalences can be further split into the PD gains of this work.

D.II Derivation of Flexible Link Robot and SEA Equivalence

For the following section bar notation $\bar{\cdot}$ is used for an estimated parameter, and tilde notation $\tilde{\cdot}$ for a measured variable. This more clearly differentiates between methods. The motor force of this work using D.3 is:

$$f_m = G_{a_2} \tilde{a}_l + G_f \tilde{\tau}_e + G_{x_1} \tilde{x}_m. \quad (D.4)$$

To rewrite the SEA method to the format of D.4, its control is rewritten fit into G_{x_1}, G_{a_2}, G_f . The motor torque of the SEA is:

$$\begin{aligned} \tau_m &= \eta_1 \tilde{a}_l + \gamma_1 \tilde{\tau}_l + C_{FF} T_d + C_{PD}(T_d - \tilde{\tau}_l) \\ T_d &= \eta_2 \tilde{a}_l + \gamma_2 \tilde{\tau}_l + \tau_d. \end{aligned}$$

The real time virtual impedance $Z_d(s)$ is computed in real time:

$$\tau_d = (k_d + d_d s_d) \tilde{\theta}_l + m_d \tilde{a}_l,$$

where s_d is digital differentiation to obtain the velocity. The control schemes are shown in D.3. This more clearly shows that the system boundaries are different and that the SEA does not consider the end effector to have inertia, while this work does.

When all are substituted into the motor torque:

$$\begin{aligned} \tau_m &= \eta_1 \tilde{a}_l + \gamma_1 \tilde{\tau}_l \\ &+ C_{FF}(\eta_2 \tilde{a}_l + \gamma_2 \tilde{\tau}_l + (k_d + d_d s_d) \tilde{\theta}_l + m_d \tilde{a}_l) \\ &+ C_{PD}(\eta_2 \tilde{a}_l + \gamma_2 \tilde{\tau}_l + (k_d + d_d s_d) \tilde{\theta}_l + m_d \tilde{a}_l - \tilde{\tau}_l). \end{aligned}$$

Collecting feedback variables by the measured SEA signals:

$$\begin{aligned} \tau_m &= \tilde{a}_l(\eta_1 + C_{FF}(\eta_2 + m_d) + C_{PD}(\eta_2 + m_d)) \\ &+ \tilde{\tau}_l(\gamma_1 + C_{FF}\gamma_2 + C_{PD}(\gamma_2 - 1)) \\ &+ \tilde{\theta}_l(C_{FF} + C_{PD})(k_d + d_d s_d). \end{aligned}$$

The SEA motor torque can then be rewritten to that of (D.4) using the relationship of (D.3). The relationship between sensed variables (D.3) rewritten is:

$$\begin{aligned}\tau_l &= \tau_e - \tilde{m}_2 a_l \\ \theta_l &= \theta_m - a_l m_2 / k + \tau_e / k.\end{aligned}$$

Substituting and collecting feedback variables by sensed variables:

$$\begin{aligned}\tau_m &= \tilde{a}_l(\eta_1 + C_{FF}(\eta_2 + m_d) + C_{PD}(\eta_2 + m_d) \\ &\quad - \tilde{m}_2(\gamma_1 + C_{FF}\gamma_2 + C_{PD}(\gamma_2 - 1) + 1/\bar{k}(C_{FF} + C_{PD})(k_d + d_d s_d))) \\ &\quad + \tilde{\tau}_e(\gamma_1 + C_{FF}\gamma_2 + C_{PD}(\gamma_2 - 1) + 1/\bar{k}(C_{FF} + C_{PD})(k_d + d_d s_d)) \\ &\quad + \tilde{\theta}_m(C_{FF} + C_{PD})(k_d + d_d s_d).\end{aligned}$$

The equivalence is thus:

$$\begin{aligned}G_{a_2} &= (\eta_1 + C_{FF}(\eta_2 + m_d) + C_{PD}(\eta_2 + m_d) - \tilde{m}_2(\gamma_1 + C_{FF}\gamma_2 + C_{PD}(\gamma_2 - 1) + 1/\bar{k}(C_{FF} + C_{PD})(k_d + d_d s_d))) \\ G_f &= \gamma_1 + C_{FF}\gamma_2 + C_{PD}(\gamma_2 - 1) + 1/\bar{k}(C_{FF} + C_{PD})(k_d + d_d s_d) \\ G_{x_1} &= (C_{FF} + C_{PD})(k_d + d_d s_d).\end{aligned}$$

Appendix E

Appendix to Chapter 8

E.1 Flexible Link Discrete-Time Controller (Mixed) Stability Tradeoff

Because the mixed system contains the sampler, the stability analysis of the hybrid system of app. C.9 is used. Approximate noise spectra are obtained by adding the ZOH and discrete controller to the flexible link spectra of sec. 6.5:

$$W_{n,\text{mixed}}(s) = \frac{Z_{12}(s)h(s)\tilde{G}_n(s)M_n(s)\sigma_n}{Z_1(s) + h(s)\tilde{G}_x(s)s^{-1} + Z_{12}(s)(1 + h(s)\tilde{G}_f(s))}.$$

The optimization problem is defined the same, as in (3.8):

$$\min \left(\alpha \|W_{\text{mixed}}(s)\|_2 + \frac{1 - \alpha}{\hat{k}_h} \right), \quad \alpha \in [0, 1],$$

where \hat{k}_h is the marginally stable spring following from the stability conditions and α is a linear tradeoff between costs.

Fig. E.1 (a) shows an example of all gains, fig. E.2 shows each reduction case and the derived optimal curves. Fig. E.1 (b) shows the combination of all four the optimal curves. Almost all results from this optimization are analogous to those of the hybrid system, such that all comments of ch. 5.6 apply. In addition, the top-right bending curves of fig. E.2 indicate quickly reducing stability. Because the marginally stable spring quickly becomes more compliant, the system is less stable for large gains. Simulation stability results of Controllab's 2o-sim are shown in either figure, and have good agreement with the numerical approach of less than 1% error on average.

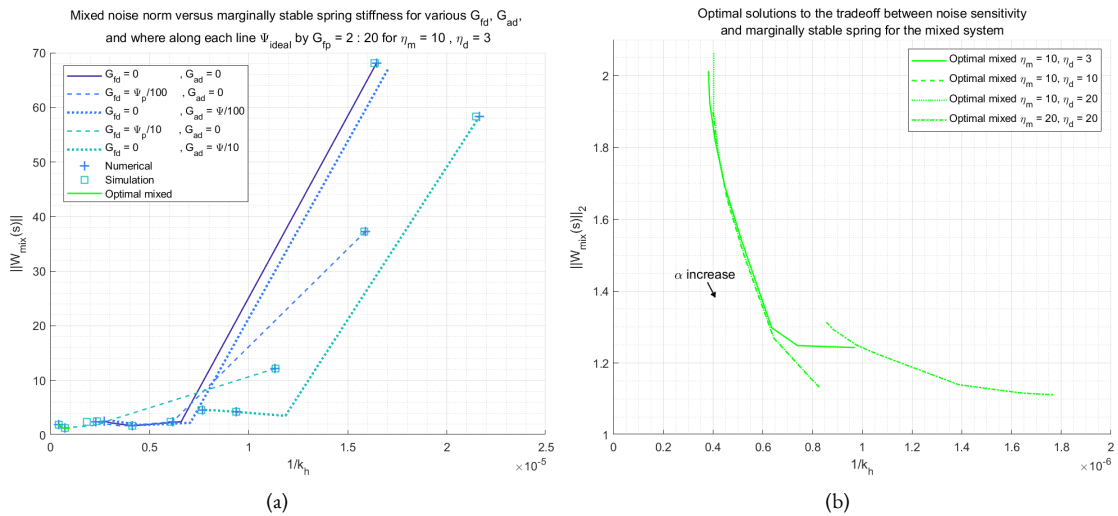


Figure E.1: Noise norms versus marginally stable stiffness, for varying gains. The stiffness axis is inverted such that the bottom and left is more desirable. (a) shows an example of the effect of increasing G_{ad} , G_{fd} . (b) is the combination of optimal curves derived from the graphs of type a., shown in fig. E.2.

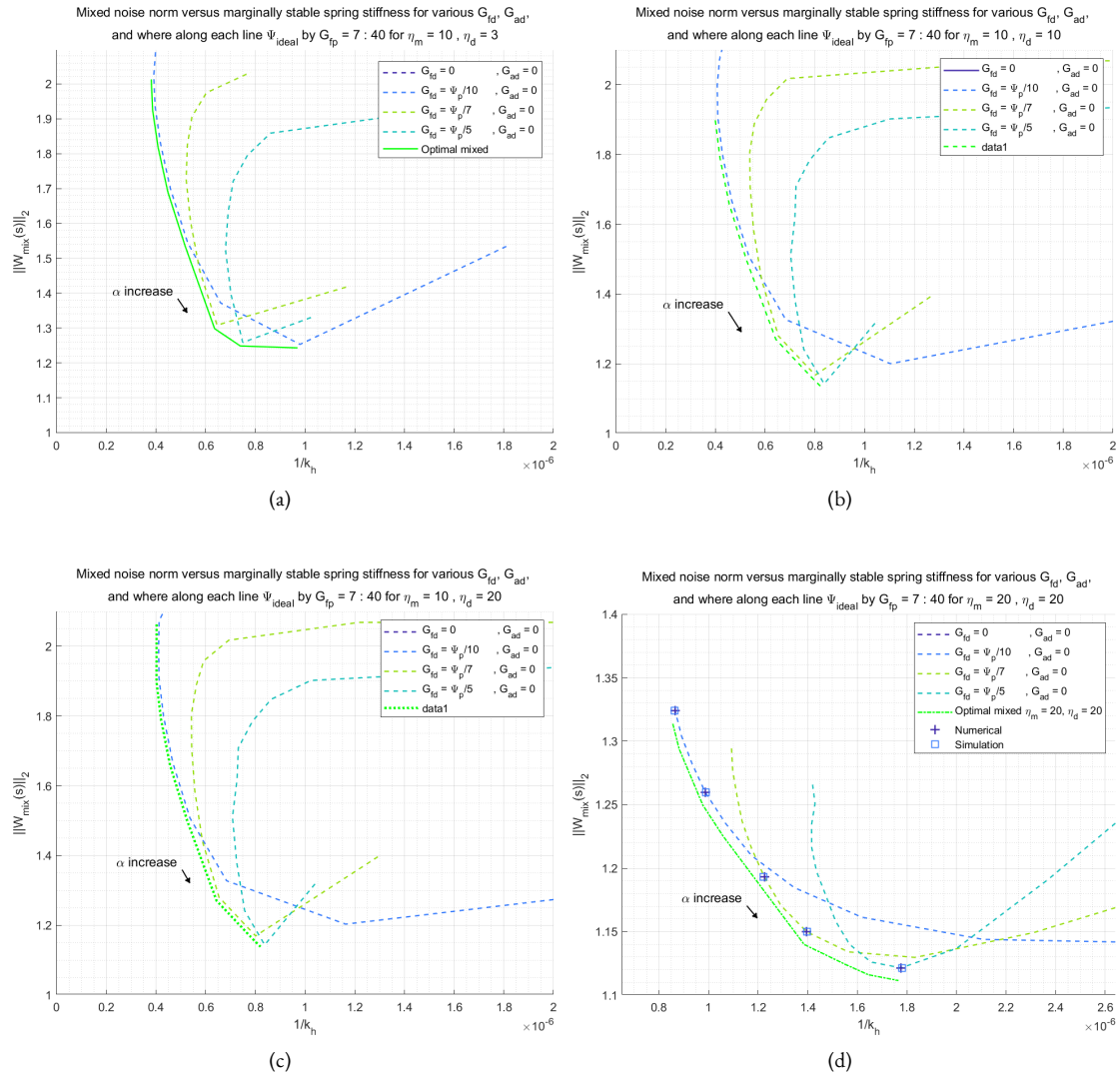


Figure E.2: Noise norms versus destabilizing stiffness for varying G_{fp} , G_{fd} , G_{ad} and four different η_m , η_d . Optimal paths are obtained by following the bottom-most and left-most curves, and are shown slightly offset for visibility reasons. Note that (d) has different axes.

Bibliography

- [1] J. E. Colgate and G. G. Schenkel, "Passivity of a class of sampled-data systems: Application to haptic interfaces," *Journal of Robotic Systems*, vol. 14, no. 1, pp. 37–47, 1997.
- [2] A.-N. Sharkawy, "Human-Robot Interaction: Applications," vol. 0, no. February, pp. 3–5, 2021.
- [3] J. E. Colgate, "Robust control of dynamically interacting systems," *International Journal of Control*, vol. 48, no. 1, pp. 65–88, 1988.
- [4] N. Hogan, "Impedance control: An approach to manipulation: Part III-applications," *Journal of Dynamic Systems, Measurement and Control, Transactions of the ASME*, vol. 107, no. 1, pp. 17–24, 1985.
- [5] N. Hogan, "Impedance control: An approach to manipulation: Part III-applications," *Journal of Dynamic Systems, Measurement and Control, Transactions of the ASME*, vol. 107, no. 1, pp. 17–24, 1985.
- [6] N. Hogan, "On the Stability of Manipulators Performing Contact Tasks," *IEEE Journal on Robotics and Automation*, vol. 4, no. 6, pp. 677–686, 1988.
- [7] H. Kazerooni, T. Sheridan, and P. Houpt, "Robust compliant motion for manipulators, part I: The fundamental concepts of compliant motion," *IEEE Journal on Robotics and Automation*, vol. 2, no. 2, pp. 83–92, 1986.
- [8] H. Kazerooni, P. Houpt, and T. Sheridan, "Robust compliant motion for manipulators, part II: Design method," *IEEE Journal on Robotics and Automation*, vol. 2, no. 2, pp. 93–105, 1986.
- [9] J. E. Colgate, M. A. Peshkin, and W. Wannasuphprasit, "Nonholonomic haptic display," *Proceedings - IEEE International Conference on Robotics and Automation*, vol. 1, no. April, pp. 539–544, 1996.
- [10] J. E. Colgate, P. E. Grafing, M. C. Stanley, and G. Schenkel, "1. (also," pp. 202–208, 1993.
- [11] J. E. Colgate, "Coordinate Transformations and Logical Operations for Minimizing Conservativeness in Coupled Stability Criteria," *Journal of Dynamic Systems, Measurement, and Control*, vol. 116, pp. 643–649, dec 1994.
- [12] J. P. Kim and J. Ryu, "Stable haptic interaction control using energy bounding algorithm," *2004 IEEE/RSJ International Conference on Intelligent Robots and Systems (IROS)*, vol. 2, pp. 1210–1217, 2004.
- [13] A. Haddadi and K. Hashtrudi-Zaad, "Stability analysis of haptic interfaces for different types of sampled signals and virtual environment implementations," *2010 IEEE Haptics Symposium, HAPTICS 2010*, pp. 293–299, 2010.
- [14] Y. Liu, "Passivity analysis of haptic interfaces based on frequency response approach," *Proceedings - 2010 IEEE International Conference on Intelligent Computing and Intelligent Systems, ICIS 2010*, vol. 2, no. 1, pp. 679–683, 2010.
- [15] Y. Liu, X. Liu, Z. Qi, and Y. Wang, "Passivity analysis and design of a haptic interface," *2015 IEEE International Conference on Mechatronics and Automation, ICMA 2015*, no. 2, pp. 2129–2133, 2015.
- [16] J. E. Colgate, M. C. Stanley, and J. M. Brown, "Issues in the haptic display of tool use," *IEEE International Conference on Intelligent Robots and Systems*, vol. 3, pp. 140–145, 1995.
- [17] R. J. Adams and B. Hannaford, "Stable haptic interaction with virtual environments," *IEEE Transactions on Robotics and Automation*, vol. 15, no. 3, pp. 465–474, 1999.
- [18] M. Brown, *Passive implementation of multibody simulations for haptic display*. PhD thesis, NORTHWESTERN UNIVERSITY, 1998.
- [19] S. Stramigioli, "Creating artificial damping by means of damping injection," *American Society of Mechanical Engineers, Dynamic Systems and Control Division (Publication) DSC*, vol. 58, pp. 601–606, 1996.

- [20] W. S. Newman, “Stability and Performance Limits of Interaction Controllers,” *Journal of Dynamic Systems, Measurement, and Control*, vol. 114, pp. 563–570, dec 1992.
- [21] M. Dohring and W. Newman, “The passivity of natural admittance control implementations,” *Proceedings - IEEE International Conference on Robotics and Automation*, vol. 3, pp. 3710–3715, 2003.
- [22] M. J. Kim, W. Lee, C. Ott, and W. K. Chung, “A passivity-based admittance control design using feedback interconnections,” in *IEEE International Conference on Intelligent Robots and Systems*, vol. 2016-Novem, pp. 801–807, Institute of Electrical and Electronics Engineers Inc., nov 2016.
- [23] A. Keemink, *Haptic physical human assistance*. PhD thesis, University of Twente, Enschede, The Netherlands, oct 2017.
- [24] A. Albu-Schäffer, C. Ott, and G. Hirzinger, “A passivity based cartesian impedance controller for flexible joint robots - Part II: Full state feedback, impedance design and experiments,” *Proceedings - IEEE International Conference on Robotics and Automation*, vol. 2004, no. 3, pp. 2666–2672, 2004.
- [25] C. Ott, A. Albu-Schäffer, A. Kugi, S. Stramigioli, and G. Hirzinger, “A passivity based cartesian impedance controller for flexible joint robots - Part I: Torque feedback and gravity compensation,” *Proceedings - IEEE International Conference on Robotics and Automation*, vol. 2004, no. 3, pp. 2659–2665, 2004.
- [26] C. Ott, A. Albu-Schäffer, A. Kugi, and G. Hirzinger, “On the passivity-based impedance control of flexible joint robots,” *IEEE Transactions on Robotics*, vol. 24, no. 2, pp. 416–429, 2008.
- [27] C. Ott, R. Mukherjee, and Y. Nakamura, “Unified impedance and admittance control,” *Proceedings - IEEE International Conference on Robotics and Automation*, pp. 554–561, 2010.
- [28] Y. Ye, C. Y. Chen, P. Li, G. Yang, and C. A. Zhu, “Cartesian admittance control with on-line gravity and friction observer compensation for elastic joint robots,” *2016 IEEE International Conference on Robotics and Biomimetics, ROBIO 2016*, pp. 725–730, 2016.
- [29] J. J. Abbott and A. M. Okamura, “Effects of position quantization and sampling rate on virtual-wall passivity,” *IEEE Transactions on Robotics*, vol. 21, no. 5, pp. 952–964, 2005.
- [30] N. Colonnese and A. Okamura, “M-Width: Stability and accuracy of haptic rendering of virtual mass,” *Robotics: Science and Systems*, vol. 8, pp. 41–48, 2013.
- [31] B. Hannaford and J. H. Ryu, “Time-domain passivity control of haptic interfaces,” *IEEE Transactions on Robotics and Automation*, vol. 18, no. 1, pp. 1–10, 2002.
- [32] J. H. Ryu, Y. S. Kim, and B. Hannaford, “Sampled and continuous time passivity and stability of virtual environments,” *Proceedings - IEEE International Conference on Robotics and Automation*, vol. 1, pp. 822–827, 2003.
- [33] J. H. Ryu, D. S. Kwon, and B. Hannaford, “Stability guaranteed control: Time domain passivity approach,” *IEEE Transactions on Control Systems Technology*, vol. 12, no. 6, pp. 860–868, 2004.
- [34] J. H. Ryu, C. Preusche, B. Hannaford, and G. Hirzinger, “Time domain passivity control with reference energy following,” *IEEE Transactions on Control Systems Technology*, vol. 13, no. 5, pp. 737–742, 2005.
- [35] J. H. Ryu, J. H. Kim, D. S. Kwon, and B. Hannaford, “A simulation/experimental study of the noisy behavior of the time domain passivity controller for haptic interfaces,” *Proceedings - IEEE International Conference on Robotics and Automation*, vol. 2005, no. April, pp. 4321–4326, 2005.
- [36] Y. Ye, Y. J. Pan, Y. Gupta, and J. Ware, “A power-based time domain passivity control for haptic interfaces,” *IEEE Transactions on Control Systems Technology*, vol. 19, no. 4, pp. 874–883, 2011.
- [37] T. Maneewarn and P. Tothawornyuenyong, “Effects of system delay in passivity-based haptic system,” *2006 IEEE Conference on Robotics, Automation and Mechatronics*, pp. 1–6, 2006.
- [38] R. Balachandran, M. Jorda, J. Artigas, J. H. Ryu, and O. Khatib, “Passivity-based stability in explicit force control of robots,” *Proceedings - IEEE International Conference on Robotics and Automation*, pp. 386–393, 2017.
- [39] S. Stramigioli, C. Secchi, A. J. Van Der Schaft, and C. Fantuzzi, “A novel theory for sample data system passivity,” *IEEE International Conference on Intelligent Robots and Systems*, vol. 2, no. October, pp. 1936–1942, 2002.

- [40] S. Stramigioli, E. D. Fasse, and J. C. Willems, "A rigorous framework for interactive robot control," *International Journal of Control*, vol. 75, no. 18, pp. 1486–1503, 2002.
- [41] S. Stramigioli, C. Secchi, A. J. van der Schaft, and C. Fantuzzi, "Sampled data systems passivity and discrete port-Hamiltonian systems," *IEEE Transactions on Robotics*, vol. 21, no. 4, pp. 574–587, 2005.
- [42] M. Franken and S. Stramigioli, "Internal dissipation in passive sampled haptic feedback systems," *2009 IEEE/RSJ International Conference on Intelligent Robots and Systems, IROS 2009*, pp. 1755–1760, 2009.
- [43] J. Kim, C. H. Seo, and J. Ryu, "Six degree-of-freedom energy bounding algorithm for stable and directionally transparent haptic interaction," *2008 International Conference on Control, Automation and Systems, ICCAS 2008*, no. 1, pp. 260–265, 2008.
- [44] J. Kim, J. P. Kim, C. Seo, and J. Ryu, "An energy bounding approach for directional transparency in multiple degree-of-freedom haptic interaction," *Proceedings - 3rd Joint EuroHaptics Conference and Symposium on Haptic Interfaces for Virtual Environment and Teleoperator Systems, World Haptics 2009*, pp. 320–325, 2009.
- [45] J. P. Kim and J. Ryu, "Robustly stable haptic interaction control using an energy-bounding algorithm," *International Journal of Robotics Research*, vol. 29, no. 6, pp. 666–679, 2010.
- [46] J. P. Kim, C. Seo, and J. Ryu, "A preliminary test for bilateral teleoperation using energy bounding algorithm," *Proceedings - IEEE International Workshop on Robot and Human Interactive Communication*, pp. 304–309, 2007.
- [47] D. Lee and K. Huang, "Passive-set-position-modulation framework for interactive robotic systems," *IEEE Transactions on Robotics*, vol. 26, no. 2, pp. 354–369, 2010.
- [48] K. Lee and Y. L. Doo, "Adjusting output-limiter for stable haptic interaction with deformable objects," *2007 Mediterranean Conference on Control and Automation, MED*, 2007.
- [49] K. Lee and D. Y. Lee, "Adjusting output-limiter for stable haptic rendering in virtual environments," *IEEE Transactions on Control Systems Technology*, vol. 17, no. 4, pp. 768–779, 2009.
- [50] J. P. Kim, S. Y. Baek, and J. Ryu, "A force bounding approach for stable haptic interaction," *2011 IEEE World Haptics Conference, WHC 2011*, pp. 397–402, 2011.
- [51] M. J. Kim and W. K. Chung, "Robust control of flexible joint robots based on motor-side dynamics reshaping using disturbance observer (DOB)," *IEEE International Conference on Intelligent Robots and Systems*, no. Iros, pp. 2381–2388, 2014.
- [52] S. Y. Baek, S. Park, and J. Ryu, "Force bounding approach for stable haptic interaction with dynamic virtual environments," *IEEE/ASME International Conference on Advanced Intelligent Mechatronics, AIM*, pp. 34–39, 2017.
- [53] S. Y. Baek, S. Park, and J. Ryu, "A Force Bounding Approach in Joint Space for Interacting With Dynamic Multi-Degrees of Freedom Virtual Objects," *IEEE Transactions on Haptics*, vol. 12, no. 2, pp. 217–223, 2019.
- [54] A. Jafari, M. Nabeel, and J. H. Ryu, "The Input-to-State Stable (ISS) approach for stabilizing haptic interaction with virtual environments," *IEEE Transactions on Robotics*, vol. 33, no. 4, pp. 948–963, 2017.
- [55] A. Morbi and M. Ahmadi, "Safely Rendering Small Impedances in Admittance-Controlled Haptic Devices," *IEEE/ASME Transactions on Mechatronics*, vol. 21, no. 3, pp. 1272–1280, 2016.
- [56] J. H. Ryu and M. Y. Yoon, "Memory-based passivation approach for stable haptic interaction," *IEEE/ASME Transactions on Mechatronics*, vol. 19, no. 4, pp. 1424–1435, 2014.
- [57] M. De Stefano, J. Artigas, W. Rackl, and A. Albu-Schaeffer, "Passivity of virtual free-floating dynamics rendered on robotic facilities," *Proceedings - IEEE International Conference on Robotics and Automation*, vol. 2015-June, no. June, pp. 781–788, 2015.
- [58] M. Nabeel, J. Lee, U. Mehmood, A. Jafari, J. H. Hwang, and J. H. Ryu, "Increasing the impedance range of admittance-type haptic interfaces by using Time Domain Passivity Approach," *IEEE International Conference on Intelligent Robots and Systems*, vol. 2015-December, pp. 585–590, 2015.
- [59] K. Totorkulov and J. H. Ryu, "Stable haptic interaction with admittance type virtual environments based on time-domain passivity approach," *2012 9th International Conference on Ubiquitous Robots and Ambient Intelligence, URAI 2012*, no. 1, pp. 111–113, 2012.

- [60] D. Ryu, J. B. Song, S. Kang, and M. Kim, “Frequency domain stability observer and active damping control for stable haptic interaction,” *IET Control Theory and Applications*, vol. 2, no. 4, pp. 261–268, 2008.
- [61] T. Hulin, A. Albu-Schäffer, and G. Hirzinger, “Passivity and stability boundaries for haptic systems with time delay,” *IEEE Transactions on Control Systems Technology*, vol. 22, no. 4, pp. 1297–1309, 2014.
- [62] J. E. Colgate and J. M. Brown, “Factors affecting the Z-width of a haptic display,” *Proceedings - IEEE International Conference on Robotics and Automation*, no. pt 4, pp. 3205–3210, 1994.
- [63] G. Meinsma, C. Heida, and M. J. van Putten, “Advanced Techniques for Signal Analysis,” pp. 1–93, 2011.
- [64] S. Skogestad and I. Postlethwaite, “Multivariable Feedback Control,” in *Optimal Real-time Control of Sewer Networks*, pp. 55–64, London: Springer-Verlag, 2001.
- [65] J. Doyle, K. Glover, P. Khargonekar, and B. Francis, “State-space solutions to standard H/sub 2/ and H/sub infinity / control problems,” *IEEE Transactions on Automatic Control*, vol. 34, no. 8, pp. 831–847, 1989.
- [66] J. R. Ragazzini and L. A. Zadeh, “The analysis of sampled-data systems,” *Electrical Engineering*, vol. 71, pp. 1102–1102, dec 1952.
- [67] S. Engelberg, *A Mathematical Introduction to Control Theory*, vol. 2 of *Series in Electrical and Computer Engineering*. London: IMPERIAL COLLEGE PRESS, v. 2 ed., jun 2005.
- [68] E. I. Jury, “Analysis and synthesis of sampled-data control systems,” *Transactions of the American Institute of Electrical Engineers, Part I: Communication and Electronics*, vol. 73, no. 4, pp. 332–346, 1954.
- [69] M. C. Smith, “Synthesis of mechanical networks: The inerter,” *Proceedings of the IEEE Conference on Decision and Control*, vol. 2, no. 10, pp. 1657–1662, 2002.
- [70] M. Spiegel and L. Seymour, “Schaum’s Outline: Mathematical Handbook of Formulas,” p. 278, 1968.
- [71] K. J. Åström and B. Wittenmark, *Computer-Controlled Systems: Theory and Design, Third Edition*. Dover Books on Electrical Engineering, Dover Publications, 2011.
- [72] M. Sytsma, *Comparing Torque Control Approaches for Series Elastic Actuators, Relating Bandwidth and Passivity To*. PhD thesis, University of Twente, 2020.